Potential Application of Nanotechnology on Cement Based Materials

R. Panneer Selvam, Vikramraja J. Subramani, Shanique Murray and Kevin Hall

Project Number: MBTC DOT 2095/3004
Date: August 06, 2009

ACKNOWLEDGEMENTS

Special thanks to Arkansas Highway and Transportation Department (AHTD) and Mack-Blackwell Rural Transportation Center (MBTC) for their financial support. This work was also supported in part by the National Science Foundation under Grant MRI 0421099 (Red Diamond) and Grant MRI #072265 (Star of Arkansas).

TABLE OF CONTENTS

ACKNOWLEDGEMENTS i

TABLE OF CONTENTS i

LIST OF FIGURES v

LIST OF TABLES ix

ABSTRACT iv

CHAPTER 1: INTRODUCTION 1

1.1 Overview 1

1.2 Origin of Strength in Cement Paste 1

1.3 The Use of Nanotechnology to Determine the Structure and Mechanical Properties of Calcium Silicate Hydrate (C-S-H) gel 2

1.4 Research Need 3

1.5 Importance of Molecular Modeling 4

1.6 Research Objectives 4

CHAPTER 2: LITERATURE REVIEW 6

2.1 Hydration of Cement 6

2.2 Microstructure of Hardened Cement Paste 7

2.3 Calcium Silicate Hydrate (C-S-H) Gel 9

2.4 Understanding the Structure-Property Relationship in Cement Paste 9

2.5 Experimental Investigation of C-S-H Gel 10

2.5.1 XRD Studies of C-S-H Gel 11

2.5.1.1 Atomic Structure of a Perfect Crystal versus Atomic Structure of C-S-H Gel 11

2.5.2 Transmission Electron Microscopy (TEM) Studies of C-S-H Gel 17

2.5.3 Scanning Electron Microscopy (SEM) Studies of C-S-H Gel 18

2.5.4 Nanoindentation Studies of C-S-H Gel 22

2.6 Models of the Structure of C-S-H Gel 22

2.6.1 Crystalline Models of the Structure of C-S-H Gel 24

2.6.2 Colloidal Model of the Structure of C-S-H Gel 25

2.7 Computational Studies of C-S-H Gel 28

CHAPTER 3: INTRODUCTION TO MOLECULAR MODELING 30

3.1 Introduction 30

3.2 Techniques of Molecular Modeling 30

3.2.1 Molecular Statics (MS) 30
3.2.1.1 Energy Minimization 31
3.2.1.2 Energy Minimization Algorithms 31
3.2.1.3 Determination of Bulk Properties 36
3.2.1.4 Elastic Constants 36
3.2.1.5 Bulk Modulus (K) & Shear Modulus (G) 37
3.2.1.6 Young's Modulus 37
3.2.1.7 Poisson's Ratio 38
3.2.2 Molecular Dynamics (MD) 38
3.2.2.1 Governing Equations 38
3.2.2.2 Ensembles 39
3.2.2.3 Steps in MD 40
3.2.2.4 Initialization 41
3.2.2.5 Energy Minimization 41
3.2.2.6 Integrating the Equations of Motion 41
3.2.2.7 Periodic Boundary Conditions 42
3.2.2.8 Verlet Neighbor List 43
3.2.2.9 Calculation of Properties 44
3.2.2.10 Kinetic, Potential and Total Energy 45
3.2.2.11 Temperature 45
3.2.2.12 Pressure 45
3.3 Atomic Interactions 46

3.3.1 Long Range Interactions (Coulombic interactions) 47
3.3.2 Short Range Interactions 49
3.3.3 Three Body Interactions 49
3.4 Modern Programs to Perform Molecular Modeling 51

CHAPTER 4: DATA PREPARATION FOR MOLECULAR MODELLING 52

4.1 Procedures for Modeling Crystalline Calcium Silicate Hydrate Structures using Molecular Statics (MS) 52

4.1.1 Identification of Crystal Parameters in Crystalline Calcium Silicate Hydrate Structures 52
4.2 Molecular Dynamic Simulation of C-S-H structures 57

4.2.1 Steps to generate Input File 57
4.2.2 Data File Generation 58
4.2.3 Atomic Interactions 63
4.2.4 MD Simulation Conditions 63

4.2.5 Determination of Strain and Young's Modulus 64
4.3 Procedures for determining the Mechanical Properties of Packed Tobermorite Structures 65
4.2.1 Generating the Structure of Packed Tobermorite Unit Cells 67
4.2.2 Atomic Interactions 71
CHAPTER 5: RESULTS AND DISCUSSION 72
5.1 Crystalline Calcium Silicate Hydrates 72
5.1.1 Mechanical Properties of Crystalline C-S-H Models 73
5.2 Breaking the Bonds in Crystalline C-S-H Models 75
5.2.1 Approach 1 75
5.2.2 Approach 2 76
5.2.2.1 Site Potentials of Silicon Atoms 77
5.2.2.2 A Possible Structure of C-S-H 79
5.3 Stress–Strain Behavior of Calcium Silicate Hydrate structures 82
5.3.1 Computation of Elastic Modulus and Tensile Strength 92
5.3.2 Limitations of Computational Model 94
5.4 Mechanical Properties of Tobermorite structures Packed Together 94
5.5 Case study 1: Mechanism of deterioration of concrete structures upon subjection to aggressive environment 96
5.5.1 Site potentials of Calcium atoms 97
5.5.2 Substitution of Calcium by Magnesium 98
5.6 Case study 2: Chemical and physical compatibility of composite cement 101
5.6.1 Substitution of Silicon by Aluminium 101
CHAPTER 6: SUMMARY 105
6.1 Summary 105
6.2 Future Work 108
REFERENCES 112
Appendix A: Input parameters to GULP 117
Appendix B: Sample Gulp Input File 121
Appendix C: Data File for Atomic Structure of Tobermorite 124
Appendix D: Data File for Atomic Structure of Proposed C-S-H 129
Appendix E: Input Parameters into Lammps 134
Appendix F: Sample Input File for Lammps 137

Appendix G: Input Parameters into GULP for Packed Tobermorite Structures 139

Appendix H: Fortran Code to Build the Atomic Structure of Packed Tobermorite Structures 140

LIST OF FIGURES

Figure 2.1 Sequence of Cement Hydration [17]. 6

a) Cement particles in water b) Formation of C-S-H c) C-S-H growth around the cement grains 6

d) Fully grown C-S-H and Calcium hydroxide 6

Figure 2.2 Microstructure of Hardened Cement Paste [19]. 8

c = Unreacted cement grains, ip = Calcium Silicate Hydrate, inner product, op = Calcium Silicate Hydrate, outer product, ch = calcium hydroxide, p = capillary pores 8

Figure 2.3 Complexity of Microstructure- Property Relationship [23]. 10

Figure 2.4 Illustrations of Crystal (a) and Unit Cell (b) [15]. 12

Figure 2.5 Classifications of Crystal Systems – 14 Bravais Lattices [25]. 13

Figure 2.6 X-Ray Diffraction Patterns of Cement Pastes [26]. 14

Figure 2.7 Typical Silica Tetrahedron [27]. 15

Figure 2.8 Illustration of Tetrahedral Silicate Chains, Inter Layer Calcium Atoms and Water Molecules [15]. 15

Figure 2.9 C-S-H layer (lamella) [28]. 16

Orange Atom = Calcium, Purple Atom = Silicon, Red Atom = Oxygen and White Atom = Hydrogen. 16

Figure 2.10 Dimmer Silicate Chains [15]. 16

Figure 2.11 Pentamer Silicate Chains [15]. 17

Figure 2.12 TEM Micrograph of HD C-S-H in hardened cement paste [29]. 17

Figure 2.13 TEM Micrographs of Inner and Outer Product of C-S-H [30]. 18

Figure 2.14 Scanning Electron Micrograph of the Fracture Surface of Portland cement after 1 Hour Hydration[31]. 19
Figure 2.15 Scanning Electron Micrograph of the Fracture Surface of Portland cement after 24 Hours Hydration [31]. 20
Figure 2.16 Higher Magnification of the Fibres[31]. 21
Figure 2.17 Scanning Electron Micrograph of the Fracture Surface of a Portland cement Paste after 21 days[31]. 21
Figure 2.16 (a) Colloidal- particle Model of C-S-H (Powers-Brunauer Model) (b) Extended Sheet Model of C-S-H (Feldman- Serada Model)[33]. 23
Figure 2.17 Atomic Configuration of Three Mineral Structures: 1) Tobermorite (11 A°) - Hamid [34] 2) Tobermorite - (11 A°) -Merlino [35] 3) Jennite- Merlino [36]. 25
Figure 2.18 Colloidal Structure of C-S-H [11]. 26
Figure 2.19 HD and LD C-S-H [11]. 27
Figure 3.1 Energy Surface of an Atomic Structure [15]. 31
Figure 3.2 Steepest descent method [44]. 33
Figure 3.3 Conjugate gradient method [44]. 34
Figure 3.4 Comparison between conjugated gradient and simple gradient methods[25]. 35
Figure 3.5 MD sequence chart [15]. 40
Figure 3.6 Periodic boundary Conditions[15]. 43
Figure 3.7 Neighbor List [15]. 44
Figure 3.8 Electrostatic (Coulombic) interactions [15]. 48
Figure 3.9 Three Body Interactions. 50
Figure 4.1 Structure of Tobermorite [15]. 62

Figure 4.2 Structure of Proposed C-S-H [15]. 62

Figure 4.3 Illustration of applying strain rate to the atomic structure of C-S-H. 64

Figure 4.4 A Possible Configuration of C-S-H Units [15]. 66

Figure 4.5 Illustration of Stack 1 69

Figure 4.6 Illustration of Stack 2 70

Figure 4.7 Illustration of Stack 3 71

Figure 5.1 Atomic Configuration of Three Mineral Structures 1) Tobermorite 11A° [Hamid (34)] 2) Tobermorite [Merlino(35)] 3) Jennite [Merlino(36)]. Visualized using Diamond (demo) Version and Xtal Software 72

Figure 5.2 Snapshot of C-S-H Structure from GDIS Visualization Software 76

Figure 5.3 Drierketten Type of Silicate Chains Observed in Tobermorite. 77

Figure 5.4 Site Potentials of Silicon Atoms 78

Figure 5.5 Breaking the Silicate Chains in Tobermorite 79

Figure 5.6 Proposed Structure for C-S-H 81

Figure 5.7(a) Tensile Stress-Strain Behavior of Tobermorite 84

Figure 5.7 (b) Compressive Stress-Strain Behavior of Tobermorite 85

Figure 5.8 (a) Tensile Stress-Strain Behavior of Proposed C-S-H 86

Figure 5.8 (b) Compressive Stress-Strain Behavior of Proposed C-S-H 87

Figure 5.9 (a) Tensile Stress-Strain Behavior of Tobermorite 88

Figure 5.9 (b) Compressive Stress-Strain Behavior of Tobermorite. 89

Figure 5.10 (a) Tensile Stress-Strain Behavior of Proposed C-S-H 90

Figure 5.10 (b) Compressive Stress-Strain Behavior of Proposed C-S-H 91

Figure 5.11 Magnification of the Tensile Stress-Strain Behavior of Proposed C-S-H ... 92

Figure 5.12 Packing of Crystalline Calcium Silicate Hydrate . (a) Stack 1, (b) Stack 2 and (c) Stack 3 96

Figure 5.13 Site potentials of Calcium atoms 98

Figure 5.14 Magnesium substituted C-S-H. 99

Figure 5.15 Aluminium substituted C-S-H 102

Figure 6. 1 Schematic diagram of the packing of C-S-H nanoparticles[15] 110

LIST OF TABLES

Table 2. 1 Composition of Hardened Cement Paste (w/c = 0.5) [16] 8

Table 4.1 Atoms in unit cell 53

Table 4.2 Normalized Monoclinic Atomic Coordinates in Tobermorite 11 Aº 54

Table 4.3 Core-Spring Potential 55

Table 4.4 Charges of the Atoms 56

Table 4.5 Charges of the Atoms 60

Table 4.6 Normalized Orthorhombic Atomic Coordinates in Proposed C-S-H Structure (a = 11.18Å, b =7.39Å, c =22.77Å) (x=a, y=b and z=c) [15] 60

Table 4.7 Normalized Orthorhombic Atomic Coordinates in Tobermorite Structure (Crystalline Calcium Silicate Hydrate) (a = 11.18Å, b =7.39Å, c =22.77Å) (x=a, y=b and z=c) [34] 61

Table 4.8 Dimensions of Simulation Cells 68

Table 5.1 Optimized Parameters of Tobermorite Structure Ca/Si-0.83 73

Table 5.2 Bulk Properties of Crystalline Calcium Silicate Hydrate 74

Table 5.3 Elastic Modulus and strength of Calcium Silicate Hydrate Structures 93

Table 5.4 Mechanical Properties of Tobermorite Structures Packed Together 95

Table 5.5 Comparison of the bulk properties of Magnesium substituted Tobermorite with unsubstituted Tobermorite 100

Table5.6 7.5 Comparison of the bulk properties of C-S-H with/without Aluminium substitution. 104

ABSTRACT

The tensile strength of cement paste is one of the most important mechanical properties that influence shrinkage cracks in cementious materials. Cement pastes which exhibit low tensile strength, tend to exhibit greater shrinkage crack potential and reduced durability. If the tensile strength in cement paste can be increased, then the shrinkage cracking potential can be minimized. It is believed that the strength and cohesion of cement paste is controlled by the formation of Calcium Silicate Hydrate (C-S-H) gel. In order to be able to enhance macroscopic mechanical properties (tensile strength) it is necessary to understand the structure and behavior of C-S-H gel at the atomic level.

Molecular statics was used to determine minimal potential energy, and the mechanical properties of crystalline calcium silicate hydrate structures. It was found that when bonds in the silicate chains of crystalline calcium silicate hydrate structures were broken at certain places, the computed elastic modulus was comparable with macro level experimental values. From this study a plausible atomic structure of C-S-H gel is proposed. Further research effort builds upon the previous work by using molecular dynamics to derive tensile and compressive strength of calcium silicate hydrate structures from uniaxial stress-strain data.

The results from the molecular dynamics simulations showed that the maximum strength (i.e. compressive and tensile) for the proposed calcium silicate hydrates are magnitudes higher than the strength at the macro level. However, the tensile strength of the proposed C-S-H gel is 23% of the compressive strength. This research also concludes that electrostatic forces and bond forces in the silicate chains are the main contributors to cement strength at the atomic level and that breakage in the silicate chains leads to low tensile strength in C-S-H gel.

CHAPTER 1: INTRODUCTION

1.1 Overview

Concrete is as essential to our modern world as are computers or electricity. In fact it is employed extensively in the construction industry and consumed at a rate of 6 billion tonnes per year. However, conventional concrete suffers from a number of inherent deficiencies, such as its low tensile strength. As a result, concrete structures undergo significant shrinkage cracking. One way of improving the tensile strength of concrete is by improving the mechanical properties of the binder, cement paste. In the past, progress in this direction has been achieved mainly by adding reinforcement (steel), adding chemical agents to reduce porosity and/or lower the water/cement ratio in cement paste. These methods have improved the tensile capacity of the concrete structure but also increase the cost of construction. In addition, many concrete infrastructures are deteriorating faster than expected due to the corrosion of steel in marine environments. Reinforcing steel corrodes because chlorides and other ions present in marine environments move through the pores or cracks in the cement paste and disrupts the layer protecting the steel, causing it to rust. The deterioration of concrete structures has resulted in a need to understand the internal structure of concrete and its effect on concrete properties (strength). Researchers are now investigating alternative approaches for enhancing the performance of cement paste by means of manipulating the internal structure of cement paste.

1.2 Origin of Strength in Cement Paste

The strength of concrete originates from the strength of the hardened cement paste, which in turn originates from the hydration products [1]. The major portion of the hydration products is in the form of a rigid gel, called Calcium Silicate Hydrate (C-S-H). It is believed that C-S-H gel is responsible for strength and cohesion of concrete structures. Currently, there is not an adequate theory for describing the source of the strength or cohesion in C-S-H gel. The forces that give C-S-H gel cohesion are still being debated. Pellenq et.al [2] provided limited insight about the factors that affect setting and

hardening of the cement paste. Pellenq suggested that the short and medium range attractive electrostatic forces are the prime components of the cohesion of C-S-H gel. Other evidences indicate that the surface force between C-S-H nano particles is solely responsible for the cohesion [3-6]. While other evidence suggests that it's a combination of various forces that contribute to cohesion in C-S-H gel [7].

If C-S-H gel can be made more functionalize i.e. C-S-H gel with improved cohesive properties; this can lead to better improvements in mechanical properties (strength and stiffness) of cement based materials. The process of making C-S-H gel more functional requires reliable information about the structure and properties of C-S-H gel.

1.3 The Use of Nanotechnology to Determine the Structure and Mechanical Properties of Calcium Silicate Hydrate (C-S-H) gel

Calcium Silicate Hydrate (C-S-H) gel is a complex structure comprising of elements and pores of various sizes. Over the past decade there have been several experimental investigations of the structure of C-S-H gel. X-ray diffraction (XRD) data of C-S-H gel suggests that the structure is amorphous. In other words, it lacks the orderliness in the arrangement of atoms unlike a perfect crystal (bulk Copper). The amorphous nature of C-S-H makes it very difficult to measure the amount of "bound" and "unbound" water in C-S-H gel and thus, makes the quantitative measurements (such as surface area) extremely challenging. Also, other compounds such as Calcium Hydroxide ($Ca(OH)_2$) coexist with the C-S-H gel. Hence, it is very difficult to separate $Ca(OH)_2$ from C-S-H gel. In addition, C-S-H has no fixed stoichiometry, the chemical composition of C-S-H gel changes from point to point within cement paste and hence, C-S-H gel is often defined by its Calcium-Silica (Ca/Si) ratio [8]. Experimental techniques such as Scanning Electron Microscopy (SEM) and Transmission Electron Microscopy (TEM) found that Ca/Si ratio within C-S-H gel ranges from 0.6 to 2.0 [8].

Experiments are unable to give complete information about its atomic structure, hence; the atomic structure of C-S-H gel is not completely resolved. However, experiments have revealed that C-S-H gel has a layered structure, at short length scales (1 to 5) nanometers (10^{-9}m) and the layers stack to form compact domains in which the

distance between individual C-S-H layers is of the order of a few nanometers, i.e. the same order as the interlayer distance in a Tobermorite or Jennite crystals [7]. At larger length scales (5 to 100) nanometers, these ordered stacks form three dimensional structures called C-S-H particles. Transmission Electron Microscopy (TEM) revealed that the actual C-S-H particle is disk shape and has a thickness of 5 nanometers with the long axis in the 60 nanometer range. During hydration these C-S-H particles multiply and aggregate to form low-density and high-density C-S-H gel at the micro length scale (10^{-6}m) [9].

Nano indentation experiments have revealed mechanical properties (stiffness [elastic modulus] and hardness) of C-S-H gel at the micro length scales. These studies revealed that the two forms of C-S-H gel (low density and high density C-S-H gel) exhibit different mechanical behaviors. High density C-S-H gel has a higher stiffness and hardness values than low density C-S-H gel. The proportion of high and low density C-S-H in cement paste depends on the mix design of cement paste, however, the stiffness and hardness of low density and high density C-S-H do not change from one cement-paste to another. The stiffness and hardness values are intrinsic properties of the C-S-H gel [10].

1.4 Research Need

Progress in understanding and quantifying structure-property relationships for concrete has been difficult because C-S-H gel is extraordinary difficult to characterize. However, novel characterization techniques such as nano indentation and small –angle neutron scattering have provided new information about the C-S-H gel, and this has lead the development of several models of the nanostructure of C-S-H gel. Jennings [11] developed a colloidal model of C-S-H that rationalizes numerous experimental observations, including surface area measured by different techniques and density. The colloidal model describes the structure of C-S-H gel at length scales (5 to 100) nanometers. According to the model, a key feature of the structure of C-S-H is the presence of regions of different density that arise due to packing densities of the same fundamental unit [12]. As the packing density increases, the number of contacts between the particles increases [13-14]. Therefore, the HD C-S-H will have higher stiffness and

hardness compared to LD C-S-H since the greater number of contact points in H-D C-S-H favors a more stabilized structure. However, the model does not quantify the strength of the bond between C-S-H particles. Experiments such Atomic Force Microscope are now being used to measure the pressure between C-S-H particles [5]. A computational approach is needed to determine the strength and nature of the bond between C-S-H particles and determine ways to improve the bond. These proceedings will ultimately lead to determining a structure of C-S-H gel that has improved cohesive properties. As a start, it is necessary to determine the structure and properties of C-S-H at length scales (1 to 5) nanometers.

1.5 Importance of Molecular Modeling

Molecular modeling (molecular statics and molecular dynamics) is a tool that can be effectively used to investigate the mechanical properties, structure, energy potentials, behavior of cement based materials at the atomic level.

A computational model can reduce the number of time consuming laboratory experiments required for testing and hence it saves a lot of time and money. Advances will only be possible if experimental and computational results support each other. In this way computational modeling will aid researchers in explaining experiments. Any findings that bring the structure into contact with the mechanical properties of cement paste may modify the actual view of the gel.

1.6 Research Objectives

The main objective of this project is to determine the atomic structure of C-S-H. Knowing the atomic structure one can manipulate this structure and improve the mechanical properties of cement based materials. To achieve this objective the following procedures are followed:

1. Consider different possible atomic structures of C-S-H and compute mechanical properties (Bulk modulus, Shear Modulus, Elastic Modulus and Poison Ratio) of those C-S-H structures using molecular mechanics and compare results with macro level experimental properties.

a. The atomic structures considered are (1) crystalline calcium silicate hydrates (Tobermorite, Jennite and Foshagite minerals) and (2) crystalline calcium silicate hydrates with bonds broken

2. Using these studies as a base, propose a possible C-S-H atomic structure for further modifications or further studies.
3. Apply uniaxial strain rate to the atomic structure of C-S-H using molecular dynamics and determine the strength of the C-S-H structure.

CHAPTER 2: LITERATURE REVIEW

2.1 Hydration of Cement

Cement is a complex mixture of numerous compounds. The major compounds found in cement are Tricalcium Silicate (C_3S), Dicalcium Silicate (C_2S), Tricalcium Aluminate (C_3A), Tetra calcium Aluminoferrite (C_4AF) and gypsum [16]. Tricalcium Silicate produces C-S-H gel and Calcium Hydroxide at the early stage of hydration while Dicalcium Silicate produces C-S-H gel and Calcium Hydroxide at a later stage in the hydration process [16]. The reaction is typically expressed as:

$2\ Ca_3SiO_5 + 7\ H_2O \longrightarrow 3\ CaO \cdot 2\ SiO_2 \cdot 4\ H_2O + 3\ Ca(OH)_2$

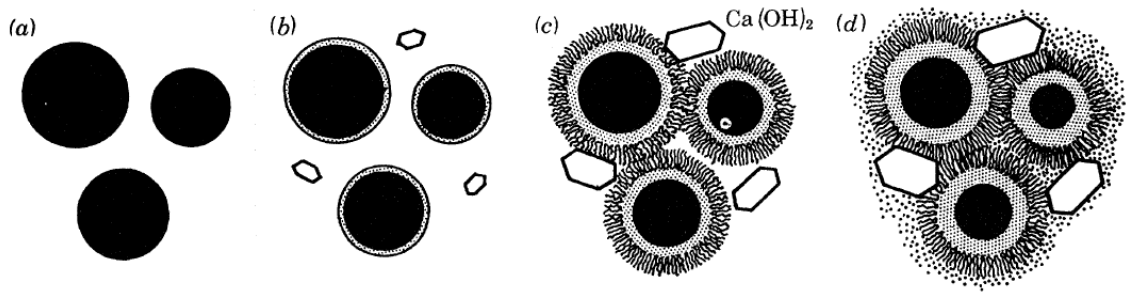

Figure 2.1 Sequence of Cement Hydration [17]. a) Cement particles in water b) Formation of C-S-H c) C-S-H growth around the cement grains d) Fully grown C-S-H and Calcium hydroxide

Figure 2.1 illustrates the sequence of cement hydration. The hydration process also consists of simultaneously occurring reactions of other anhydrous compounds with water, although the compounds do not hydrate at the same time. The aluminates are known to hydrate at a much faster rate and therefore stiffening and setting of cement pastes is generally attributed to aluminate minerals. The hardening of cement paste is attributable mainly to the silicate minerals. Hydration products formed during the

hydration of Aluminate (C_3A) and Tetra calcium Aluminoferrite (C_4AF) are Ettringite and Monosulfate. Ettringite is a hydrated Sulfoaluminate compound and is commonly formed in concrete during curing. Monosulfate is a related Sulfoaluminate compound. In cement nomenclature Ettringite is referred to as AFt and Monosulfate is called AFm.

2.2 Microstructure of Hardened Cement Paste

Hardened cement paste (HCP) microstructure is composed of a highly heterogeneous system of several kinds of solids and pores of various sizes and shape. The composition of mature cement paste is shown in Table 2.1, from which it can be seen that C-S-H gel, the principal hydration product, is the predominant solid volume in hardened cement paste. C-S-H gel has a poorly crystalline structure. There are two generic forms of C-S-H; low density C-S-H gel (outer product) and high density C-S-H gel (inner product). Another primary hydration product is calcium hydroxide ($CaOH_2$) which has a crystalline structure. There are also some minor components such as AFm and Aft phases (Ettringite and monosulphate) which are generally crystalline and vary considerably in morphology and size. Additionally, unhydrated cement particles may occupy the volume depending on the degree of hydration or water/cement (w/c) ratio.

Pores are also components of HCP microstructure. Two major classes of pores are recognized. The first class, gel pores, is conceived to be part of the C-S-H gel with characteristic diameters <10 nm. The second class of pores is the large capillary pores, which are on the order of 10 nm to 10 μm. Water not consumed in the hydration reaction will remain in the microstructure pore space (capillary pores). These pores make the concrete weaker due to the lack of strength-forming Calcium Silicate Hydrate bonds [18]

In addition there may be accidental or deliberately entrained air voids, and larger empty spaces where the pastes has not been properly consolidated. The total pore volume depends on the water/cement ratio, degree of hydration, curing condition etc. Figure 2.2 displays the microstructure of hardened cement paste.

Table 2. 1 Composition of Hardened Cement Paste (w/c = 0.5) [16]

Component	Approximate Volume (%)	Remarks
Calcium Silicate Hydrate(C-S-H)	50	Amorphous structure, includes gel pores
Calcium Hydroxide (CH)	12	Crystalline structure
AFm and Aft phases	13	Crystalline structure
Unreacted Cement particles	5	Depends on hydration
Capillary pores	20	Depends on the water-cement-ratio

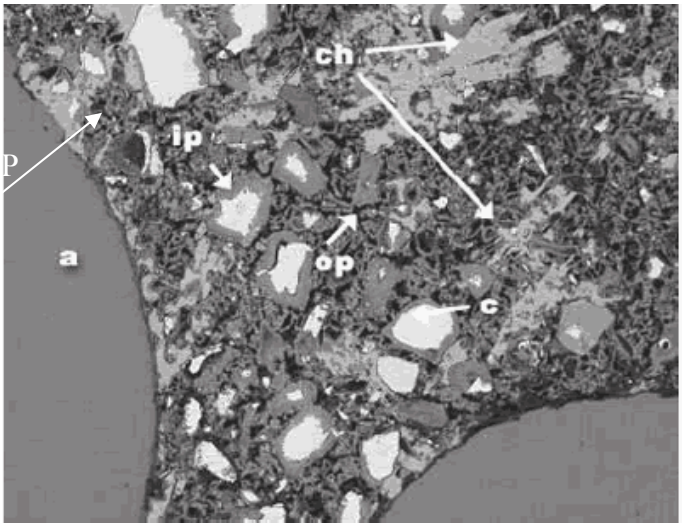

Figure 2.2 Microstructure of Hardened Cement Paste [19].

c = Unreacted cement grains, ip = Calcium Silicate Hydrate, inner product, op = Calcium Silicate Hydrate, outer product, ch = calcium hydroxide, p = capillary pores

2.3 Calcium Silicate Hydrate (C-S-H) Gel

C-S-H gel has high surface areas and shows excellent adhesive characteristics [20]. The dashes in the term C-S-H means no chemical composition implied.

C-S-H gel is primarily responsible for the strength and cohesion in cement based materials. The complex nature of concrete is attributable to the behavior of the C-S-H gels subjected to a) external loading as in the case of creep and b) changes in relative humidity during shrinkage- both of which critically affects the performance of concrete [21].

2.4 Understanding the Structure-Property Relationship in Cement Paste

The structure of hardened cement paste is fundamental to the understanding of the performance of cement paste. To understand the behavior and to predict the properties of cement paste, one has to understand the structure–property relationship. In addition, one has to identify and quantify the structural elements that affect the properties in cement paste.

Currently, theoretical understanding of how the properties and performance of cement-based materials relate to structure is complicated by the large range of length scales (from nanometer to millimeter). For example, in Figure 2.3, concrete at the scale of millimeters can be viewed as a composite mixture of aggregates and air voids embedded in cement paste matrix. At the scale of micrometers, the cement paste is comprised of unhydrated cement particles, hydration products (C-S-H gel and calcium hydroxide) and capillary porosity. Furthermore, the major hydration product of cement paste, Calcium Silicate Hydrate (C-S-H) gel is a porous material, being composed of nanometer-sized “particles” and pores [22].

A better theoretical understanding of these phases occurring at each of these length scales and how they react with other scales is still needed to increase the predictability of the performance of cement-based materials.

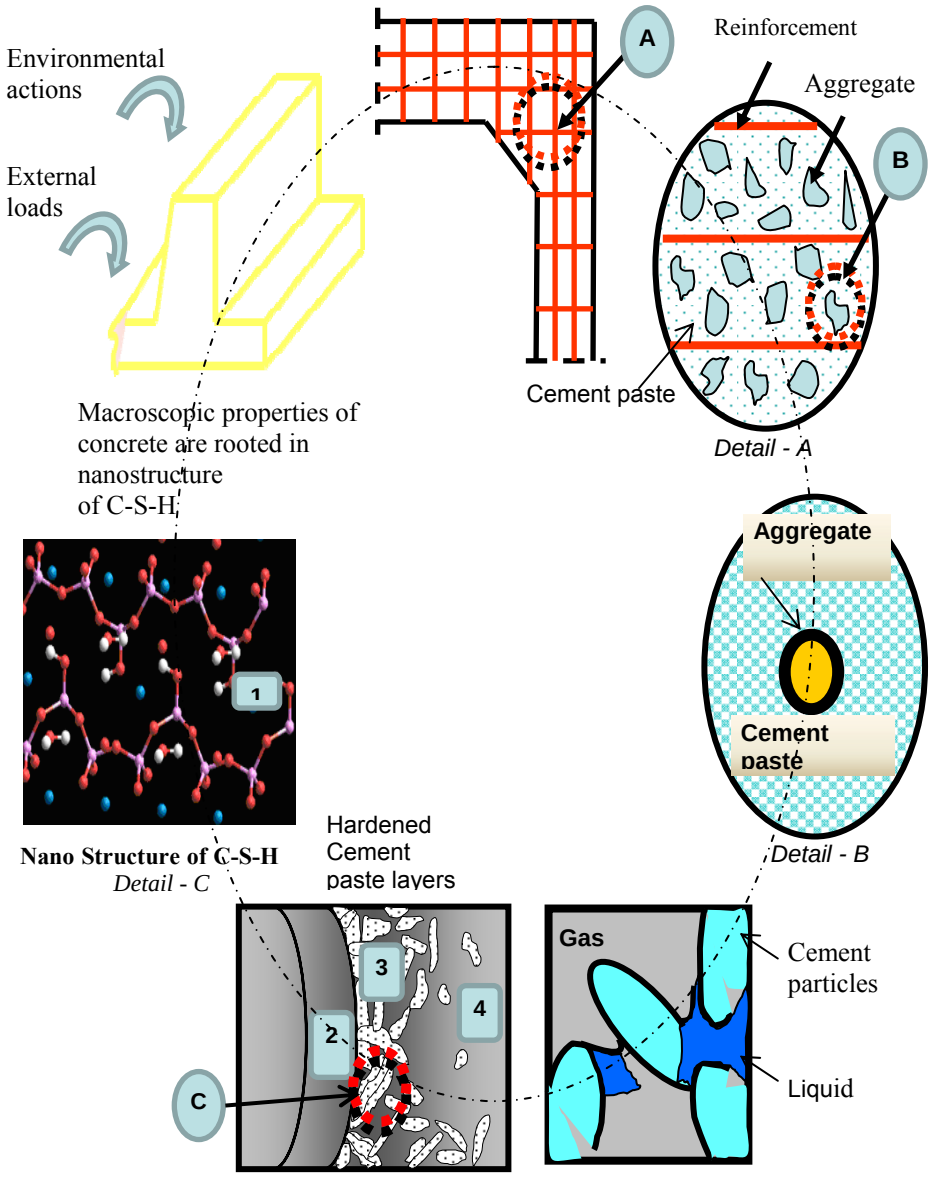

Figure 2.3 Complexity of Microstructure-Property Relationship [23].

2.5 Experimental Investigation of C-S-H Gel

Due to the importance of C-S-H gel in cement based materials, there have been numerous experimental studies of the structure and nature of C-S-H gel. Some techniques used to investigate the nanostructure for C-S-H gel are XRD, Scanning Electron Microscopy (SEM), Transmission Electron Microscopy (TEM) and Nanoindentation Studies.

2.5.1 XRD Studies of C-S-H Gel

XRD is a non destructive technique for characterizing crystalline materials. It provides information on structures, phases, preferred crystal orientations (texture) and other structural parameters such as average grain size, crystallinity, strain and crystal defects [24].

2.5.1.1 Atomic Structure of a Perfect Crystal versus Atomic Structure of C-S-H Gel

In crystalline materials such as copper, silicon, table salt etc., the atoms are arranged in an orderly and unique fashion called Bravais lattices. A crystal is made up of several small identical volume elements called unit cells. A unit cell is a tiny box containing atoms in a particular arrangement. The unit cells are repeated and stacked periodically in three dimensional spaceS to form a bulk crystal (Figure 2.4 (a)). A unit cell is defined by lattice parameters such as length of the sides and angles between their axes as shown in Figure 2.4(b). The positions of the atoms within the unit cell are given by the x, y, z coordinates gauged from a reference point in the lattice [15].

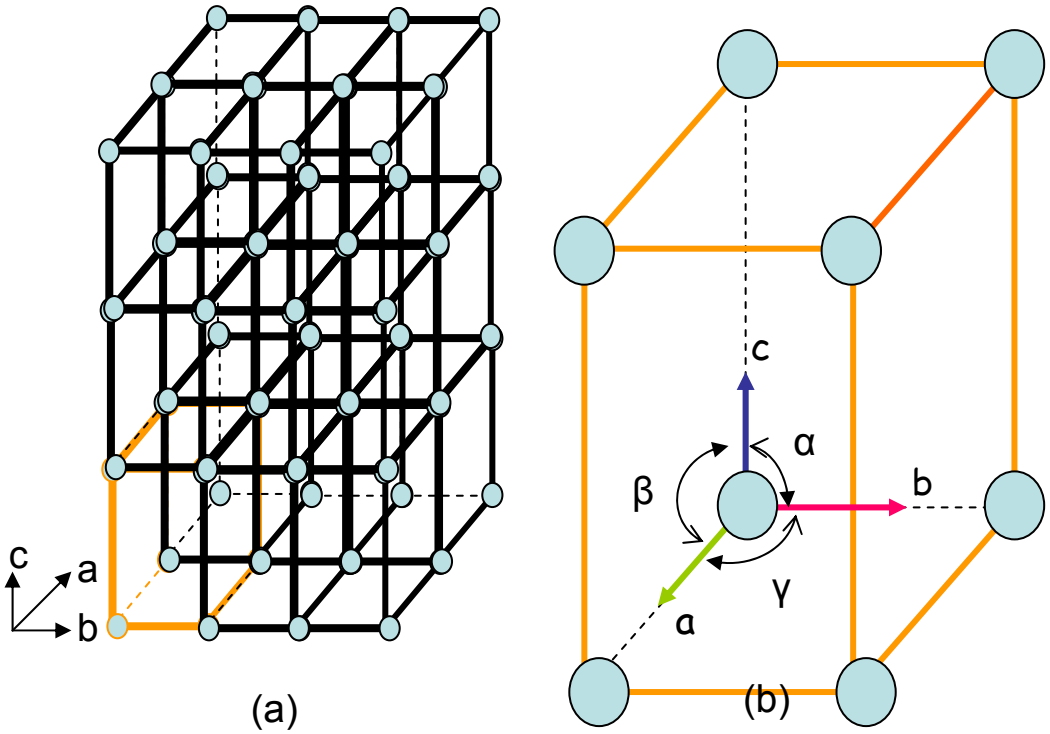

Figure 2.4 Illustrations of Crystal (a) and Unit Cell (b) [15].

Figure 2.5 shows the classification of the crystal systems. The crystal systems can be classified into seven different point groups based on symmetry namely Triclinic, Monoclinic, Hexagonal, Rhombohedral, Orthorhombic, Tetragonal and Cubic.

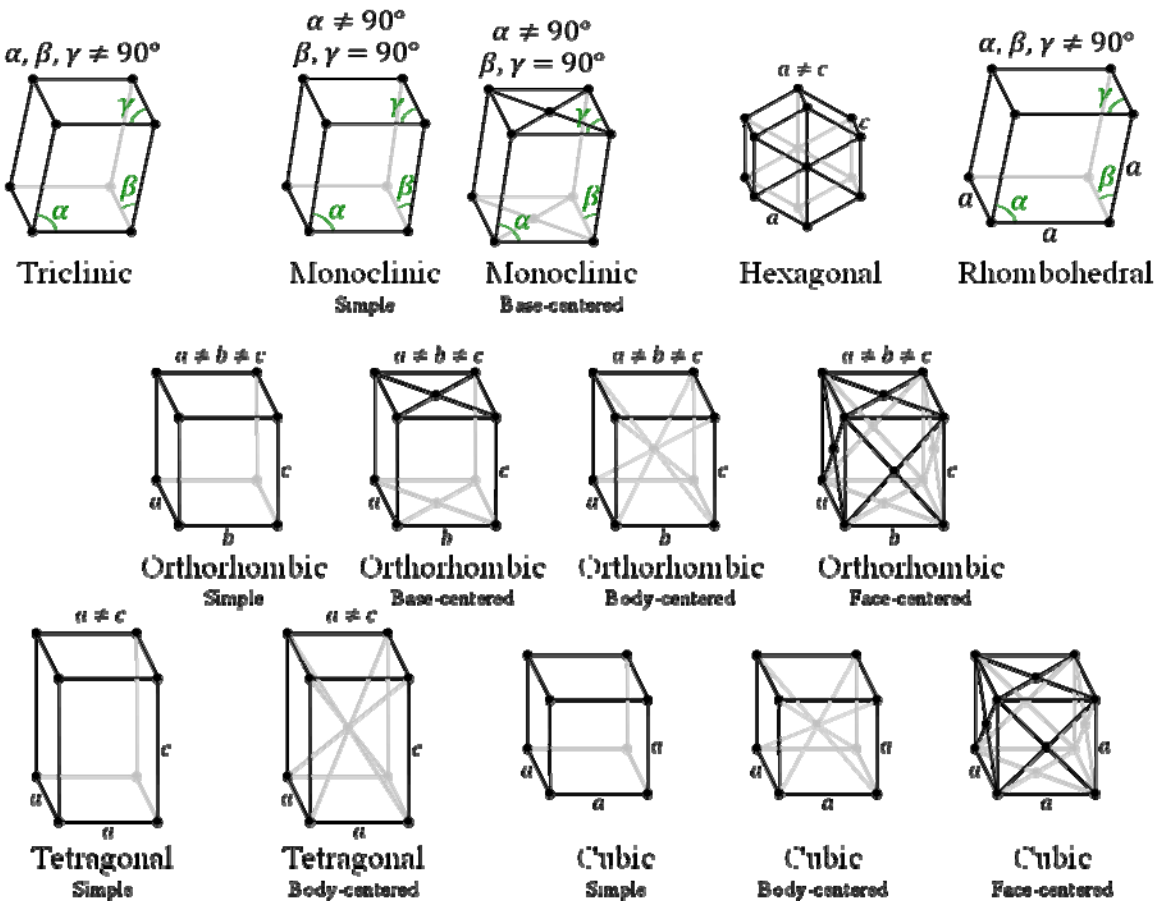

Figure 2.5 Classifications of Crystal Systems – 14 Bravais Lattices [25].

Solid crystals may also be classified based on the nature of their atomic bonds viz.: a) Ionic Crystal b) Covalent Crystal c) Molecular Crystal d) Metallic Crystal. A crystal can be distinguished from an amorphous solid by its order and disorder over longer distances [15].

XRD patterns of C-S-H gel suggested that no long range order exist in their structures. The diffraction peaks or the peak intensities for perfect crystals are narrow and sharp. For imperfect crystals or amorphous materials, the peaks are broadened. In case of liquids, it will be a continuous and gradually varying function [15]. Figure 2.6 shows the XRD pattern of the cement pastes. C-S-H gel is amorphous in nature while $Ca(OH_2)$ is a crystalline substance. The sharper and narrow peaks in Figure 2.6 are those that are due to the presence of $Ca(OH_2)$ in the cement pastes. Apart from the $CaOH_2$ peaks, there are

only few other noticeable peaks in the XRD pattern. The peaks observed at 2.79 - 3.04 A° and at 1.82 A° are the only ones attributable to the C-S-H gel in the cement paste. Also, note that the C-S-H peaks are much broader compared to CH peaks. Therefore, the cement paste as a whole cannot be treated as a crystalline substance. [15]

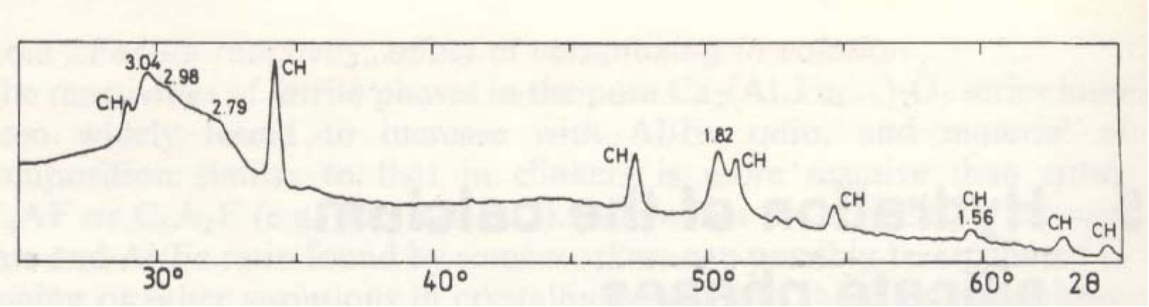

Figure 2.6 X-Ray Diffraction Patterns of Cement Pastes [26].

Since C-S-H gel is amorphous, the X-ray diffraction techniques could not give complete information about its atomic structure. However, experiments have revealed that C-S-H gel has a layered structure, at short length scales (1 to 5) nanometers and the layers stack to form compact domains in which the distance between individual C-S-H layers is of the order of a few nanometers, i.e. the same order as the interlayer distance in a Tobermorite or Jennite crystals [7]. These are crystalline calcium silicate hydrates.

Crystalline calcium silicate hydrate is primarily composed of tetrahedral chains of silica that run between layers of calcium atoms and water molecules. These tetrahedral chains of silica are infinite. However there is still a debate about the short range ordering of silicate chains in C-S-H gel. Figure 2.7 shows a typical silica tetrahedron and Figure 2.8 illustrates silicate chains, interlayer calcium atoms and water molecules. Figure 2.9 illustrates a C-S-H layer. At larger length scales (5 to 100) nanometers ordered stacks of C-S-H layers form three dimensional structures called C-S-H particles.

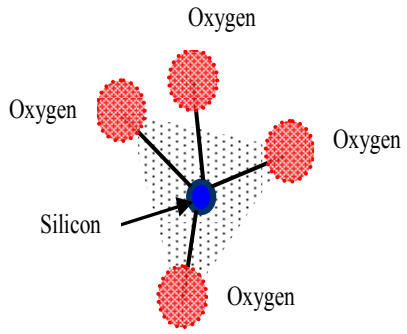

Figure 2.7 Typical Silica Tetrahedron [27].

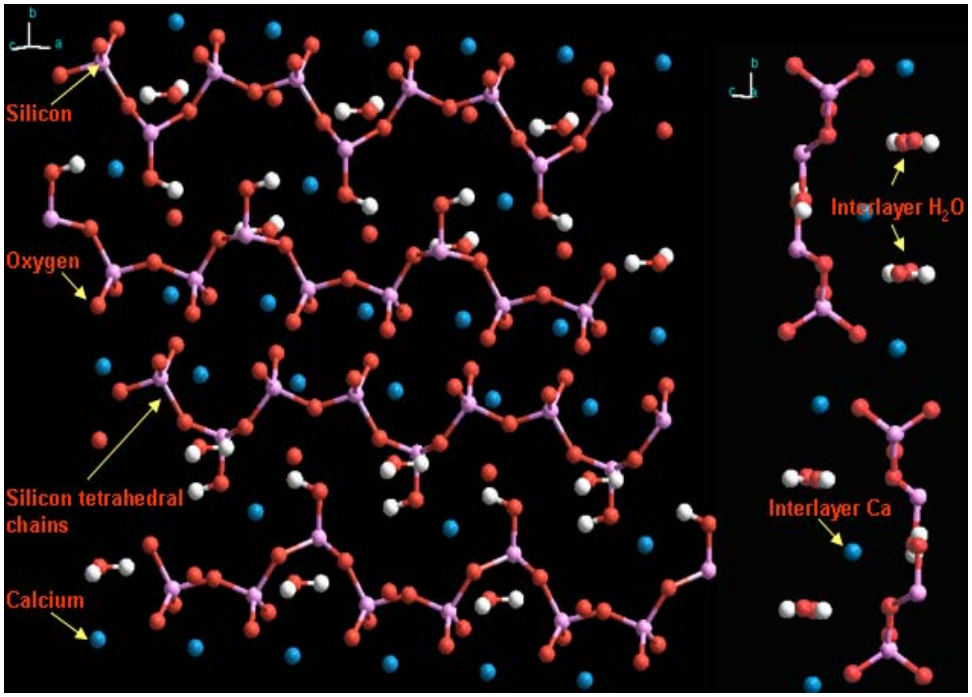

Figure 2.8 Illustration of Tetrahedral Silicate Chains, Inter Layer Calcium Atoms and Water Molecules [15].

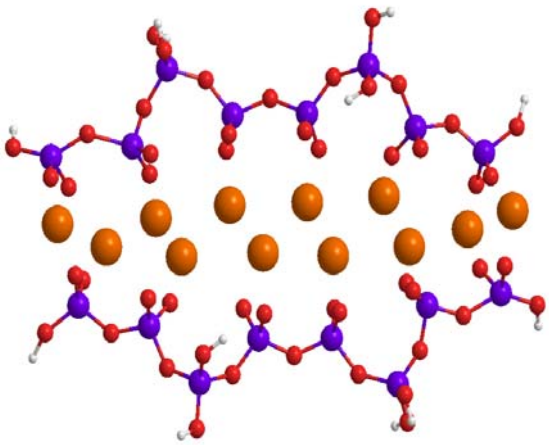

Figure 2.9 C-S-H layer (lamella) [28].
Orange Atom = Calcium, Purple Atom = Silicon,
Red Atom = Oxygen and White Atom =
Hydrogen.

Plassard et al [5] reported that sometimes a bridging silicon tetrahedron might be missing in the silicate chains of C-S-H gel, in which case it may form dimmers and pentamers. A dimmer is formed when a bridging silica tetrahedron is missed at intervals of every two silica tetrahedra. Figure 2.10 shows the dimmer silicate chain. Similarly, when a bridging silica tetrahedron is missed at intervals of every five silica tetrahedra it forms pentamer silicate chains. Figure 2.11 shows the pentamer silicate chains as well as a bridging silicon tetrahedron.

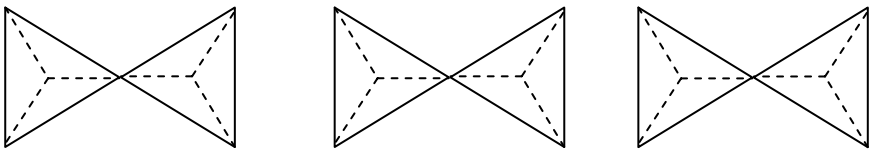

Figure 2.10 Dimmer Silicate Chains [15].

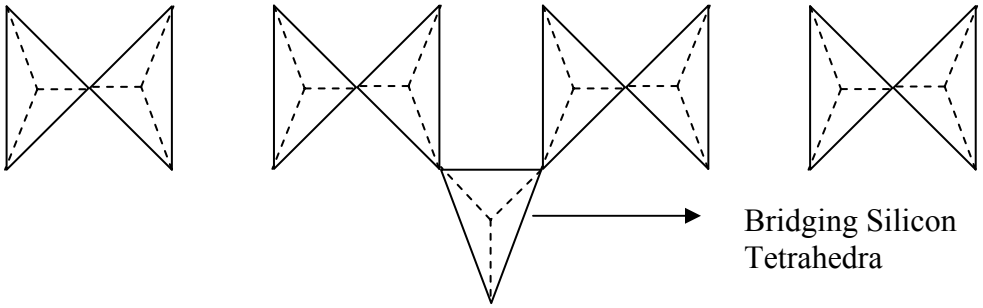

Figure 2.11 Pentamer Silicate Chains [15].

2.5.2 Transmission Electron Microscopy (TEM) Studies of C-S-H Gel

Transmission Electron Microscopy experiments are used to determine the chemical composition of the main hydration product. Transmission Electron Microscopy (TEM) revealed that the actual C-S-H particle is disk shape and has a thickness of 5 nanometers with the long axis in the 60 nanometer range. During hydration these C-S-H particles multiply and aggregate to form low-density and high-density C-S-H gel at the micro length scale (10^{-6}m) [9].

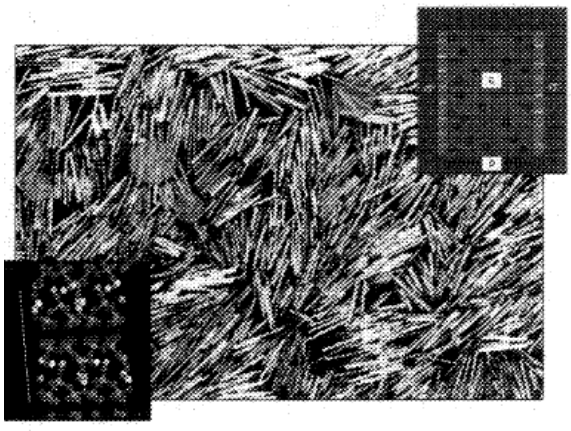

Figure 2.12 TEM Micrograph of HD C-S-H in hardened cement paste [29].

I.G.Richardson et al [30] also performed extensive TEM studies on hardened cement paste of various ages. In their studies they found that the inner and outer product differed in morphology but not substantially in the Ca/Si ratio. The TEM analysis indicates no

systematic variation in C-S-H composition with age; they found that the Ca-Si ratio ranges from 0.6 to 2.0.

They also found that the inner C-S-H gel product contained small amounts of Aft, Afm, a magnesium rich phase and Calcium Hydroxide. Figure 2.13 shows TEM micrographs of inner and outer C-S-H gel products.

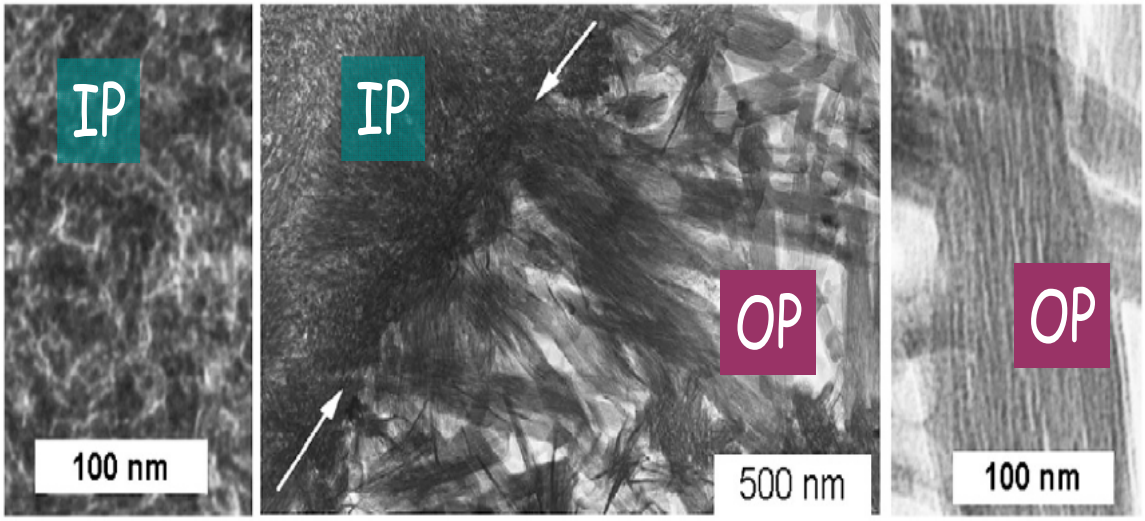

IP = Inner Product – High Density C-S-H

OP = Outer Product –Low Density C-S-H

Figure 2.13 TEM Micrographs of Inner and Outer Product of C-S-H [30].

2.5.3 Scanning Electron Microscopy (SEM) Studies of C-S-H Gel

The Scanning Electron Microscope (SEM) is a type of electron microscope that images the sample surface by scanning it with a high-energy beam of electrons in a raster scan pattern. The electrons interact with the atoms that make up the sample producing signals that contain information about the sample's surface topography, composition and other properties such as electrical conductivity.

Walsh et al.[31] performed a detailed scanning electron study with respect to the fracture surface of Portland cement hydrated for various times. It was shown that after one day, the individual calcium silicate grain is covered with dense spherulite network of Calcium Silicate Hydrate fibers, radiating out from the initial unhydrated particles.

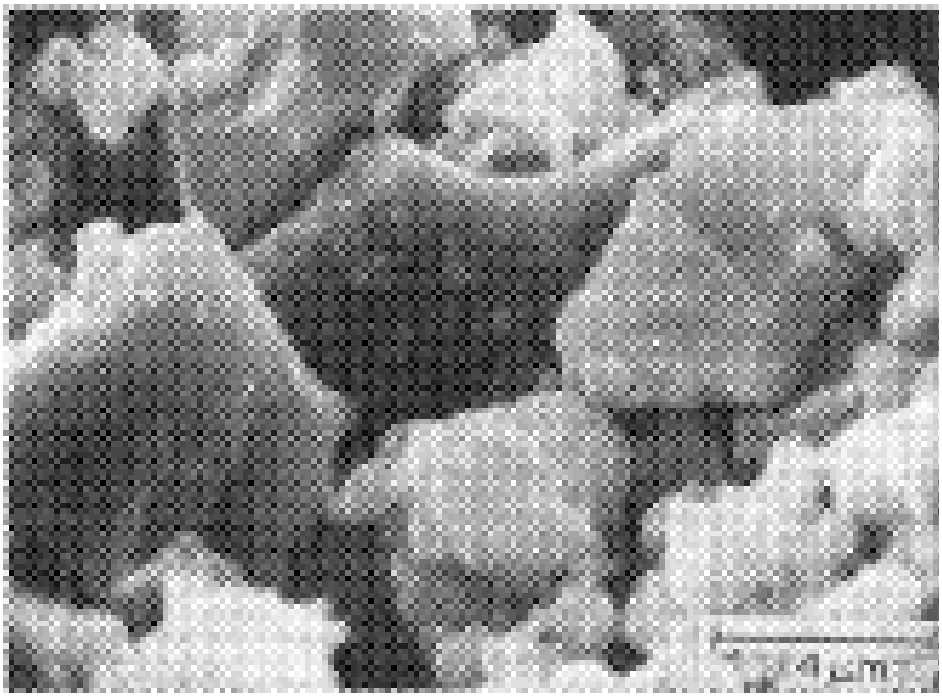

Figure 2.14 Scanning Electron Micrograph of the Fracture Surface of Portland cement after 1 Hour Hydration[31].

Figure 2.14 shows a scanning electron micrograph of the fracture surface of Portland cement after 1 hour hydration. The fracture surface is seen to be entirely intergranular in nature, consisting essentially of the unbounded grain which comprises the cement powder. The fracture surface is continuously changing throughout the hydration process.

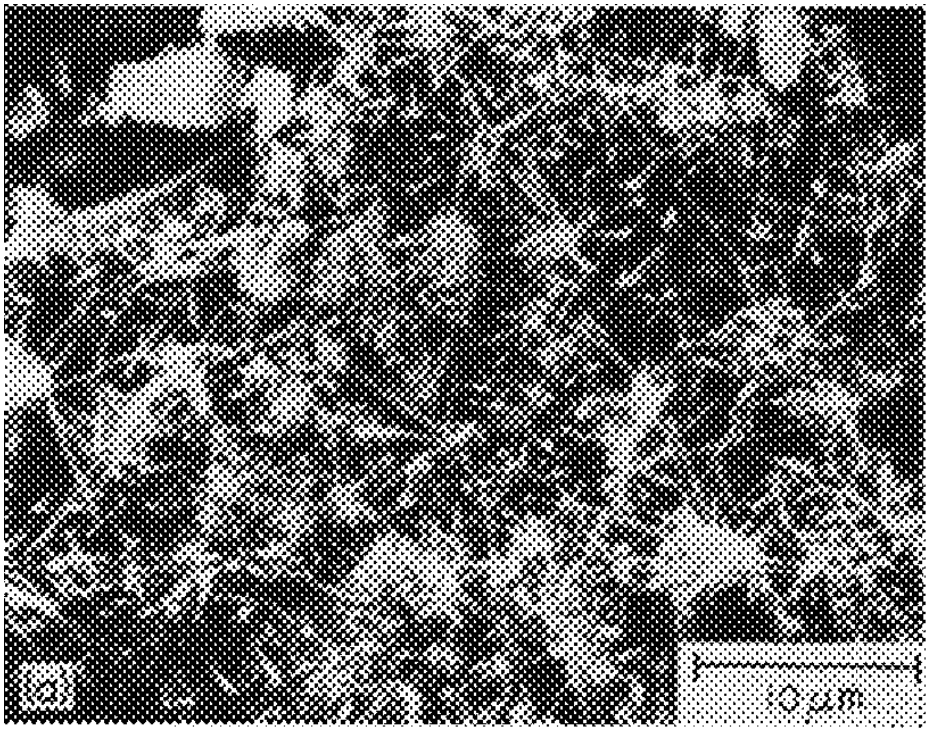

Figure 2.15 Scanning Electron Micrograph of the Fracture Surface of Portland cement after 24 Hours Hydration [31].

Figure 2.15 shows scanning electron micrograph of the fracture surface of Portland cement after 24 hours hydration showing the network of fibers. The morphology of the fibers is shown in more detail in the higher magnification micrograph in Figure 2.16. They are seen to be in the order of 100 nm in diameter and quite long as compared to this diameter. The fibers are seen to have geometrical cross section which can sometimes be identified as a square. In many other cases, the fibers are seen to bend and form bonded junctions with one another at their crossing points.

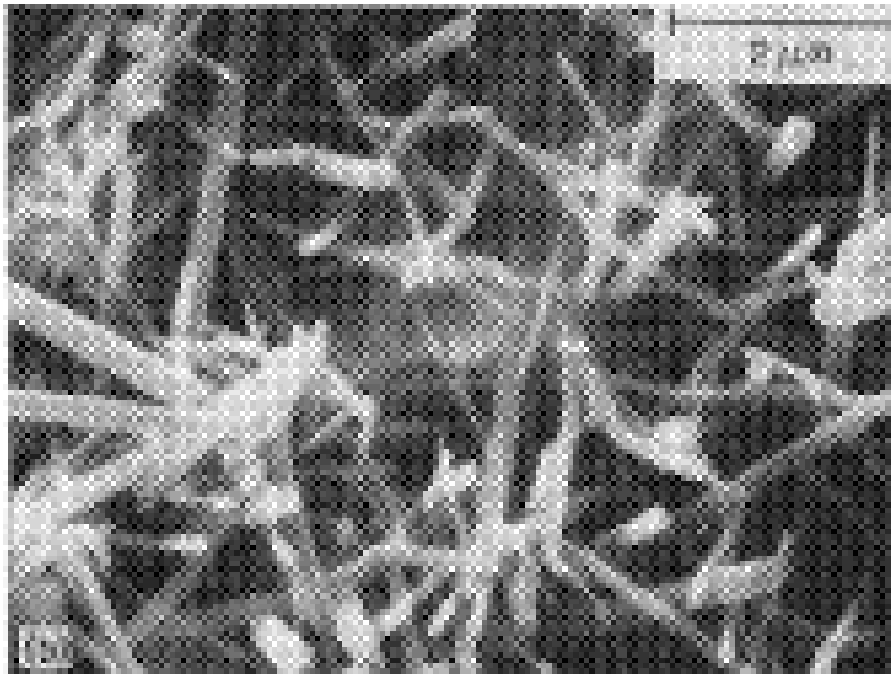

Figure 2.16 Higher Magnification of the Fibres[31].

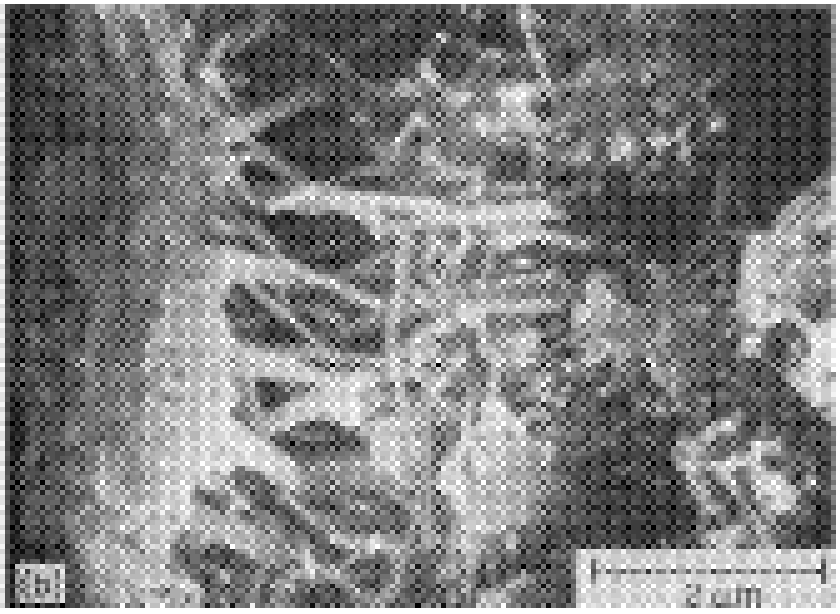

Figure 2.17 Scanning Electron Micrograph of the Fracture Surface of a Portland cement Paste after 21 days[31].

After 21 days, fibers from the neighboring spherulites bond with each other. In addition, large plate-like crystals of calcium hydroxide are found between the sperulites. The SEM micrographs of C-S-H do not show any specific crystalline form. Figure 2.17, scanning electron micrograph of the fracture surface of a Portland cement paste after 21 days, shows the inner growth of Calcium Silicate Hydrate fibres from adjacent sperulites.

2.5.4 Nanoindentation Studies of C-S-H Gel

Nano-indentation tests measure hardness and elastic modulus of materials by indenting on small volumes using very small, on the order of 1 nano-Newton, indentation forces and measuring the depth of the indention. These tests are based on new technology that allows precise measurement and control of the indenting forces and precise measurement of the indentation depths. By measuring the depth of the indentation, progressive levels of forcing are measurable on the same piece.

Nanoindentation experiments of Constantines et al [10] revealed that there are two phases of C-S-H gel, which exhibit dissimilar mechanical properties. The two phases of C-S-H gel are Low Density (LD) C-S-H gel and High Density (HD) C-S-H gel. The nanoindentation results suggested that the elastic property is an intrinsic material property that does not depend on the mix proportions of cement based materials. The elastic properties for LD C-S-H and HD C-S-H were found to be between 21.4 and 29.4 GPa respectively. Acker [32] performed microindentation experiments on C-S-H phases and determined the elastic modulus for a C-S-H structure with a Ca/Si ratio <1 is 20 GPa and C-S-H structure with Ca/Si ratio >1 is 31.4 GPa. The hardness was determined as 0.8 and 0.9 GPa respectively. Plassard et.al [6] carried out nanoindentation hardness measurements on synthetic Tobermorite crystals and reported the Young's modulus values to be 151 GPa.

2.6 Models of the Structure of C-S-H Gel

C-S-H gel has been intensively characterized by techniques such as SEM, TEM, XRD, NMR, etc, however the complex and poorly organized nanostructure of the C-S-H gel has not been completely elucidated. SEM can only resolve the structure of C-S-H gel at the micrometer level. This means that there is no hard evidence of any specific structure of

C-S-H gel at the nanometer scale. Nevertheless certain structural features are already recognized. For instance, C-S-H gel is comprised of silicate chains held together by calcium oxide layer. In fact, several models have been proposed, which represent the nanostructure of C-S-H gel. The Powers-Brunauer model is historically the first model of the structure of C-S-H gel at the nano level [33]. This model is based on indirect tests such as adsorption measurements and porosimetry. These indirect tests give no information as to how the pores are arranged in C-S-H gel; thus conclusions about the pore and nano structure of C-S-H gel have been drawn by inference. Feldman and Sereda[33] made several modifications to Powers and Bruner model of the nanostructure of C-S-H. One modification made is the assumption of a layered structure of the C-S-H gel having pores as spaces between the C-S-H layers as shown in Figure 2.16 b. Another modification is the assumption concerning a special form of water, interlayer water present in C-S-H gel. It is assumed generally that the major portion of volume change of concrete, such as shrinkage and creep, is a result of the loss of interlayer space. These models are capable of simulating, at least qualitatively, the observed strength, deformability, volume changes, permeability, and durability characteristics of hardened paste and concretes. However theses models cannot quantitatively characterize properties of C-S-H gel.

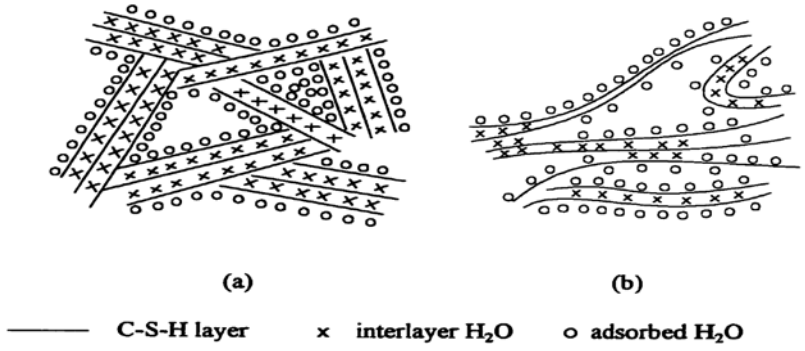

Figure 2.16 (a) Colloidal- particle Model of C-S-H (Powers-Brunauer Model) (b) Extended Sheet Model of C-S-H (Feldman- Serada Model)[33].

2.6.1 Crystalline Models of the Structure of C-S-H Gel

As mentioned above, the atomic structure of C-S-H gel is believed to be similar to crystalline calcium silicate hydrate structures such as Tobermorite, Jennite, Clinotobermorite, Foshagite etc. In Tobermorite, the Si-O chains are linked together in a fashion that repeat at intervals of three tetrahedra and forms a type of chain known as Dreierketten. Tobermorite and Jennite are layered crystalline minerals that have infinite chains of silicon tetrahedral which run between layers of calcium atoms. Two widely used crystalline C-S-H models are Tobermorite 11 A °(Hamid's [34] and Merlino et.al [35] and Jennite (Merlino et.al [36]) ,these models are shown in Figure 2.17. Tobermorite has a monoclinic lattice structure and it is available in three different (layer) thicknesses, namely 14, 11, 9 A°.

The layer between the top and bottom Calcium layer (also known as interlayer) is called "labile". The interlayer is filled up as the Ca/Si ratio increases. The chemical composition of Tobermorite for various Ca/Si ratios can be written as follows:

Ca4 [Si6O14 (OH) 4].2H2O, Ca/Si =0.667 (no Ca atoms in labile layers)

Ca5 [Si6O16 (OH) 2].2H2O, Ca/Si =0.83, [either Ca (5) or Ca (6) is present]

Ca6 [Si6O18].2H2O, Ca/Si = 1.0 [both Ca (5) and Ca (6) are present]

The main difference between Hamid's [34] and Merlino's [35] Tobermorite model is the bonding scheme in the silica chains. In Merlino's model, the silicon tetrahedra are bonded between interlayers.

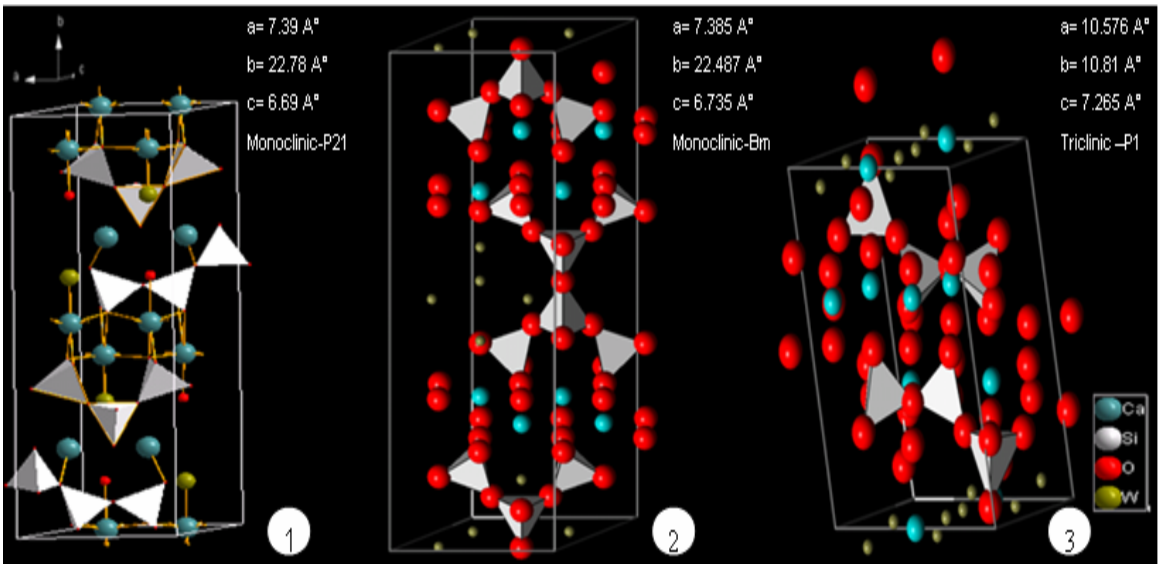

Figure 2.17 Atomic Configuration of Three Mineral Structures: 1) Tobermorite (11 A°) - Hamid [34] 2) Tobermorite - (11 A°) -Merlino [35] 3) Jennite- Merlino [36].

Analogies to Tobermorite and Jennite have also led to a deeper understanding of the atomic structure of C-S-H, including the observed Ca/Si and the chain length of the silicates. The structural models have generally focused on chemical and physical changes in the structure of the interlayer space (space between silicate chains and calcium oxide layer). The “interlayer spaces" in the C-S-H gel contain water that is removed on drying and re-enters on rewetting, causing shrinkage and swelling. These structural models have been fairly successful at qualitatively explaining the shrinkage behavior and gas sorption properties of cement paste

2.6.2 Colloidal Model of the Structure of C-S-H Gel

As shown above there are quite a few studies devoted to understanding the atomic structure of C-S-H, considering it as a layered structure similar to Tobermorite and Jennite. However, the relationship between structure and mechanical behavior of cement paste still remains a great challenge. Jennings [11] developed a colloidal model to study the relationship between morphology and mechanical properties of C-S-H.

The colloidal structure of C-S-H is shown in Figure 2.18. The basic building blocks flock together to form a cluster of globules and these globules form the C-S-H gel. Based on the packing density of these globule clusters, Jennings model shows the two types of C-S-H: Low Density (LD) C-S-H and High Density (HD) C-S-H gel. Figure 2.19 shows the colloidal model for HD and LD C-S-H.

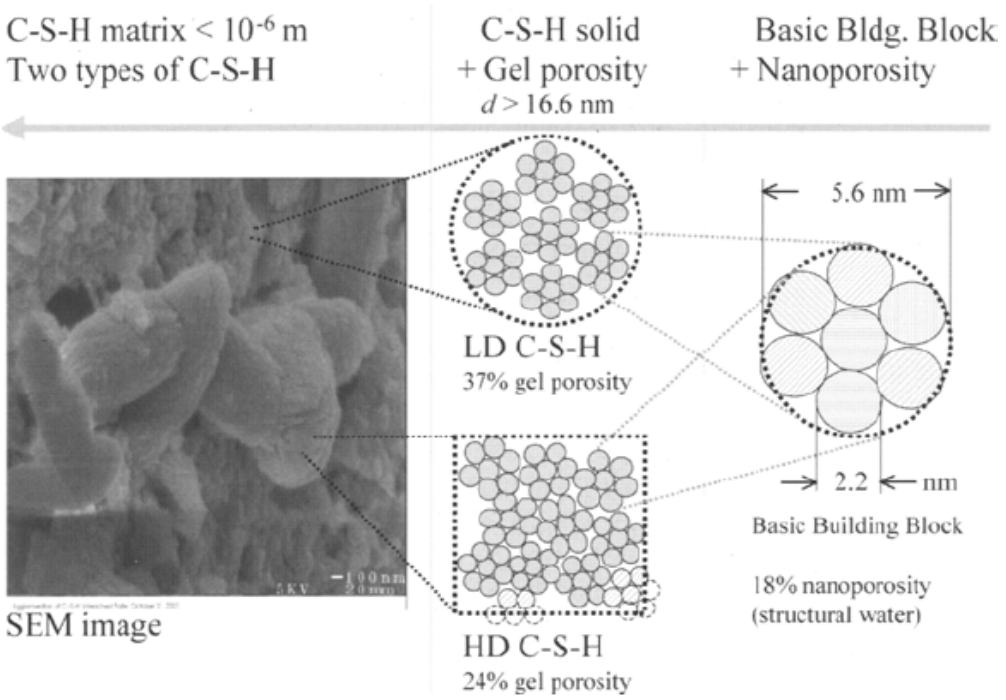

Figure 2.18 Colloidal Structure of C-S-H [11].

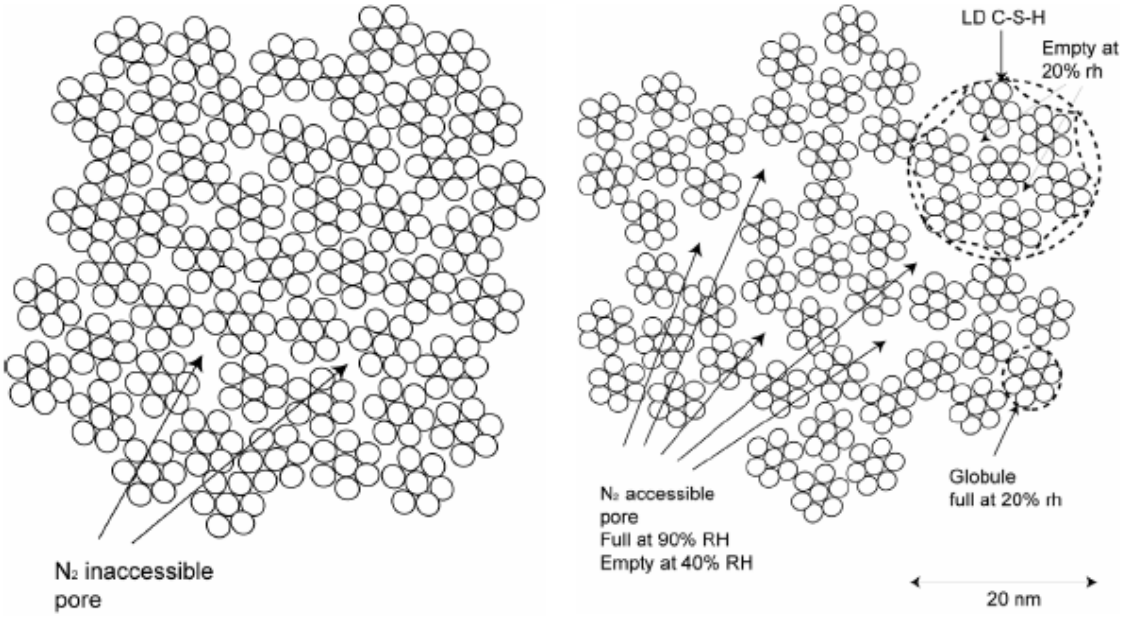

Figure 2.19 HD and LD C-S-H [11].

As the packing density increases, the number of contacts between the particles increases [13-14]). Therefore, the HD C-S-H will have higher stiffness and hardness compared to LD C-S-H since the greater number of contact points in H-D C-S-H favors a more stabilized structure.

According to Jennings, the basic building block is assumed to be roughly spherical and approximately 2 nm across with a specific surface area of about 1000 m^2/g. These building blocks flocculate to form larger units of C-S-H. According to Jennings and Tennis, these basic building blocks are comparable to a unit cell of a crystalline Calcium Silicate Hydrate. The diameter of a spherical unit is 2.2nm, which corresponds to the largest lattice dimension of Tobermorite unit cell (c=2.2nm).

In addition porosity of a globule of C-S-H (LD or HD) is 18%. This porosity is an intrinsic property of C-S-H solid phase and can be associated as nanoporosity filled with structural water. The C-S-H globule has been found to be of a characteristic size of 5.6 nanometer. Above this scale, there is a second type of porosity, the gel porosity, which is found to be different from one C-S-H to another (LD or HD). The C-S-H globules together with gel porosity form different types of C-S-H (LD or HD). These combined

phases are roughly larger than 16.6 nm. The difference between the two types of C-S-H relates to the gel porosity of roughly 24% for HD C-S-H, and 37% for LD C-S-H.

2.7 Computational Studies of C-S-H Gel

Molecular Dynamic has been used in recent years to simulate the structure of calcium silicate hydrates (C-S-H). Faucon et. al [37-38] used molecular dynamics to simulate the structure of calcium silicate hydrates having Ca/Si ratios between 0.66 and 0.83. This simulation was done to identify structural instability and to understand the mechanisms causing breaks in the Si-O chains. According to nuclear magnetic resonance (NMR) tests tetrahedral chains in the C-S-H atomic structure (with Ca/Si between 0.66 and 0.83) move closer together in the absence of labile calcium. This proximity may lead to bridging between the chains. In addition, when there is increase in the amount of labile calcium, there is partial rupture of the Si-O chains. In other words as Ca/Si ratio increases in the CSH, brakes occur in the silicate chains. These chains are of infinite length in crystalline calcium silicate hydrate.

Dolado et al. [39] studied the formation and the structure of C-S-H by means of molecular dynamics simulation of the polymerization of silicic acids ($Si(OH)_4$) in the presence of solvated calcium ions ($Ca(OH)_2$ $4H_2O$). The structure was studied to determine whether the nanostructure of C-S-H gel favors Tobermorite crystals or Jennite crystals. Tobermorite has mostly Si-OH bonds whereas Jennite crystal has mostly Ca-OH bonds. They determined that the concentration of Si-OH bonds in the C-S-H gel decreases with an increase of the Ca/Si ratio whereas the number of Ca-OH bonds increases in increasing Ca/Si ratio.

Gmira et al [40] made the first attempt to calculate the bulk properties of a C-S-H mineral Tobermorite. The Bulk Modulus and Young's Modulus determined using energy minimization studies was reported to be 71.8 GPa and 17 GPa respectively. Manzano [41] also performed energy minimization studies to calculate the key mechanical properties of cement-based materials using different crystalline C-S-H models. Their calculation showed that the bulk (K), shear (G) and Young's Modulus (E) decrease slightly when Ca/Si of C-S-H increases and when more water molecules enter into the composition of C-S-H. In addition, they found that the mechanical properties of C-S-H

structures with dimer or pentamer silicate chains were lower than the mechanical properties for C-S-H with infinite silicate chains. They also showed that their results were in good agreement when they include gel porosity.

Pellenq [9] reported a maximum cohesion pressure (tensile strength) of 5,000 MPa between C-S-H lamella (layers) structures in C-S-H units using Ab Inito modeling techniques.

CHAPTER 3: INTRODUCTION TO MOLECULAR MODELING

3.1 Introduction

Molecular modeling is defined as the use of computational techniques to construct molecules and perform a variety of calculations on these molecules in order to predict their chemical characteristics and behavior [42]. Molecular modeling allow users to determine three fundamental items about an individual molecule or system of molecules: its chemical structure (number and type of atoms, bonds, bond lengths, angles, and dihedral angles); its properties (basic characteristics of the molecule, such as its molecular energy, enthalpy, and vibrational frequencies); and its activity (those characteristics that describe how the molecule behaves in the presence of other molecules, such as its nucleophilicity, electrophilicity, and electrostatic potentials). These determinations can validate experimental studies or be carried out to predict experimental results [42].

3.2 Techniques of Molecular Modeling

There are a number of techniques employed in molecular modeling. However, for the purpose of this work, two methods will be discussed: molecular statics and molecular dynamics.

3.2.1 Molecular Statics (MS)

This method uses traditional classical mechanics to model molecular systems. Classical mechanics is used to describe the motion of macroscopic objects according to Newton's second law. In MS, atoms are considered to be spheres that are connected to other atoms by springs. The springs are considered as bonds. Various properties of the molecule can be calculated by measuring the motion of atoms and the changing energies in the springs. Molecular statics is well suited for providing excellent information such as bond distances, angles, and the most stable configuration of a molecule. Determining the most stable configuration of atoms is called 'energy minimizations'. Energy minimization is often used before any other calculation is performed [43].

3.2.1.1 Energy Minimization

As mentioned above, energy minimization is the process of determining the most stable configuration of molecules. The most stable configuration of a molecular system should correspond to a local minimum energy. The energy surface of a molecular system (Figure 3.1) may have multiple minima. Each point on the energy surface of a molecular system corresponds to a local atomic configuration of the molecules in that system. The objective of energy minimization is to find the local minimum energy in which the corresponding atomic configuration is closest to the initial atomic configuration. This is done to insure that the molecule or system of molecules is in its lowest energy state so that the calculated results can be compared with experiments.

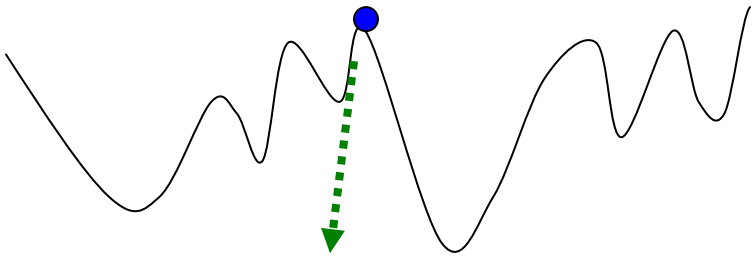

Figure 3.1 Energy Surface of an Atomic Structure [15].

The filled circle in the above figure represents the initial configuration of the atomic structure

3.2.1.2 Energy Minimization Algorithms

Some of the energy minimization algorithms available are Simplex, Steepest Descent, Conjugate Gradients method, Newton-Raphson method or Broyden–Fletcher–Goldfarb–Shanno (BFGS) method. These algorithms are derivative–based, meaning that these

techniques employ the derivatives of the potential energy. The negative first derivative of the potential energy with respect to inter-atomic distance (r) is the force (F) acting on an atom.

$$F = -\frac{\partial U}{\partial r} \tag{3.1}$$

The potential energy of a system may be expressed by a Taylor series expansion as follows:

$$U(r+\delta r) = U(r) + \frac{\partial U}{\partial r}\delta r + \frac{1}{2!}\frac{\partial^2 U}{\partial r^2}(\delta r)^2 + ... \tag{3.2}$$

The potential energy expression is usually truncated to either first derivative, also called the gradient vector (g) or second derivatives, termed as Hessian matrix (H). In Steepest descent methods, equation 3.2 is approximated to the first derivative of the potential energy. For every iterative step of this algorithm a line search or an arbitrary step size is used to determine the direction of steepest decent. The net force acting on individual atoms is computed from the potential energy expression and the atomic positions are computed according to equation 3.3. The procedure is repeated for every time step (j) until the force (F) on the individual atoms reaches zero.

$$r_i^{\,j} = r_i^{\,j-1} + \alpha . F_i \tag{3.3}$$

where, i is the atom number, j is the time step, α is the multiplication factor, F_i is the net force on an atom at that time step. In this method, the successive step directions in the iterative process are perpendicular to each other (as shown in Figure 3.2). The steepest descent method is quite effective when the initial configuration is far away from the minimum energy configuration i.e., when the gradient of the potential energy is large. This method will not be efficient when it is close to approaching a minimum configuration because of the smaller gradient of the potential energy. However, these algorithms are known to have great numerical stability for the fact that the potential energy of the system could never increase for a reasonable assumption of α. Hence, this could be used along with the conjugate gradient method, a relatively efficient and quicker method.

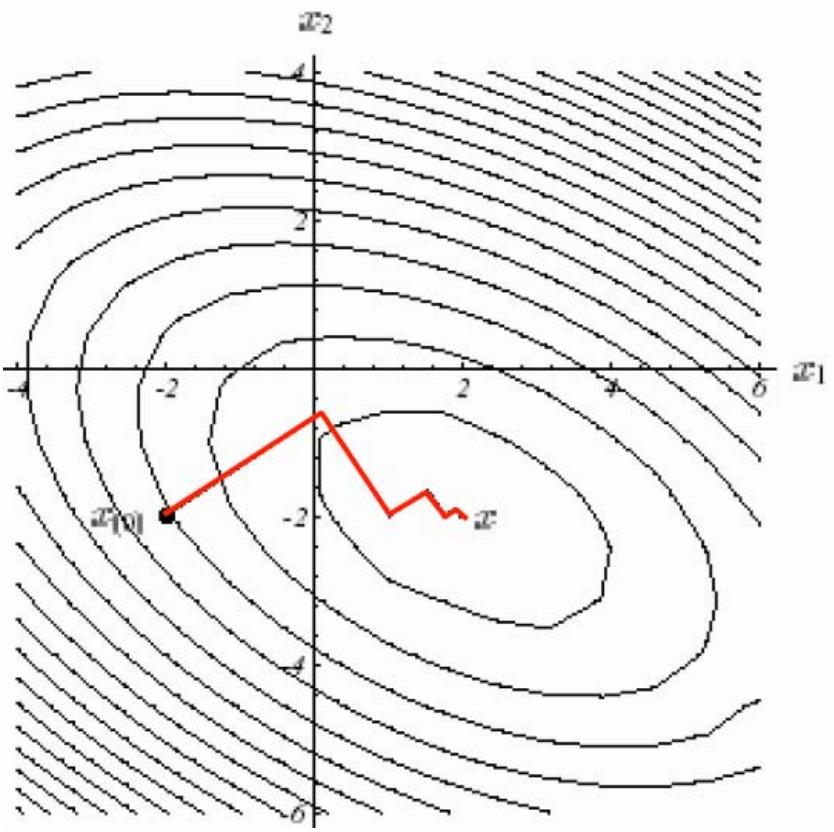

Figure 3.2 Steepest descent method [44].

The conjugate gradient method is an effective method when the gradient of the potential energy is smaller. In this method, the succeeding search directions are made conjugate i.e., the step directions are made orthogonal to its preceding search vector. This algorithm introduces a vector perpendicular to the direction of search and moves it in another direction which is orthogonal to that vector.

The residuals calculated in the method of conjugate gradient methods (as shown in Figure 3.3) are orthogonal to preceding directional search vectors. This property warrants production of fresh and independent directional search vector throughout the iteration process until the residue becomes zero. This method finds the minima in lesser number of steps compared to the steepest gradient methods [44].

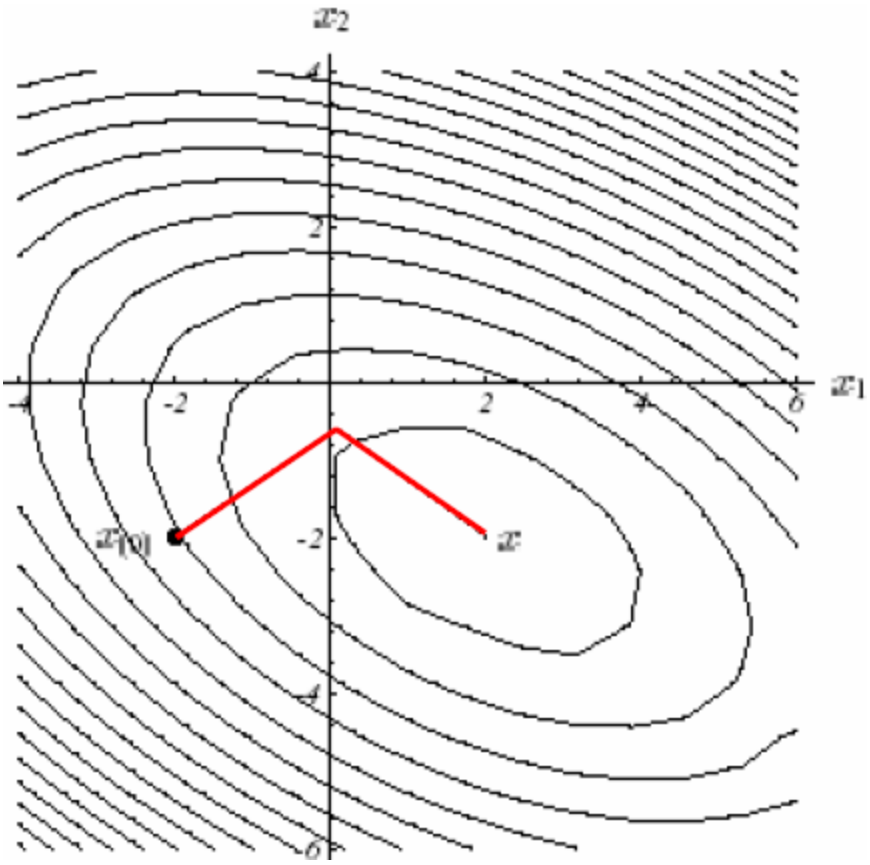

Figure 3.3 Conjugate gradient method [44].

Figure 3.4 shows a simplified version of a comparison between simple gradient and conjugated gradient method.

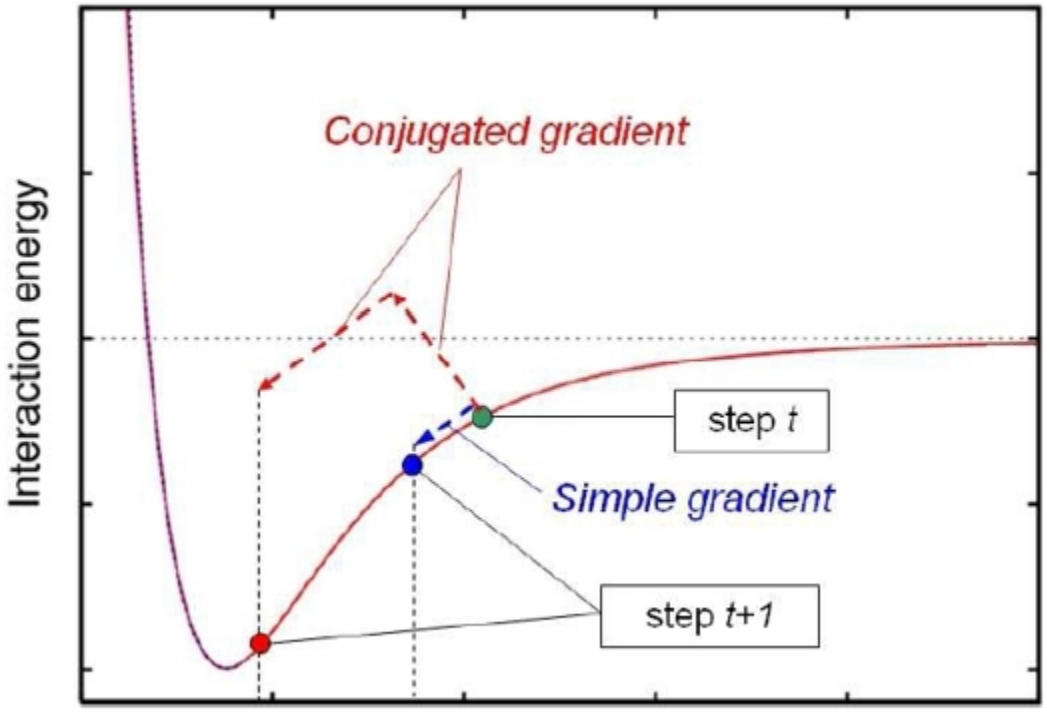

Figure 3.4 Comparison between conjugated gradient and simple gradient methods[25].

In the Newton-Raphson method, the Taylor series is expanded to the second derivative (H). The first derivatives (g) should be set to zero and the second derivative (H) should be positive definite in the calculation of local minima. The displacement vector (Δr) is determined by the following equation:

$$\Delta r = \alpha H^{-1} g \tag{3.4}$$

where, α is the scalar quantity ascertained by a line search algorithm and updated every step. In this method, much of the time is spent in inverting the Hessian (H) matrix. The changes in the Hessian matrix are very small for every step. This calculation can be avoided in the Broyden-Fletcher-Goldfarb-Shanno (BFGS) scheme where the inversion of Hessian matrix is modified suitably at every time step instead of recalculating the inversion of Hessian matrix (H). The BFGS expression is given by:

$$H_{i+1}^{BFGS} = H_i^{BFGS} + \frac{\Delta r \otimes \Delta r}{\Delta r.\Delta g} - \frac{(H_i^{BFGS}.\Delta g) \otimes (H_i^{BFGS}.\Delta g)}{(\Delta g.H_i^{BFGS}.\Delta g)} + \left[\Delta g.H_i^{BFGS}.\Delta g\right] \upsilon \otimes \upsilon \tag{3.5}$$

$$\upsilon = \frac{\Delta r}{\Delta r.\Delta g} - \frac{H_i^{BFGS}.\Delta g}{\Delta g.H_i^{BFGS}.\Delta g} \tag{3.6}$$

The BFGS algorithm is rated as one of the most efficient method used in optimization studies. This method is very efficient when it is used for smaller systems and less number of variables.

3.2.1.3 Determination of Bulk Properties

Bulk moduli, elastic constants, dielectric properties of a molecular system are dependent on the curvature of the energy surface about its minimum. The equations used to determine some of the key properties are briefly discussed here.

3.2.1.4 Elastic Constants

The calculation of elastic constants is very useful considering the fact that experimental determinations of these values are practically difficult. The elastic constants (Cij) are determined by calculating the second derivatives of the energy density (energy/volume) with respect to lattice strain components

$$C_{ij} = \frac{1}{V}\left(\frac{\partial^2 U}{\partial \varepsilon_i \partial \varepsilon_j}\right) \tag{3.7}$$

The six possible strains denoted by a 6 x 6 symmetric matrix represents the hardness of the material with respect to the deformations [45].

$$C_{ij} = \begin{bmatrix} C_{11} & C_{12} & C_{13} & C_{14} & C_{15} & C_{16} \\ C_{21} & C_{22} & C_{23} & C_{24} & C_{25} & C_{26} \\ C_{31} & C_{32} & C_{33} & C_{34} & C_{35} & C_{36} \\ C_{41} & C_{42} & C_{43} & C_{44} & C_{45} & C_{46} \\ C_{51} & C_{52} & C_{53} & C_{54} & C_{55} & C_{56} \\ C_{61} & C_{62} & C_{63} & C_{64} & C_{65} & C_{66} \end{bmatrix} \tag{3.8}$$

36 elements of Elastic constants get reduced to 21 due to crystal symmetry (Cij=Cji). In case of cubic crystals, C11=C22=C33 and C44=C55=C66. The elastic compliance matrix, S, is obtained by finding the inverse matrix of C (i.e. $S = C^{-1}$).

3.2.1.5 Bulk Modulus (K) & Shear Modulus (G)

Experimental determination of bulk modulus is much simpler compared to the elastic constant tensor. If the structure is subjected to a uniform pressure in all three directions, then the bulk modulus can be determined from the plot of pressure versus volume. As the bulk and shear modulus are interrelated with the elastic constants, they can be obtained by establishing a relationship with the elastic constants. However, no unique expression relating the constants and modulus are available [38]. The three different versions of defining the relationship between bulk & shear modulus and elastic constants are Reuss, Voight and Hill. Reuss and Voight's definition of bulk and shear modulus are given by [46]:

$$K_{Voight} = \frac{1}{9}(C_{11} + C_{22} + C_{33} + 2(C_{11} + C_{13} + C_{23})) \tag{3.9}$$

$$K_{Reuss} = (S_{11} + S_{22} + S_{33} + 2(S_{12} + S_{13} + S_{23}))^{-1} \tag{3.10}$$

$$G_{Voight} = \frac{1}{15}(C_{11} + C_{22} + C_{33} + 3(C_{44} + C_{55} + C_{66}) - C_{12} - C_{13} - C_{23}) \tag{3.11}$$

$$G_{Reuss} = \frac{15}{4(S_{11} + S_{22} + S_{33} - S_{12} - S_{13} - S_{23}) + 3(S_{44} + S_{55} + S_{66})} \tag{3.12}$$

The Hill definition of bulk and shear modulus is basically the average of the previous two methods [46]. The values reported in this work for Bulk and Shear moduli are according to the Voight's definition.

3.2.1.6 Young's Modulus

If a uniaxial tension is applied to a material, the stretching of the material is calculated as the strain. The ratio of stress to strain yields the Young's modulus (E) for that material.

$$E_a = \frac{\sigma_{aa}}{\varepsilon_{aa}} \tag{3.13}$$

Young's modulus in its respective directions can be computed from the elastic compliance elements as follows:

$$E_x = S_{11}^{-1} \tag{3.14}$$

$$E_y = S_{22}^{-1} \tag{3.15}$$

$$E_z = S_{33}^{-1} \tag{3.16}$$

3.2.1.7 Poisson's Ratio

Poisson's ratio (ν) is defined as the ratio of lateral to longitudinal strain under the application of a uniform, uni-dimensional stress. Poissons ratio and Young's modulus are calculated from the following expressions.

$$\nu = \frac{3K - 2G}{6K + 2G} \tag{3.17}$$

$$E = 2G(1 + \nu) \tag{3.18}$$

3.2.2 Molecular Dynamics (MD)

Molecular Dynamics is a numerical tool used to simulate the movement of the atoms and molecules in a given system throughout a period of interaction time [47]. Molecular dynamic methods are also based on Newton's laws of classical mechanics. Molecular dynamic methods basically generate atomic trajectories i.e., atomic positions, velocities. If the atomic positions and velocities of the individual atoms are known, then the properties/state of the system can be determined [47].

3.2.2.1 Governing Equations

Molecular dynamic methods rely on Newton's second law of classical mechanics, which is given by:

$$F_i = m_i a_i \tag{3.19}$$

where, F_i is the force acting on the atom, m_i is the mass of the atom and a_i is the acceleration of the atom. The total potential energy of the system is determined by

summing up the potential energy associated with all types of interactions. The total potential energy (U) is expressed as follows:

$$U = U^{bonded} + U^{nonbonded}$$
$$U^{bonded} = U^{bond-stretch} + U^{bond-angle} + U^{rotation}$$
$$U^{nonbonded} = U^{electrostatic} + U^{VanderWaals} \quad (3.20)$$

The force (F_i) acting between a pair of atoms is determined by evaluating the negative gradient of the potential energy with respect to the separation distance (r_{ij}). This is given by:

$$F_i = -\frac{\partial U}{\partial r_{ij}} \quad (3.21)$$

The net force acting on an atom 'i' is calculated by summing up all the interactions between atom 'i' and the surrounding atoms. Once the net force is known, the acceleration of the individual atoms can be determined from equation 3.19. By integrating the equations of motion, velocities and positions are obtained.

3.2.2.2 Ensembles

The microscopic state of a system is defined by the atomic positions and momenta; which are the coordinates in a multidimensional imaginary space called phase space. For a system of N particles, this space has 6N dimensions and hence a single point in phase space represents the state of a system. A molecular dynamic simulation generates a collection of points in phase space as a function of time. An ensemble can be defined as a collection of points in phase space satisfying the conditions of a particular thermodynamic state [47]. There are three commonly used ensembles in MD:

1) Micro Cannonical (N, V, E) – Number of atoms, Volume and Energy of the system are maintained constant.

2) Cannonical (N, V, T) – Number of atoms, Volume and Temperature of the system are constant.

3) Gibb's ensemble (N, P, T) - Number of atoms, Pressure and Temperature of the system are kept constant.

Depending on the type of ensemble used, a thermostat or barostat need to be chosen for the Molecular dynamic simulations. Generally, thermostats are intended to control the temperature of the system. There are different methods to control the temperature of the system and hence have different types of thermostats: a) Velocity scaling methods - simple velocity scaling and the Berendsen thermostat, b) Adding stochastic forces or velocities - the Andersen, Langevin, and Dissipative Particle Dynamics thermostats, c) Extension of Lagrangian form- Nosé-Hoover thermostat. Some of the popular barostats used to control the pressure of the system (N,P,T) are Berendsen and Nose-Hoover barostat [47].

3.2.2.3 Steps in MD

Figure 3.5 shows the various steps involved in a typical Molecular dynamics algorithm.

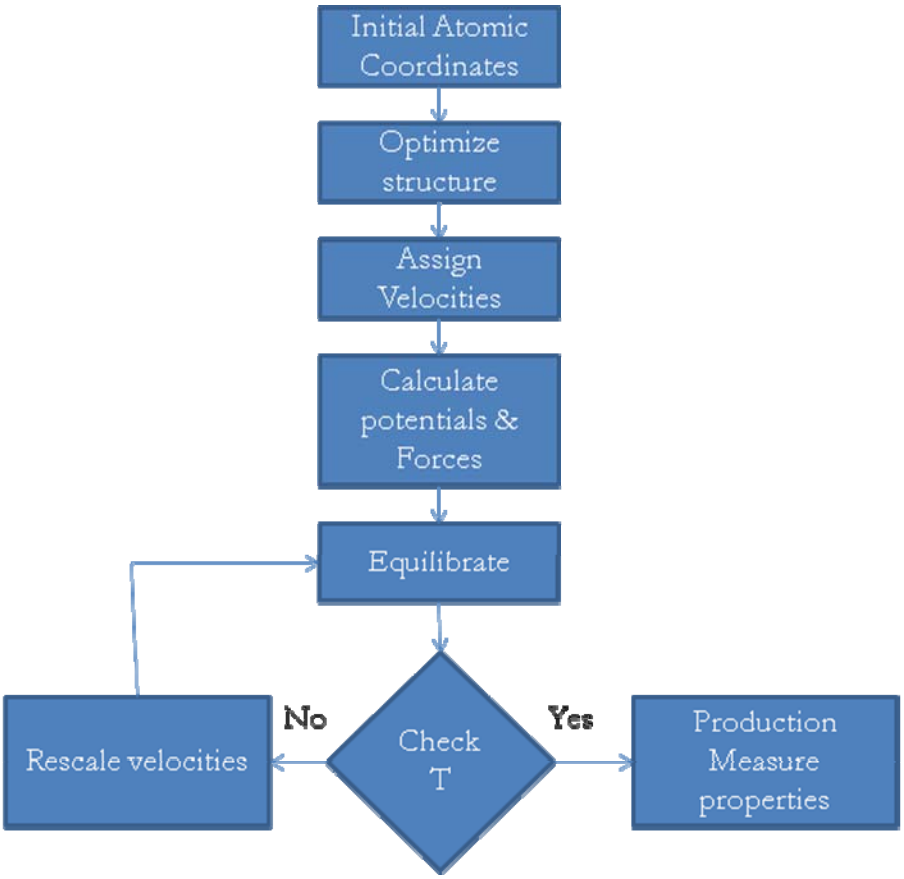

Figure 3.5 MD sequence chart [15].

3.2.2.4 Initialization

Initial positions of all the atoms are defined by the coordinates of the corresponding atoms in the simulation cell. Every atom is assigned a velocity. A number generator is used to introduce random velocity to each atom in the simulation cell. When doing this, the system will have a small total linear momentum, corresponding to a translational motion of the whole system. To nullify this effect, it is common practice to subtract this component from the velocity of each particle in order to operate in a zero total momentum condition. The velocity is then scaled to the desired temperature. The new position of the atoms is then calculated using the generated velocity [15].

3.2.2.5 Energy Minimization

The structure is then optimized so that the net force acting on the structure will be zero and hence it will serve as an excellent starting point for Molecular Dynamic simulations.

3.2.2.6 Integrating the Equations of Motion

The time integration algorithm is the most important part of a MD program. The MD program integrates Newton's equation of motion of each atom and generates atomic positions and velocities. The most popularly used methods are Verlet, Velocity Verlet, Leap Frog algorithms. Most of these schemes are based on finite difference algorithms. In finite difference methods, time is discretized into timesteps Δt on a finite grid [15]. If the atomic positions and velocities at a given time t are known, then the same entities at a future time, $t + \Delta t$, can be predicted. The expressions for atomic positions and velocities in the Verlet scheme are given below. The basic idea is to write two third-order Taylor expansions for the positions r(t), one forward and one backward in time. The atomic positions at a time $(t+\Delta t)$ and time $(t-\Delta t)$ can be expressed by a Taylor series expansion [10]:

$$r(t+\Delta t) = r(t) + v(t)\Delta t + (1/2!)a(t)\Delta t^2 + (1/3!)b(t) + O(\Delta t^4) \tag{3.22}$$

$$r(t-\Delta t) = r(t) - v(t)\Delta t + (1/2!)a(t)\Delta t^2 - (1/3!)b(t) + O(\Delta t^4) \tag{3.23}$$

Adding the above two equations

$$r(t+\Delta t) = 2r(t) - r(t-\Delta t) + a(t)\Delta t^2 + O(\Delta t^4) \tag{3.24}$$

where, a(t) is the acceleration of the atoms at time t which can be determined as follows:

$$a(t) = -(1/m)\nabla U(r(t)) \tag{3.25}$$

Velocity of an atom at a time t can be computed from the atomic positions using the following formula:

$$v(t) = \frac{r(t+\Delta t) - r(t-\Delta t)}{2\Delta t} \tag{3.26}$$

The acceleration term is not needed for the velocity calculation and velocity term is not required for calculating the atomic positions. The expressions for the leap frog schemes are given by:

$$r(t+\Delta t) = r(t) + \Delta t v(t+1/2\Delta t) \tag{3.27}$$

$$v(t+1/2\Delta t) = v(t-1/2\Delta t) + \Delta t a(t) \tag{3.28}$$

In this method (leap frog), the velocities at half time steps are initially calculated and the atomic positions are calculated based on the midstep velocities. One major disadvantage of this scheme is that the positions and velocities are not known at the same time and hence, the potential energy and kinetic energy of the system cannot be determined at the same time t and ultimately not able to evaluate the total energy of the system at time t [15]. A better implementation of the same basic algorithm is the so-called *velocity Verlet* scheme. This algorithm is most preferred in most molecular dynamics calculations. The equations associated with the Velocity verlet algorithm are given by:

$$r(t+\Delta t) = r(t) + \Delta t v(t) + \frac{1}{2}\Delta t^2 a(t) \tag{3.29}$$

$$v(t+1/2\Delta t) = v(t) + \frac{1}{2}\Delta t a(t) \tag{3.30}$$

$$a(t+\Delta t) = -(1/m)\nabla U(r(t+\Delta t)) \tag{3.31}$$

$$v(t+\Delta t) = v(t+1/2\Delta t) + \tfrac{1}{2}\Delta t a(t+\Delta t) \tag{3.32}$$

3.2.2.7 Periodic Boundary Conditions

To mimic the behavior of the bulk material, periodic boundary condition is applied to the simulation box in which case the unit cell is replicated to infinity in all three directions. Therefore, individual atoms in a unit cell interact with not only with the other atoms in it but also with their images outside the unit cell [15] Figure 3.6 shows the schematic sketch

of periodic boundary conditions employed in a two dimensional system. If an atom in a unit cell moves out of the box then the atom appears in the opposite side of the box with the same velocity so that the number of atoms in a unit cell is conserved. The advantage of using this periodic boundary condition is that a very small system size could be used for investigating the macroscopic properties of bulk materials[15]

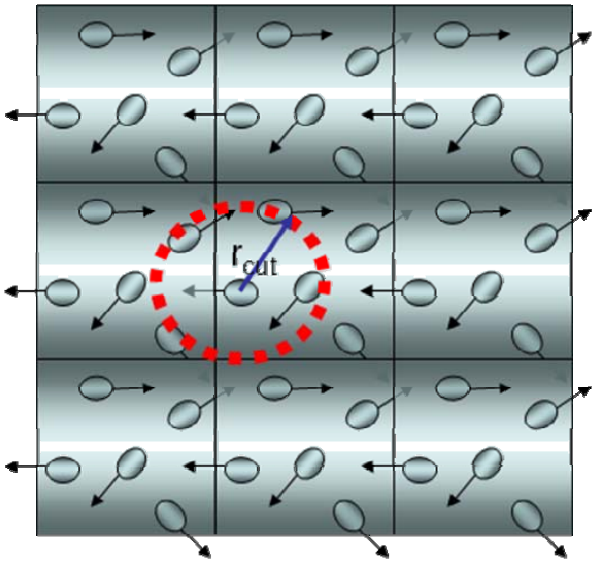

Figure 3.6 Periodic boundary Conditions[15].

3.2.2.8 Verlet Neighbor List

A cut off radius (r_{cut}) as shown in Figure3.6 is specified to limit the number of interactions associated with individual atoms and hence the time involved in the force calculations is appreciably reduced. A list of neighboring atoms is generated for each and every atom in the system so that only the interactions with those listed in the neighbor list is accounted for the force calculation. This avoids the time consuming step of calculating all possible interactions between an atom and the rest in the system for each time step [15]. However, the list needs to be updated for every time step which is undesirable because it consumes appreciable amount of time in generating the neighbor list. To avoid this problem, a buffer radius (r_b) is added to the cut-off radius i.e., a neighbor list cut-off radius (r_{nl}) is chosen such that it is greater than the cut-off radius as shown in Figure 3.7. This buffer radius is provided to account for the movement/displacement of the atoms

beyond the cut-off radius but within the neighbor list radius [15]. This eliminates the necessity to update the list for every single time step. Instead, the neighbor list is refreshed and re-constructed whenever the atoms move beyond the neighbor list radius or when the maximum displacement of the atoms exceeds the buffer radius [15].

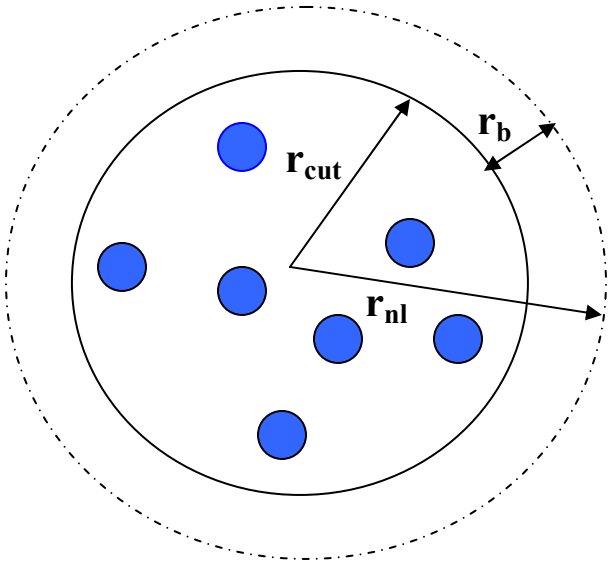

Figure 3.7 Neighbor List [15].

3.2.2.9 Calculation of Properties

Measuring quantities in MD usually means performing time averages of physical properties. Physical properties are usually a function of the particle coordinates and velocities. Whenever the system state changes, the system goes out of thermodynamic equilibrium for a while. But it is relaxing towards a new value i.,e. fluctuating around a

value which is slowly drifting with time. The state change may be induced by a change in parameter of the simulation such as the temperature, thereby disturbing the system, and then wait for a new equilibrium to be reached.

3.2.2.10 Kinetic, Potential and Total Energy

The average potential energy U is obtained by averaging its instantaneous value, which is usually obtained straightforwardly at the same time as the force computation is made. Knowledge of average potential energy U is required to verify energy conservation. This is an important check to do in any MD simulation. The instantaneous kinetic energy is given by:

$$K(t) = \frac{1}{2}\sum_i m_i [v_i(t)]^2 \tag{3.32}$$

The total energy E = K + U is a conserved quantity in Newtonian dynamics. However, it is common practice to compute it at each time step in order to check that it is indeed constant with time.

3.2.2.11 Temperature

The temperature T is directly related to the kinetic energy, assigning an average kinetic energy K_B T / 2 per degree of freedom. K_B is the Boltzmann constant.

$$K = \frac{3}{2} N K_B T \tag{3.33}$$

So temperature is therefore directly derived from the average kinetic energy K.

3.2.2.12 Pressure

The pressure of the entire system of atoms is a function of the position and force on each atom. It is computed by the following formula [48].

$$P = \frac{NKT}{V} + \frac{\sum_i^N ri \bullet fi}{dV} \tag{3.34}$$

Where

N= the number of atoms in the system

K = the Boltzmann constant

T = Temperature

d = dimensionality of the system (2 or 3 for 2d/3d)

V = the system volume (or area in 2d)

P = stress in the entire system

The second term is the viral term for all pair wise as well as two-body, three-body and four-body and long range interactions.

3.3 Atomic Interactions

The first step in most of the atomistic molecular modeling techniques (molecular mechanics) is the determination of the energy (Lattice energy in this case). The lattice energy of a crystal can be computed by summing all different types of interactions that can occur in a system comprising N number of atoms in it.

$$U = \sum_{i=1}^{N} U_i + \frac{1}{2}\sum_{i=1}^{N}\sum_{j=1}^{N} U_{ij} + \frac{1}{6}\sum_{i=1}^{N}\sum_{j=1}^{N}\sum_{k=1}^{N} U_{ijk} + \ldots\ldots, \tag{3.35}$$

Where, i,j,k refers to atom 1, 2 and 3 respectively. The first term signifies self energies of the atoms, the second term is the two body interaction and the third represents the three body interactions. However, the lattice energy computed can be accurate only if higher orders of interactions are also considered for calculation. But, it is impractical to include the higher orders of interaction for computation as it will prove extremely time consuming. Also considering the fact that the contributions decrease gradually with increasing order of interactions, it is reasonable to truncate the expansion to two body and three body interactions. The atomic interactions become weaker as the distance between the atoms increases [15]. The potentials are basically empirical equations (generally involves a function of inter atomic distance) to calculate the energy associated with the specific atomic interactions.

Potentials play an important role in determining the accuracy of the computer modeling studies [49]. There are a number of potentials available in the literature and text for different species of interacting atoms. The choice of potential is left to the discretion of the user, based purely on the knowledge of nature of forces acting between two atoms.

The potential should be chosen in such a way that it best mimics the nature of atomic interactions and make the computations more realistic. There are different kinds of chemical bonds that exist in different substances for holding the material together; namely Ionic bonds, Covalent bonds, Metallic bonds, Hydrogen bonds, Van der Waals bonds. Each type of bond will have varied strength. Bonds may also be classified as intramolecular bonds and intermolecular bonds. Intramolecular bonds are those that keep the atoms together within a molecule. In addition, intramolecular bonds are those that exist between the molecules as in Van der Waals bonding, ionic bonding, covalent bonding, Dipole – Dipole interaction and Hydrogen bonding. In ionic bonding, the ions of opposite charges are attracted to each other. Sodium chloride (NaCl) is a classic example of ionic bonding. In covalent bonding, the valence electrons are shared between atoms unlike electron transfer observed in ionic bonding. Covalent bonding is observed in the case of water and diatomic molecules like H_2 etc. These atomic interactions may also be classified as long and short range interactions [49]

3.3.1 Long Range Interactions (Coulombic interactions)

When dealing with ionic crystals such as C-S-H, the long range Coulomb interactions contribute the most to the total energy of the structure. Figure 3.8 shows the sketch of Coulombic interactions. If the ions are just specified as point charges, the simplest form of Coulomb's law is defined by

$$U_{ij}^{Coulomb} = \frac{q_i \, q_j}{4\pi\varepsilon_0 r_{ij}} \tag{3.36}$$

Where,

$U_{ij}^{Coulomb}$ is the Coulomb energy.

q_i , q_j are the charges on the interacting pairs of ions.

ε_0 is the permittivity of free space.

r_{ij} is the inter-ionic distance.

The calculation of Coulomb energy becomes tedious for a three dimensional bulk material. Interactions between ions gradually decrease with increase in the inter-ionic

distances. But, on the contrary, the number of ions and hence the number of interactions between ions increases as the cut-off radius increases. This ultimately results in the increase of energy density of interactions with increase in distance. This problem could be resolved by using Ewald summation method which necessitates two important criterions for convergence: a) Sum of all the charges in the system should be zero b) Dipole moment should be zero. Ewald summation method is basically derived by taking Laplace transformation on the proceeding equation. The Coulomb energy calculation is done in two parts: a) Real space summation b) Reciprocal space summation. Real space summation part converges quickly and the Reciprocal space summation part decays rapidly. A Gaussian charge distribution is added and subtracted about each ion. The expression for the estimation of coulomb energy (UCE) as the summation of contributions from real space (U_{real}), reciprocal space ($U_{reciprocal}$) and self-energy ($U_{selfenergy}$) of the ions is given by:

$$U^{CE} = \frac{1}{2}\sum_{i=1}^{N}\sum_{j=1}^{N}\frac{q_i q_j}{r_{ij}} erfc(\eta^{1/2} r_{ij}) + \frac{1}{2}\sum_{i=1}^{N}\sum_{j=1}^{N}\sum_{G}\frac{4\pi}{V} q_i q_j \exp(iG.r_{ij})\frac{\exp(-G^2/4\eta)}{G^2} - \sum_{i=1}^{N} q_i^2\left(\frac{\eta}{\pi}\right)^{\frac{1}{2}} \quad (3.37)$$

$$U^{CE} = U^{real} + U^{reciprocal} - U^{selfenergy} \quad (3.38)$$

where, q is the charge of the ion, G is reciprocal lattice vector, V is the unit cell volume, N is the number of atoms in the system, η is the proportion of job between real and reciprocal space.

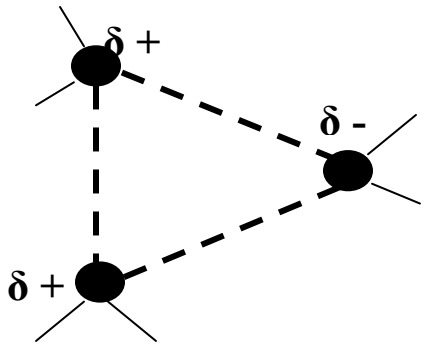

Figure 3.8 Electrostatic (Coulombic) interactions [15].

3.3.2 Short Range Interactions

Short range (non Coulombic) interactions play a vital role in estimating the location and shape of the minimum energy. Generally, the two body terms contribute to the short range interactions. Two body terms include interactions between atoms that are ions or bonded. Three popularly used two body potentials are Buckingham potential, Lennard-Jones potential and Morse potential. The expressions for the potentials are given by:

$$U_{ij}^{Buckingham} = A\exp\left(\frac{-r_{ij}}{\rho}\right) - \frac{C_6}{r_{ij}^6} \tag{3.39}$$

$$U_{ij}^{Lennard-Jones} = \frac{C_m}{r_{ij}^m} - \frac{C_6}{r_{ij}^6} \tag{3.40}$$

$$U_{ij}^{Morse} = D_e[(1-\exp(-a(r-r_o)))^2 - 1] \tag{3.42}$$

where, r_{ij} is the inter-atomic distance and all the other terms are the parameters of the potentials.

The Buckingham potential and Lennard Jones potential contains similar terms in the above expressions i.e., a repulsive part and attractive part. The C_6 part found in both the potentials is the attractive part of the potential and it is not necessary to model this in case of ionic bonds. The difference between the two potential is primarily due to the repulsive term in the potential. The repulsive part in the Buckingham potential is modeled by using negative exponential term that decays with inter atomic distance while in L-J potential, a positive term is used that varies inversely with inter-atomic distance.

3.3.3 Three Body Interactions

Three body interactions (Figure 3.9) shall be included if the atomic structure of the ionic system is complex (say if the ions form tetrahedral coordination like in silica). Three body terms will provide the angular constraints. For example, three body potentials were

used to model the bending of O-Si-O bonds of silicate chains, imposing angular constraints of 109.5.

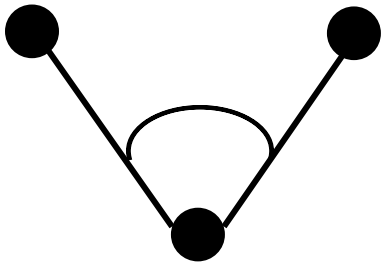

Figure 3.9 Three Body Interactions.

The general expression for three body potential is given by :

$$E = \sum_i \sum_{i=0} \phi_2(r_{ij}) + \sum_i \sum_{j \neq i} \sum_{k>j} \phi_3(r_{ij}, r_{ik}, \theta_{ijk}) \quad (3.43)$$

$$\phi_2(r_{ij}) = A_{ij} \varepsilon_{ij} \left[B_{ij} \left(\frac{\sigma_{ij}}{r_{ij}}\right)^{p_{ij}} - \left(\frac{\sigma_{ij}}{r_{ij}}\right)^{q_{ij}} \right] exp\left(\frac{\sigma_{ij}}{r_{ij} - a_{ij}\ \sigma_{ij}}\right)$$

$$\phi_3(r_{ij}, r_{ik}, \theta_{ijk}) = \lambda_{ijk} \varepsilon_{ij\,k} [cos\theta_{ijk} - cos\theta_{0ijk}]^2 exp\left(\frac{\gamma_{ij}\sigma_{ij}}{r_{ij} - a_{ij}\ \sigma_{ij}}\right) exp\left(\frac{\gamma_{ik}\sigma_{ik}}{r_{ik} - a_{ik}\ \sigma_{ik}}\right)$$

Where

i, j, k represents atom 1, 2, and 3 in the molecule

Θ is the angle between atom 1, 2, and 3

A, B, P, q, σ, ε, γ, are all parameters depending on the molecules

3.4 Modern Programs to Perform Molecular Modeling

There are a variety of programs used to perform molecular modeling. A well known program to perform molecular mechanics is a code called General Utility Lattice Program (GULP), developed by Gale [50]. GULP is free for academic purposes.

Another useful program to perform molecular dynamics is called LAMMPS; LAMMPS stands for Large -Scale Atomic /Molecular Massively Parallel simulator. It is a classical molecular dynamics code that models an ensemble of particles in a liquid, solid or gaseous state. It can model atomic, polymeric, biological, metallic, granular, and coarse-grained systems using a variety of force fields and boundary conditions. LAMMPS can model systems with only a few particles up to millions or billions. LAMMPS is a freely-available open-source code, distributed under the terms of the GNU Public License.

CHAPTER 4: DATA PREPARATION FOR MOLECULAR MODELLING

4.1 Procedures for Modeling Crystalline Calcium Silicate Hydrate Structures using Molecular Statics (MS)

Atomistic modeling of crystalline calcium silicate hydrate structures using GULP involves the following steps in sequence.

a) Identification of Crystal parameters (Unit cell dimensions, space group etc)
b) Positioning of atoms in the unit cell – Determination of x, y, z coordinates of all the atoms.
c) Identify the different types of atoms in the structure and their nature of interaction with other atomic species. Accordingly, define the Interatomic potentials.
d) Determination of optimized structure using Energy minimization methods.
e) Calculation of physical/bulk properties.
f)

To model the atomic structure of crystalline calcium silicate hydrate structures, the user had to fulfill part a through c. This information is used to generate the input file. GULP then performs part d and e; the results are placed in an output file.

4.1.1 Identification of Crystal Parameters in Crystalline Calcium Silicate Hydrate Structures

The structure of crystalline calcium silicate hydrates was constructed using the atomic coordinates of the atoms in the crystalline minerals (Tobermorite, Jennite etc). The atomic coordinates, crystal parameter and space group were obtained from XRD data and

other literatures [34-36]. A crystalline calcium silicate structure used in this study is Hamid's [34] Tobermorite model. The chosen Tobermorite crystal has a Monoclinic structure, classified under the space group P21 with unit cell dimensions: am=6.69 A°, bm =7.39 A°, cm = 22.779 A° and γ = 123.49°. The atoms in a unit cell of Tobermorite 11 Aº (Ca/Si-1.00) is given in Table 4.1.

Table 4.1 Atoms in unit cell

Unit cell	
Atoms	**Number of Atoms**
Ca	6
Si	6
O1	18
Hw	4
Ow	2
Total	36

The coordinates of the atoms in Tobermorite crystal referred in Table 4.2 are taken from Hamid[34]. The coordinates of hydrogen atoms for all the hydroxyl and water molecules was derived from the atomic positions of the oxygen atoms that are available in Table 4.2. The hydrogen atoms are located at about 1 Aº from the oxygen atoms of hydroxyl and water molecules. In case of water, hydrogen atoms are so located that H-O-H angle is 109º.

GULP can handle materials of different space groups. This eliminates the need of transforming the Monoclinic coordinates to orthorhombic coordinates. Hence, the monoclinic fractional coordinates can be directly fed into GULP code. It also has an additional feature that permits the occupancy factor of an atom to be specified along with the coordinates. This was of help when the atomic structure of Merlino's Tobermorite 11 Aº was modeled using GULP.

Table 4.2 Normalized Monoclinic Atomic Coordinates in Tobermorite 11 A°

Atom	X	Y	Z	Atom	X	Y	Z
Ca1	0.75	0.25	0	O4	0.25	0.5	0.077
Ca2	0.75	0.75	0	O5	0.015	0.622	0.0189
Ca3	0.75	0.75	0.413	O6	0.484	0.856	0.0189
Ca4	0.75	0.25	0.413	O7	0.25	0.83	0.12
Ca5	0.506	0.38	0.198	O/OH8	0.068	0.909	0.211
Ca6	0.506	0.88	0.198	O/OH9	-0.18	0.785	0.113
Si1	0.25	0.287	0.056	O10	0.25	0	0.348
Si2	0.25	0.707	0.056	O11	0.015	0.122	0.4108
Si3	0.068	0.909	0.141	O12	0.484	0.357	0.4108
Si4	0.25	0.207	0.373	O13	0.25	0.335	0.31
Si5	0.084	0.414	0.282	O14	0.1	0.425	0.213
Si6	0.25	0.787	0.373	O15	0.25	0.645	0.31
O1	0.25	0.17	0.12	O16	0.015	0.638	0.4108
O2	0.015	0.137	0.0189	O17	0.484	0.872	0.4108
O3	0.484	0.372	0.0189	O18	-0.175	0.288	0.306
H2O(1)	0.75	0.75	0.303	H2O(2)	0.75	0.25	0.11

Since the system dealt with, is an ionic crystal, polarization effect becomes an important factor in the calculation. All the anions in the Tobermorite namely the lattice oxygen, oxygen of hydroxyl and water molecule are more liable to polarization. The polarization of those anions (O1, O2 & O3) is accounted by using the 'shell model' approach by splitting those anions into a) core, representing the positively charged nucleus and b) shell, representing the polarizable valence electrons. The cations in the structure (Ca, Si, H) were considered only as cores. The coulombic interactions between a core and shell were removed from the calculation. However, they are connected together by a restoring harmonic spring force. The general expression for the spring potential is given by

$$U^{core-shell} = \frac{1}{2} k_{cs} r_{cs}^2 \tag{4.1}$$

where, $U_{core\text{-}shell}$ is the restoring spring potential energy, k_{cs} is the spring constant, r_{cs} is the distance between core and shell. The spring constants of the anions in the Tobermorite structure are provided in Table 4.3. All the potentials associated with the short range interactions i.e., Buckingham potential, Morse potential, Lennard Jones potential, Three body potential are applied only on the shells of the polarizable anions (O1,O2 & O3) while the long range Coulombic interactions are applied on both (core and shell). This accounts for the polarization of ions by making it contingent on the local environment.

Table 4.3 Core-Spring Potential

Atoms	**eV/Aº2**
O1	74.92
O2	74.92
O3	209.45

Note that O1, O2 and O3 (referred in the above table) are the oxygen ions of lattice oxygen, hydroxyl and water molecule in the Tobermorite crystal. The values for the charges of all the ions (Table 4.4) except the hydroxyl group are taken from Gmira's thesis (2003). The charge breakup of the hydroxyl molecule (not present in the Tobermorite structure Ca/Si-1) is calculated from Collins et.al (1992). From the cited work, it was known that the net charge on the oxygen atom (O2-core + O2-shell) of hydroxyl molecule should be -1.426. The charge of O2-core oxygen atom was assumed to be the same as the free oxygen (O1 core) i.e., +0.86902. The charge of O2-shell oxygen atom was back calculated and found to be -2.295. Similarly, the charge of (H1-core) hydrogen atom of the hydroxyl molecule was determined to be +0.426 and thus the net charge (O2-core + O2- shell + H1- core) on the hydroxyl molecule is -1.00.

Table 4.4 Charges of the Atoms

Sl.No.	Atom	Type	Charge	No. of atoms	Total charge
1	Ca1	Core	2	4	8
2	Ca2	Core	2	2	4
3	Si	Core	4	6	24
4	O1	Core	0.86902	18	15.64236
5	O1	Shel	-2.86902	18	-51.64236
6	O2	Core	0.86902	0	0.0
7	O2	Shel	-2.295	0	0.0
8	H1	Core	0.426	0	0.0
9	O3	Shel	-2.05	2	-4.1
10	O3	Core	1.25	2	2.5
11	H2	Core	0.4	4	1.6
Charge of the system – Neutral					0

Ca1 & Ca2 are the lattice Calcium atom and interstitial Calcium atoms respectively. O1, O2 & O3 are the free oxygen atoms, hydroxyl oxygen and water oxygen atoms respectively. H1 and H2 are the hydrogen atoms from the hydroxyl and water molecules respectively. The net charge on the water molecule should be zero i.e., (O3-shell + O3-core + 2 * (H2-core) = 0.0). In atomistic simulations of ionic solids, two important conditions are needed 1) the input atomic structure should be charge neutral 2) the total dipole moment of the system should be zero. .

4.1.2 Assigning Appropriate Potentials to the Interacting Atoms:

The potentials for the two and three body interactions are taken from the Gmira[40] and GULP library. Ewald summation method was used to compute the electrostatic interactions in the system in order to obtain quicker and accurate results The potentials

and parameters used for the atomistic calculations of C-S-H are given in Appendix A for reference.

4.2 Molecular Dynamic Simulation of C-S-H structures

Molecular Dynamics (MD) was used to simulate stress-strain test on C-S-H structures. A uniaxial strain rate is applied to the atomic structures of C-S-H and the response (stress) of structure is calculated and given as output. In MD, the strain rates are typically very high [10^6/sec -10^8/sec] to initiate motion at the atomic level. Stress-Strain graphs were derived from the MD output data and from these graphs the maximum strength [tensile and compressive], and elastic modulus were determined.

LAMMPS (Large-scale Atomic Molecular Massively Parallel Simulator) is a classical MD code used in this study. LAMMPS is developed by Steve Plimpton and his group of Sandia National Laboratories. An input file was generated for LAMMPS MD code to calculate the response of C-S-H structures to uniaxial loading.

4.2.1 Steps to generate Input File

This work used the following scheme to generate the input file

1. A data file was created to construct the atomic structure of calcium silicate hydrate. The data file is a separate file containing molecular topology information LAMMPS needs to run a simulation. Such information includes dimension of the simulation cell, the initial coordinates, charges, type and mass of atoms in the simulation cell.
2. Parameters such as units, boundary, and atom styles were set within the input file. Periodic boundary conditions are used to simulate a bulk material. When periodic boundary conditions are used, the cubical simulation box is replicated throughout space to form an infinite lattice. The atom style defines how the data file will be organized. Refer to http://lammps.sandia.gov/ for a list of the various atom styles.
3. Next, interatomic potential equations that describe the type of atomic interaction were specified as well as parameters for these equations. Inter atomic potential equations describe the forces acting between atoms.
4. The atoms were defined and read from the data file

5. Then, energy minimization algorithms were specified to stabilize the atomic structure. Once the system is set and initial coordinates are assigned, an initial round of equilibration is necessary before the simulation can begin.
6. A random number generator was assigned to set initial velocities to atoms in the simulation cell
7. A set of boundary conditions were imposed to control parameters like temperature, strain rate of the atomic structure etc. The following algorithms are implemented in the LAMMPS MD Code:
    a. Constant energy, constant number of particles (NE)
    b. Constant energy, constant volume (NVE)
    c. Constant temperature, constant volume (NVT)
    d. Constant temperature, constant pressure (NPT)
    e. Constant Strain rate
8. Time step and duration of MD simulation were specified.
9. The simulation process was started i.e. run the program with the input file and data file. Integration algorithms in LAMMPS are then used to solve Newton's equations and advance the atomic positions and velocities of atoms
10. The data from the output file was tabulated. Thermodynamic statistics like stress (pressure), energy and temperature are extracted from the atomic positions and velocity and given as output.

4.2.2 Data File Generation

This study considered two atomic structures: Tobermorite crystal structure and the proposed C-S-H structure. The data file can be found in Appendix C and D. The format of each data file is listed below:

1. Title of data file
2. Number of atoms
3. Type of atoms
    a. For example, there are four atom types – each atom is identified by a number
        i. Calcium = 1, Silicon = 2, Oxygen = 3 and Hydrogen =4

4. Dimension of Simulation Cell [Matrix Format]
    a. x,y, z direction
5. Mass of each atoms
    a. Calcium (Ca) = 40.078 amu
    b. Silicon (Si) = 28.085 amu
    c. Oxygen (O) = 15.999 amu
    d. Hydrogen (H) = 1.000 amu
6. Description of each atom
7. Atom ID, Atom Type, Charge, x-coordinate, y-coordinate, z-coordinate

Table 4.5 lists the charges on each atom used in this work. The net charge on the water molecule should be zero. Also the net charge on each system should be zero

The Tobermorite structure used in this study has continuous silicate chains and the proposed C-S-H structure has dimmer silicate chains. The Tobermorite (crystalline calcium silicate hydrate structure) was constructed using the atomic coordinates of the atoms in Hamid's [34] Tobermorite 11 Aº (Ca/Si-1.00) model. The proposed C-S-H was constructed using the atomic coordinates of the atoms in the proposed C-S-H structure of 15]. Both atomic structures are in a monoclinic crystal system; however this work adopted Subramani's [15] approach to convert the monoclinic coordinates into pseudo orthorhombic system for both atomic structures.

Table 4.6 and 4.7 present the normalized orthorhombic atomic coordinates in Tobermorite and the proposed C-S-H. In Tables 4.2 and 4.6, Ca1, Ca2, Ca3, Ca4 are the lattice calcium atoms. Ca5 and Ca6 are interstitial calcium atoms respectively. O1 to O18 are the free oxygen atoms and hydroxyl oxygen. The water oxygen is labeled H2O(1) and H2O(2) respectively. In tables 4.7, Ca1 & Ca2 are the lattice calcium atom and interstitial calcium atoms respectively. O1, O2 & O3 are the free oxygen atoms, hydroxyl oxygen and water oxygen atoms respectively. H1 and H2 are the hydrogen atoms from the hydroxyl and water molecules respectively.

Table 4.5 Charges of the Atoms

Atom Types	Atom	Charge
1	Ca	2
2	Si	4
3	O	-2
4	H	1

Table 4.6 Normalized Orthorhombic Atomic Coordinates in Proposed C-S-H Structure (a = 11.18Å, b =7.39Å, c =22.77Å) (x=a, y=b and z=c) [15]

Atom	Fractional Coordinates			Atom	Fractional Coordinates		
	X	Y	Z		X	Y	Z
Ca1	0.500	0.000	0.000	O1	0.015	0.137	0.019
Ca1	0.500	0.500	0.000	O1	0.484	0.372	0.019
Ca1	0.500	0.500	0.413	O1	0.250	0.830	0.120
Ca1	0.500	0.000	0.413	O1	0.250	0.500	0.077
Ca2	0.378	0.752	0.198	O1	0.015	0.622	0.019
Si	0.250	0.287	0.056	O1	0.484	0.856	0.019
Si	0.250	0.707	0.056	O1	0.250	0.000	0.348
Si	0.250	0.207	0.373	O1	0.484	0.357	0.411
Si	0.250	0.787	0.373	O1	0.015	0.122	0.411
H1	0.260	0.261	0.153	O2	0.250	0.335	0.310
H1	0.263	0.249	0.273	O1	0.250	0.645	0.310
H2	0.590	0.500	0.303	O1	0.015	0.638	0.411
H2	0.471	0.628	0.303	O1	0.484	0.872	0.411
H2	0.590	0.000	0.110	O3	0.750	0.750	0.303
H2	0.471	0.128	0.110	O3	0.750	0.250	0.110
O2	0.250	0.170	0.120				

Table 4.7 Normalized Orthorhombic Atomic Coordinates in Tobermorite Structure (Crystalline Calcium Silicate Hydrate) (a = 11.18Å, b =7.39Å, c =22.77Å) (x=a, y=b and z=c) [34]

Atom	Fractional Coordinates			Atom	Fractional Coordinates		
	X	Y	Z		X	Y	Z
Ca1	0.500	0.000	0.000	O4	0.250	0.500	0.077
Ca2	0.500	0.500	0.000	O5	0.133	0.740	0.019
Ca3	0.500	0.500	0.413	O6	0.367	0.739	0.019
Ca4	0.500	0.000	0.413	O7	0.250	0.830	0.120
Ca5	0.378	0.252	0.198	O/OH8	0.159	1.000	0.211
Ca6	0.378	0.752	0.198	O/OH9	0.035	1.000	0.113
Si1	0.250	0.287	0.056	O10	0.250	0.000	0.348
Si2	0.250	0.707	0.056	O11	0.133	0.240	0.411
Si3	0.159	1.000	0.141	O12	0.367	0.240	0.411
Si4	0.250	0.207	0.373	O13	0.250	0.335	0.310
Si5	0.167	0.500	0.282	O14	0.175	0.500	0.213
Si6	0.250	0.787	0.373	O15	0.250	0.645	0.310
O1	0.250	0.170	0.120	O16	0.133	0.756	0.411
O2	0.250	1.170	0.120	O17	0.367	0.755	0.411
O3	0.367	0.255	0.019	O18	0.038	0.501	0.306
H2O(1)	0.500	0.500	0.303	H2O(2)	0.500	0.000	0.110

With the help of these derived coordinates, a Fortran program was written to replicate the atomic structure of calcium silicate hydrate given by Subramani [15] and Hamid[34]. The dimension of each simulation box is a = 11.17Å, b= 7.39Å and c = 22.7Å. The simulation box of crystalline calcium silicate hydrate contained 144 atoms

and the simulation box of the proposed calcium silicate hydrate structure contained 124 atoms. Figure 4.1 and Figure 4.2 display the calcium silicate hydrate structure and the proposed calcium silicate hydrate structure in two dimensions.

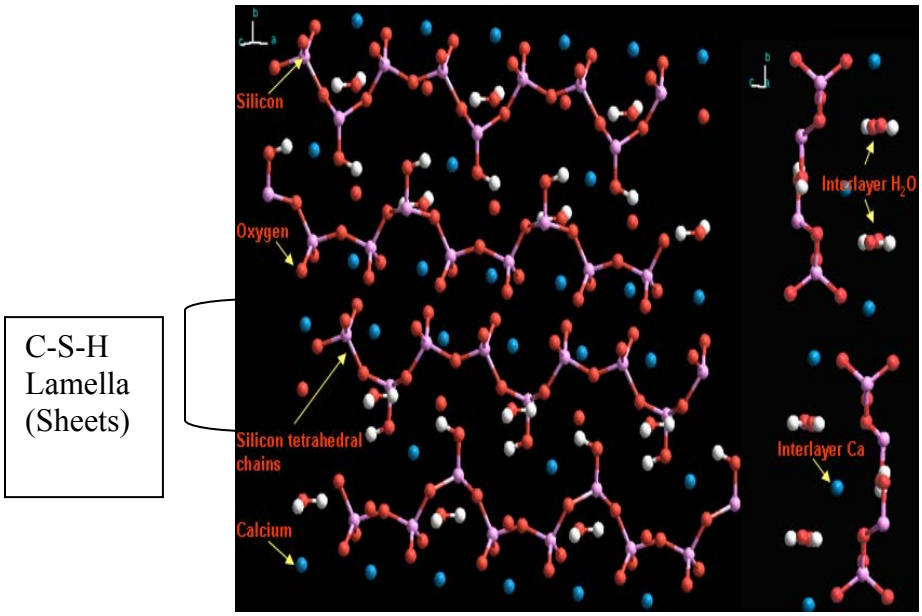

Figure 4.1 Structure of Tobermorite [15].

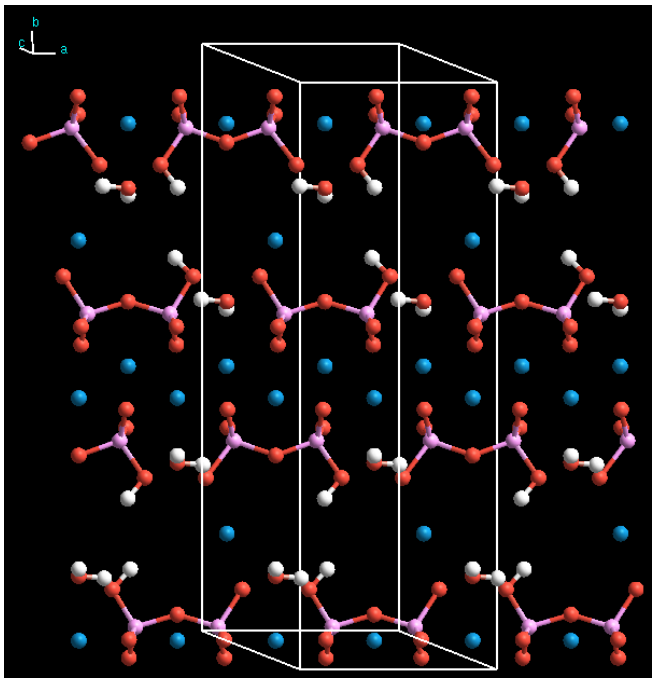

Figure 4.2 Structure of Proposed C-S-H [15].

4.2.3 Atomic Interactions

The interactions between atoms in this simulation are characterized by the interatomic potential energy. The potential energy of a structure can be computed by summing up all different types of interactions that occur in a system i.e. two body interactions and three body interactions. In this study, Buckingham, Stillinger-Weber and Coulomb Potential were used to describe atomic interactions. The parameters for Buckingham, Stillinger-Weber and Coulomb potential were found in Faucon et al [37-38] and other literature [51]. Refer to Appendix E for parameters of these potential equations.

4.2.4 MD Simulation Conditions

Periodic boundary conditions were employed to simulate a larger system of C-S-H gel. The conjugate gradient method was used to equilibrate the structure of C-S-H gel. Next, NPT (constant number of atoms, *N*, constant pressure, *P*, and constant temperature, *T*) cannonical ensemble was employed to control the temperature and pressure of the system. Initially, the temperature was set to $T=25\ ^{o}C\ (300^{o}K)$ and the pressure was set at $P=0.0\ MPa$. Nosé Hoover thermostat temperature control method and the Nosé Hoover barostat pressure method were used for NPT calculations. A time step of 1 femtosecond (fs, 10^{-15} sec) was chosen since 1fs is suitable for most purposes. The dynamic time ranges from 100 to 400 picoseconds (ps, 10^{-12} sec) depending on the size of the simulating cell, which ensures thermodynamic equilibrium and the convergence of energy with a reasonable computational time. Finally, a constant uniaxial strain rate is applied to the simulation cell along the b direction [100] and NPT conditions ($T=25\ ^{o}C\ (300^{o}K)$ and $P=0.0\ MPa$.) was applied to the other two directions (a and c). An illustration of this simulation cell is shown in Figure 4.3. The atoms will move in the direction of the deformation. Then a MD simulation is performed to equilibrate the system and measure its corresponding stress.

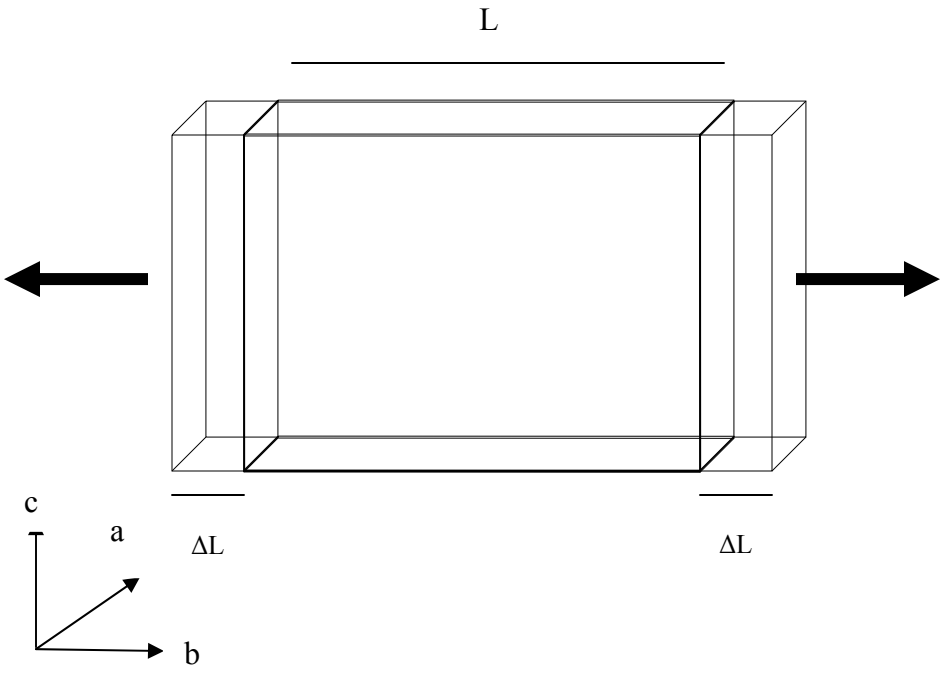

Figure 4.3 Illustration of applying strain rate to the atomic structure of C-S-H.

where

ΔL = change in length of box

L = Length of box

4.2.5 Determination of Strain and Young's Modulus

If a uniaxial tension/compression is applied to a material, the stretching or compression of the simulation cell is calculated as the strain (ε).

Where

$$\varepsilon = \frac{\Delta L}{L_0} \tag{4.1}$$

ΔL = change in length

L_o = original length

The ratio of stress to strain yields the Young's modulus (E) for that material. The equation is given by equation 4.2.

$$E = \frac{\sigma}{\varepsilon} \tag{4.2}$$

The strain is calculated after collecting data from the output file. At the end of each time interval a new box length is computed. Strain is unitless and is defined as delta/length, where length is the original box length and delta is the change relative to the original length.

The stress is also computed per time step. The elastic modulus can also be approximated from the slope of the linear portion of the curve. The elastic modulus of both C-S-H structures was computed from the slope of the linear portion of the stress-strain curve. The linear portion evaluated is from the origin to the point corresponding to 0.4 times the maximum stress.

4.3 Procedures for determining the Mechanical Properties of Packed Tobermorite Structures

Further work was done to incorporate the packing factor into the computational model of C-S-H gel. The General Lattice Utility Program or GULP software was used to model the atomic structure and predict the mechanical properties of packed C-S-H units

It is understood that C-S-H does not have a single porosity or single packing mode. But, if the C-S-H structures were to be modeled with porosity, then the input computational domain shall be constructed as shown in Figure 4.4. Figure 4.4 is not drawn to scale. The unit cells of Tobermorite could be stacked together to form a cluster of unit cells of Tobermorite. These clusters that occupy the computational domain could then be oriented in different directions while also ensuring that the density of the system matches experimental data.

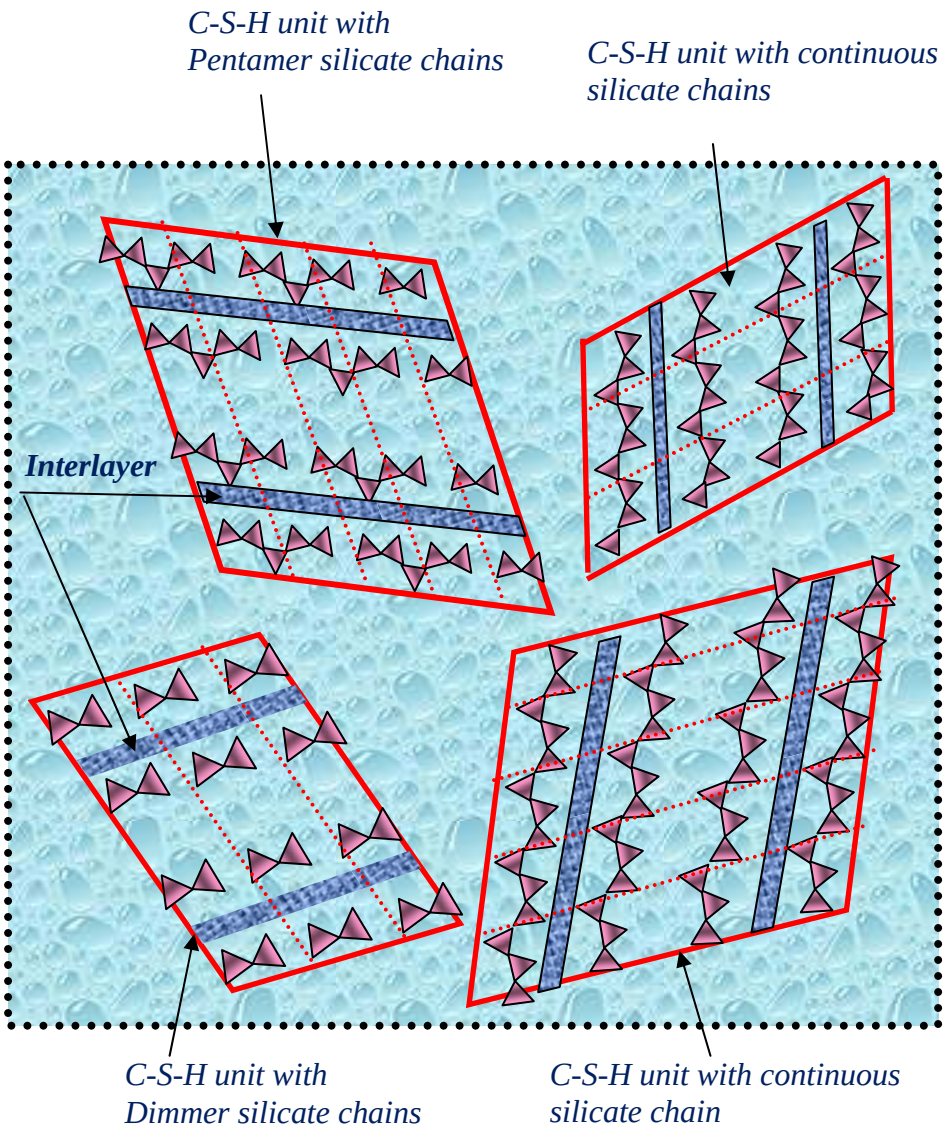

Figure 4.4 A Possible Configuration of C-S-H Units [15].

However, constructing such a domain is not possible in the current molecular static simulations. For example, to construct a single C-S-H unit of about 5nm in length, it requires about 7 number of unit cells of crystalline calcium silicate hydrate structures (Tobermorite) (~1000) atoms to be stacked together. The lattice dimension 'b' for Tobermorite is 7.39 A° and the number of atoms in a unit cell of Tobermorite is 144. In molecular static simulations, the size of the computational domain is very small. The C-S-H takes the form of very small crystals packed closely together to form a very dense structure. This work attempted to construct a smaller version of Figure 4.4 through packing unit cells crystalline calcium silicate hydrate structures. Each unit cell can represent a 5nm particle.

4.2.1 Generating the Structure of Packed Tobermorite Unit Cells

The crystalline structure chosen is Hamid's [34] Tobermorite 11 Aº (Ca/Si-1.00). Before building the structure of packed Tobermorite structures, the first task is establishing the dimensions, volume, and density of the simulation box. Once the density of the simulation cell is determined, the total mass of atoms required to occupy the simulation cell can be found. The number of Tobermorite unit cells needed in the simulation cell can be found by dividing the total mass of atoms in simulation cell by the total mass of atoms in a Tobermorite unit cell.

For this work, three simulation cells were created. The names of the simulation cell are Stack 1, Stack 2 and Stacks 3. Each simulation cell contained four (4) Tobermorite unit cell and the number of atoms in each simulation cell is 576 atoms. The dimension of each simulation cell is shown in Table 4.8. The configuration of atoms in "Stack 1" is created by translating the atoms in a Tobermorite unit cell to 4 regions (

corners) of the simulation cell . The Tobermorite unit cells are spaced angstroms apart to incorporate “breaks” in the silicate chains. Figure 4.5 illustrates a sketch of Stack 1. In Figure 4.5, Tobermorite unit cxell 1 is located at the origin. In stack 1, Tobermorite unit cell are 5.22 angstroms apart in the b direction and 6 angstrom apart in the c direction. In Stack 2, Tobermorite unit cell are 10.22 angstroms apart in the b direction and 0 angstrom apart in the c direction as shown in Figure 4.6. Stack 3 was constructed differently in that the Tobermorite unit cells are not placed at the corners. Instead, the first and forth Tobermorite unit cell are centered in the simulation box. The distance between first and forth Tobermorite unit cells is 21 angstroms in the c direction. The second and third unit cells are placed in the space between the first and forth Tobermorite and spaced 3.22 angstrom in the b direction. Figure 4.7 illustrates a sketch of Stack 3.

A Fortran program was written to translate Tobermorite unit cells in the simulation cell. The Fortran code gave the atomic coordinates of all atoms in the simulation cell. The atomic coordinates of atoms are in Cartesian coordinates, therefore γ = 90 degrees. A Sample Fortran code is presented in Appendix G. Space group chosen for Molecular Statics computation is number 1(no symmetry). Charges of atoms are the same as the previous study.

Table 4.8 Dimensions of Simulation Cells

Simulation Cell	Number of Atoms	a (Å)	B (Å)	C (Å)
Stack 1	576	10	20	50
Stack 2	576	10	25	44
Stack 3	576	13	18	65

$

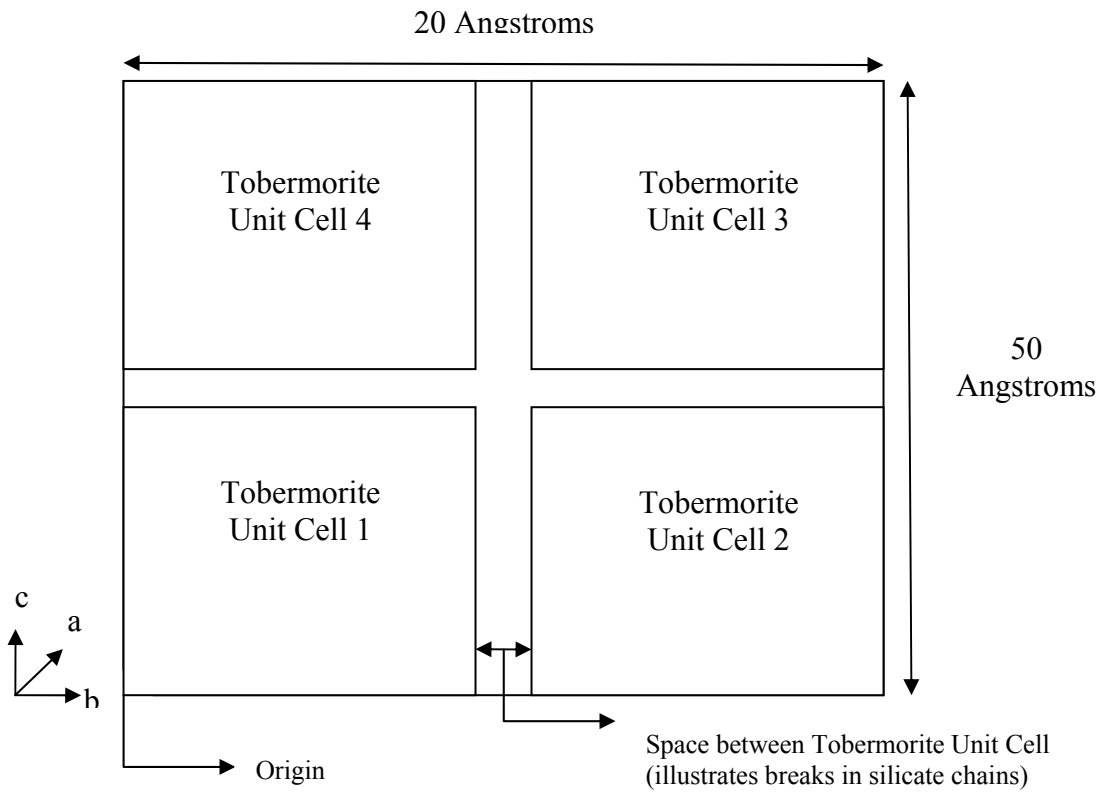

Figure 4.5 Illustration of Stack 1

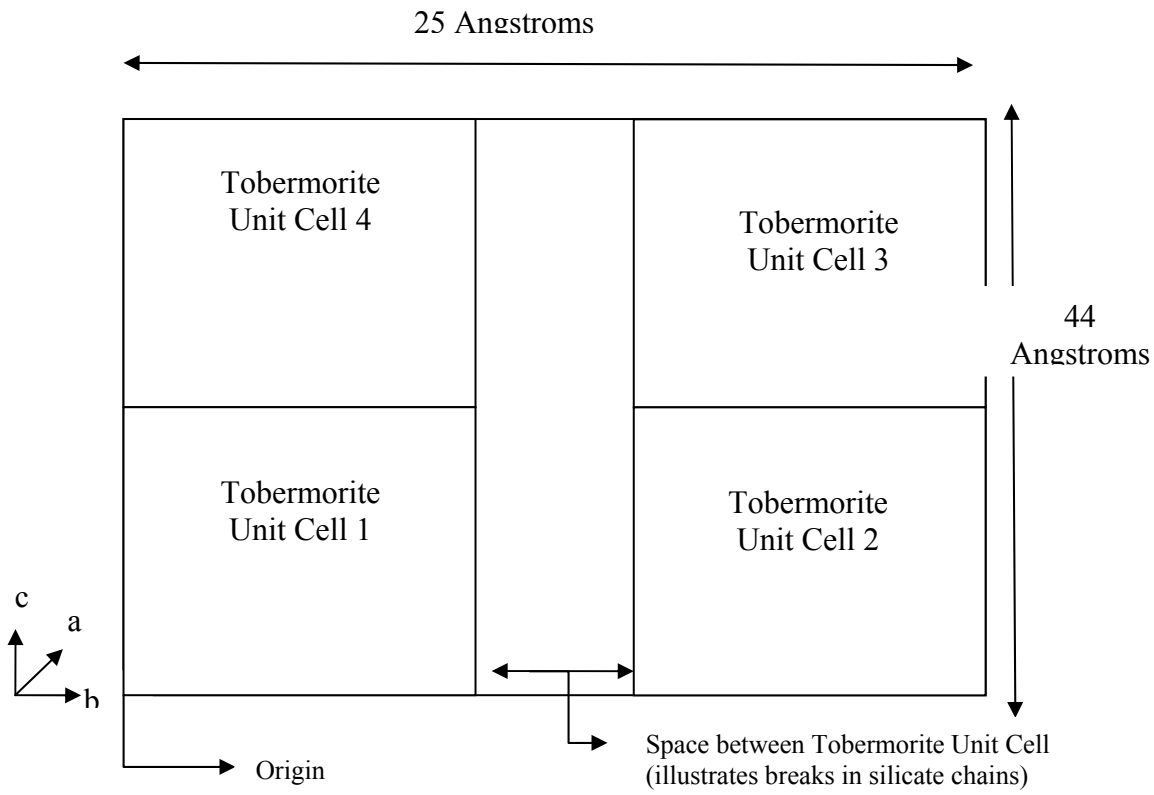

Figure 4.6 Illustration of Stack 2

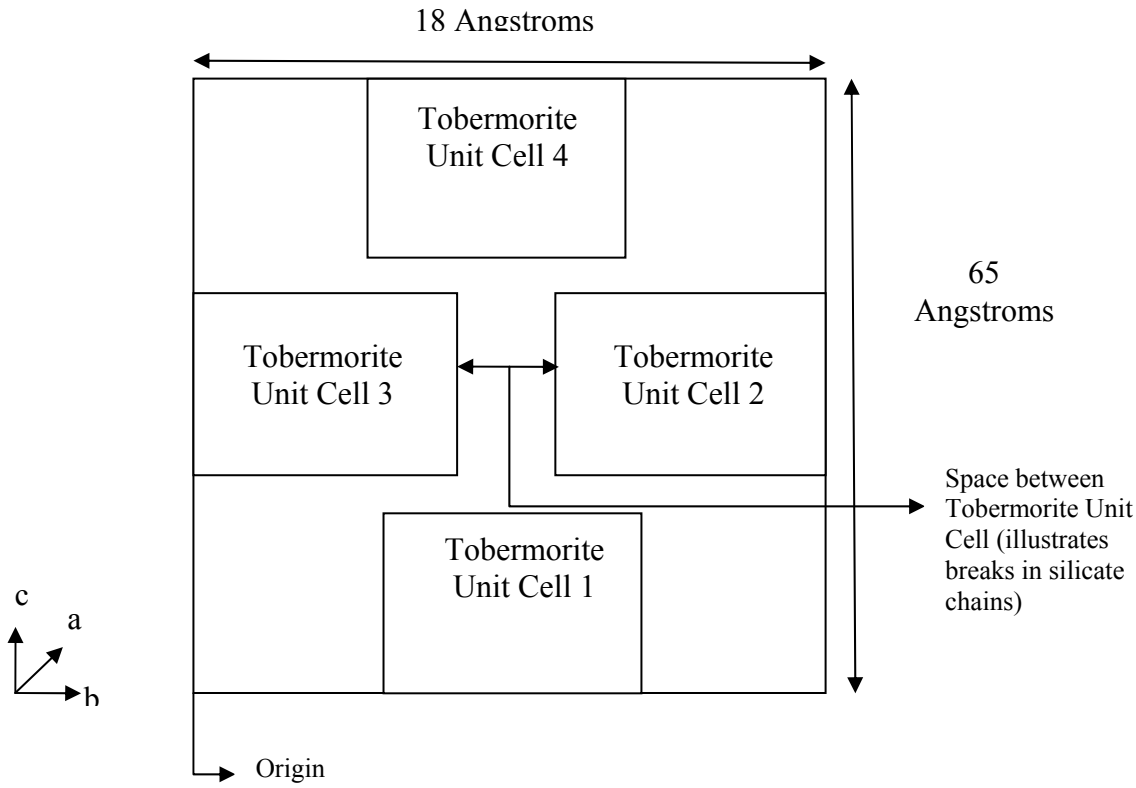

Figure 4.7 Illustration of Stack 3

4.2.2 Atomic Interactions

In this study, Buckingham, Stillinger-Weber and Coulomb Potential were used to describe atomic interactions. The parameters for Buckingham, Stillinger-Weber and Coulomb potential were found in the GULP library. Refer to Appendix G for parameters of these potential equations

CHAPTER 5: RESULTS AND DISCUSSION

5.1 Crystalline Calcium Silicate Hydrates

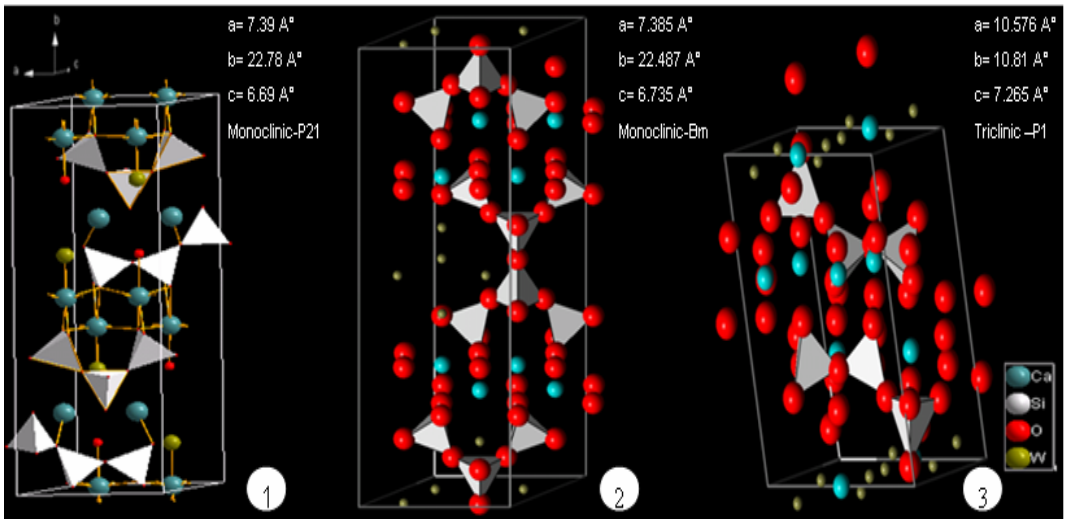

Figure 5.1 Atomic Configuration of Three Mineral Structures 1) Tobermorite 11A° [Hamid (34)] 2) Tobermorite [Merlino(35)] 3) Jennite [Merlino(36)]. Visualized using Diamond (demo) Version and Xtal Software

Atomistic simulations were carried out for different crystalline calcium silicate hydrate minerals with different Ca/Si ratio and Water/Ca ratio. Figure 5.1 shows the atomic structure of Tobermorite and Jennite. Energy minimization techniques via Molecular Statics were used to optimize each atomic structure. Table 5.1 shows the comparison of the parameters before and after the optimization of Tobermorite structure with Ca/Si-0.

Table 5.1 Optimized Parameters of Tobermorite Structure Ca/Si-0.83

Cell Parameters	Units	Before Optimization	After Optimization
A	A°	7.39	7.349935
B	A°	22.779	23.211867
C	A°	6.69	6.759629
Alpha	°	90	90
Beta	°	123.49	122.894943
Gamma	°	90	90
Volume	$A°^3$	939.208385	968.331306
Lattice energy	eV	-1767.13	-1925.93
Density	g/cm^3	2.383674	

5.1.1 Mechanical Properties of Crystalline C-S-H Models

The energy minimization calculations generated reliable estimates of the mechanical properties (Young's modulus, Bulk modulus, Shear modulus, Poisson's ratio) of the different crystalline C-S-H models. High values of Young's modulus (E) were observed for C-S-H structures that contain low Water/Ca ratio. The structure becomes relatively soft when more water is present in the structure and hence low E values were observed for higher Water/Ca ratios. Calculated values of the properties are in good agreement with the data obtained from experiments by Plassard et al [6] and simulations carried out by Manzano et al [41].

Table 5.2 Bulk Properties of Crystalline Calcium Silicate Hydrate

C-S-H Model	Chemical formula	Ca/Si	Water/Ca	Bulk modulus K Gpa	Shear modulus G Gpa	Poissons ratio γ	Elastic modulus E Gpa
Tobermorite 11A° (Hamid 1981)	$Ca_4Si_6O_{14}(OH)_4.2H_2O$	0.67	0.5	58	28	0.29	72
Tobermorite 11A° (Hamid 1981)	$Ca_5Si_6O_{14}(OH)_2.2H_2O$	0.83	0.4	60	35.5	0.25	89
Tobermorite 11A° (Hamid 1981)	$Ca_6Si_6O_{18}.2H_2O$	1	0.33	79	37	0.30	96
Tobermorite 11A° (Merlino 1999)	$Ca_4Si_6O_{15}(OH)_2.5H_2O$	0.67	1.25	46	39	0.17	91
Jennite (Merlino 2004)	$Ca_9Si_6O_{18}(OH)_6.8H_2O$	1.5	0.89	51	27	0.28	69
Foshagite	$Ca_8Si_6O_{16}(OH)_2$	1.333	0	75	39	0.28	100

Nevertheless, the mechanical properties determined from experiments for samples of bulk cement paste showed that the bulk modulus is in the range of 17-18 GPa (Cho et.al [53]). The bulk modulus values (listed in Table 5.2) for various crystalline calcium silicate hydrates overestimated the available experimental data for the cement pastes by nearly 4 to 5 times. However the values for the Poisson's ratio were in reasonable agreement with the experimental data. This could be explained by the fact that the Poisson's ratio is related to a ratio between bulk modulus (K) and shear modulus (G). Some probable factors that could be responsible for such exaggerated values are: a) Unaccountability of gel porosity in the C-S-H structure b) Modeling a defectless C-S-H structure.

5.2 Breaking the Bonds in Crystalline C-S-H Models

5.2.1 Approach 1

A super cell was constructed by replicating the unitcell of Tobermorite. In this approach, point defects were introduced to break the silicate chains by removing particular oxygen atoms that connect the silica tetrahedra chains (as marked by a yellow box shown in the Figure6.2). The length of silicate chains is thus restricted to a maximum of two tetrahedra. Energy minimization was run for the above setup with "Qok" option (to neglect the charge imbalance induced into the system) and E, K, G values were recalculated. Unfortunately, the values were not in agreement with the literature data. The reasons for the anomaly were investigated and analyzed. Since the major forces that are responsible for holding the atoms together in an ionic system like C-S-H is the electrostatic forces, the charge neutrality of the system is the most important criteria in these types of problems. If the charge neutrality of the ionic systems gets disturbed it affects the stability of the structure and thus, errors occur in the calculation of energy. Hence, an alternate method was investigated to restrict the chain length of the silicate chains without affecting the charge neutrality of the C-S-H structure.

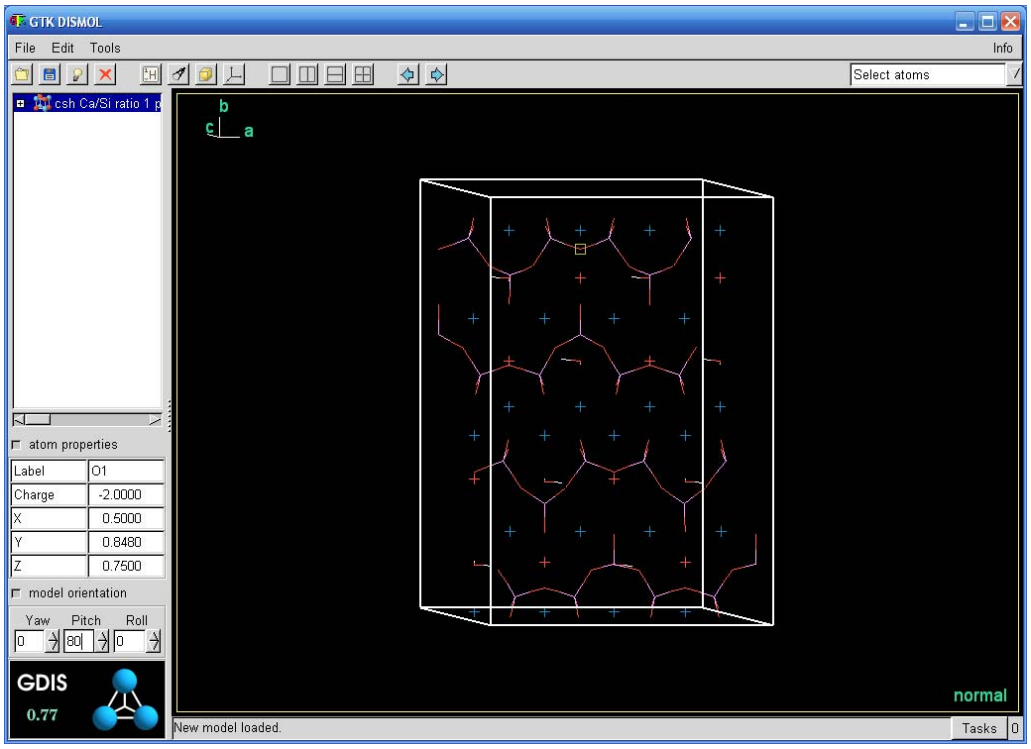

Figure 5.2 Snapshot of C-S-H Structure from GDIS Visualization Software

5.2.2 Approach 2

Plassard et [6] reported that the bridging silica tetrahedra (encircled in red in Figure 5.3) may be missing in the Drierketten type of silicate chains observed in Tobermorite like C-S-H. To corroborate the above statement, the site potentials of the silicon atoms i.e., the potential energies of silicon atoms at its position in the atomic structure were determined using Molecular Mechanics (Figure 5.3) simulations. Calculation of site potentials of the silicon atoms will provide information to identify the less stable silicon atoms in the silicate chains.

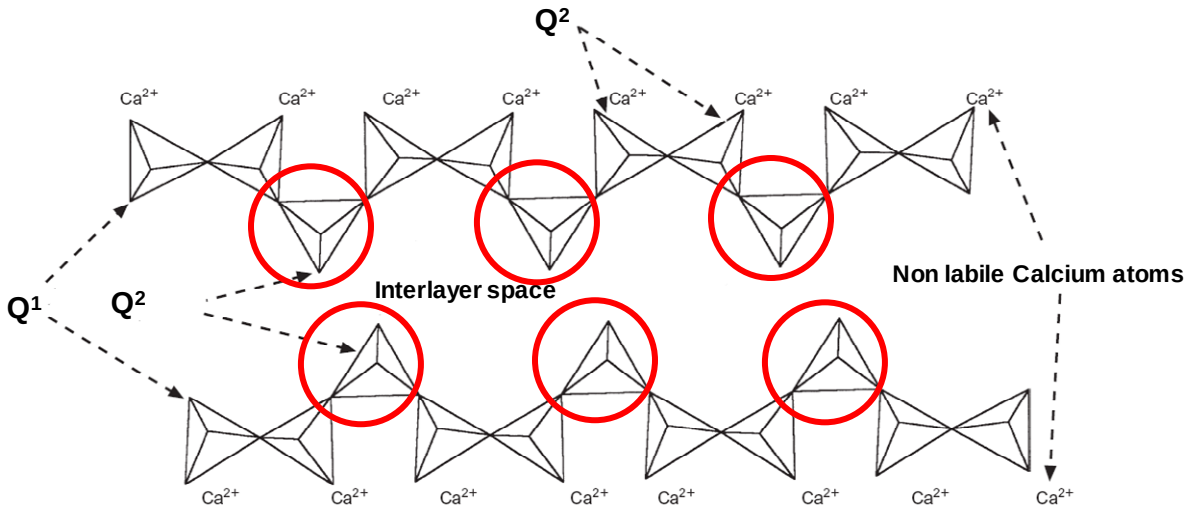

Figure 5.3 Drierketten Type of Silicate Chains
Observed in Tobermorite.
Bridging Silica Tetrahedra are Encircled in Red.

5.2.2.1 Site Potentials of Silicon Atoms

The potential energies of all six silicon atoms in the unit cell of the Tobermorite structure were determined using GULP code. The option "pot" in GULP calculates the electrostatic site potentials of the atoms. Figure 5.4 shows the site potentials of the silicon atoms in the Tobermorite structure corresponding to two different Ca/Si ratios (0.66 and 0.83). In both cases i.e., for Ca/Si ratio 0.66 and 0.83, the potential energies of silicon atoms at sites 3 and 5 are the maximum. To put it in simple terms, the more negative the potential energy, higher is the cohesive energy of an atom. If an atom has higher cohesive energy, it is energetically more stable. Therefore, the silicon atoms at sites 3 and 5 can be considered as the energetically less stable silicon atoms in the Tobermorite structure. This can also be viewed from another perspective. The bridging silica tetrahedra are the ones that carry hydroxyl molecules in the Tobermorite structure (Ca/Si-0.66 and 0.83). Each of the bridging silicon tetrahedra in the Tobermorite type C-S-H structure corresponding to Ca/Si-0.83 carries only one hydroxyl molecule with it, where as it carries two hydroxyl molecules in the case of Ca/Si-0.66. It is obvious that the presence of hydroxyl atoms increases the exchange capacity of the cation to which it is attached. Hence, the presence

of hydroxyl molecules weakens the stability of the bridging silicon atoms and makes it vulnerable for cation exchange. The potential energy of silicon atoms at sites 3 and 5 for Ca/Si-0.83 were found to be -51.872 eV and -51.861 eV and it is comparatively less than those observed for Ca/Si-0.66 (-50.243 and -50.203 eV). Thus, it can be said that the silicon atoms at sites 3 and 5 in the Tobermorite structure corresponding to Ca/Si-0.66 are energetically less stable compared to those in Ca/Si-0.83. This could be explained by the number of hydroxyl molecules present at each bridging silicon sites in the two different Ca/Si ratios. Hence, it can be concluded from this study that the bridging silica tetrahedra could be removed from the atomic structure to introduce rupture in the silicate chains.

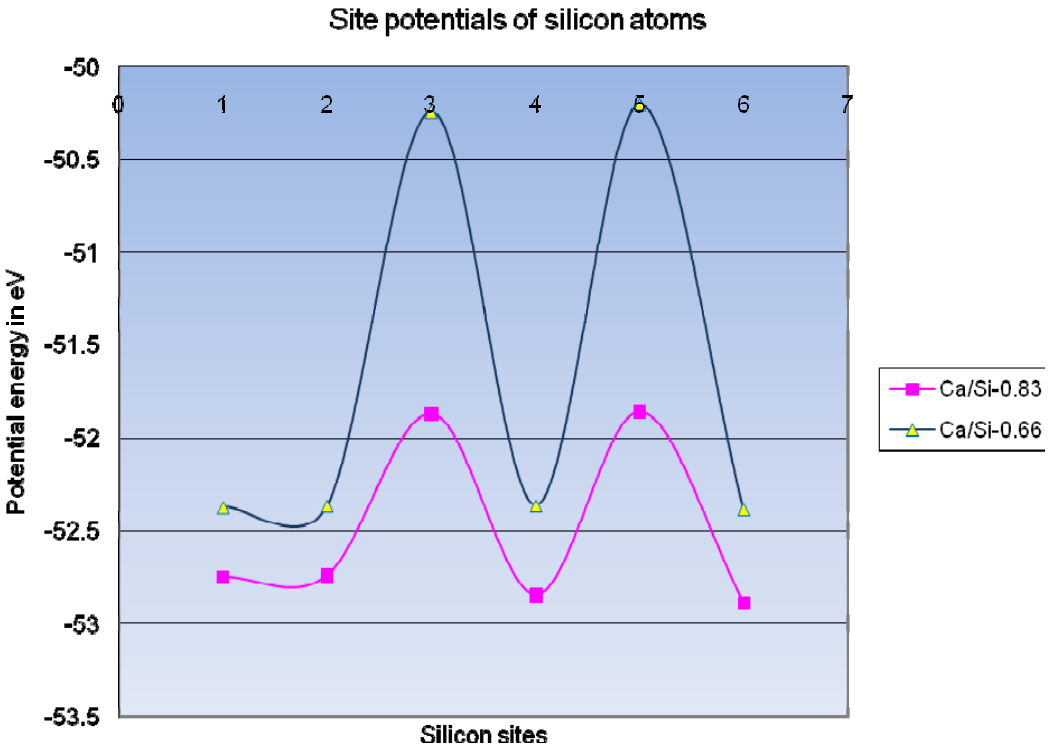

Figure 5.4 Site Potentials of Silicon Atoms

5.2.2.2 A Possible Structure of C-S-H

The removal of the bridging silica tetrahedra from the structure, however, affects the charge neutrality of the system. The charge imbalance due to the omission of bridging tetrahedra could be accounted for by adding protons to the other two oxygen atoms of the silica tetrahedra or by introducing calcium atoms in the interlayer. Therefore, the length of the silicate chains in C-S-H could be condensed to two silica tetrahedra (dimmers) instead of an infinite length as observed in those crystalline minerals.

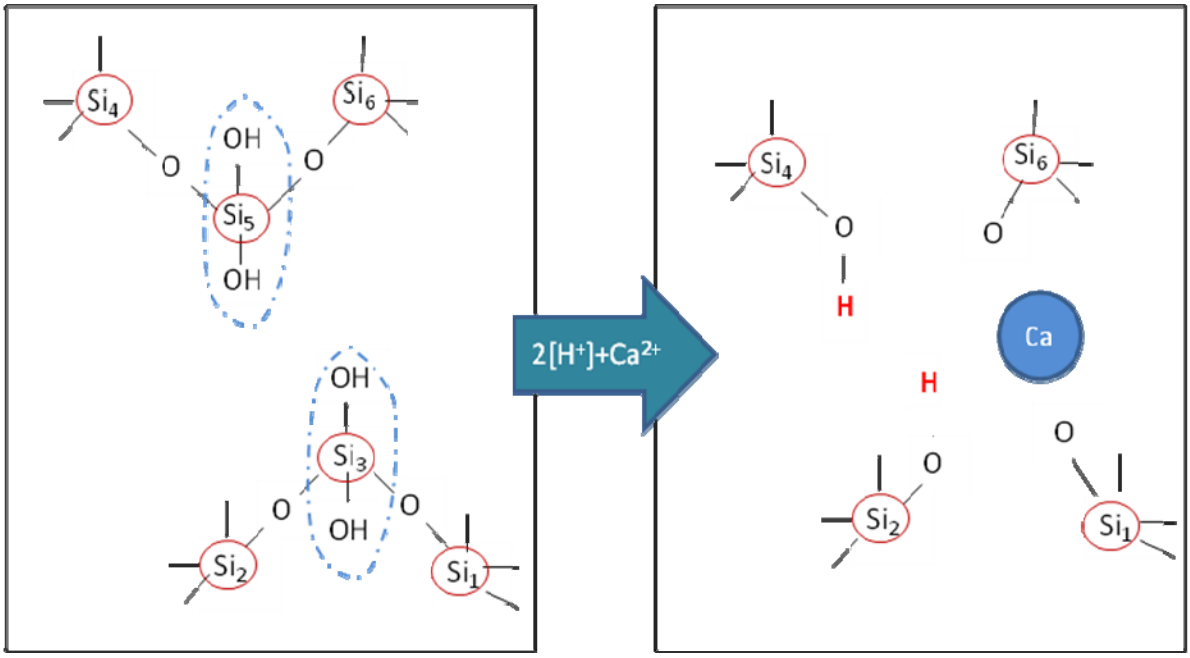

Figure 5.5 Breaking the Silicate Chains in Tobermorite

The bridging silica tetrahedra $(Si_{[3]}(OH)_2)^{2-}$ and $(Si_{[5]}(OH)_2)^{2-}$ are removed from the Tobermorite structure (Ca/Si-0.66) as illustrated in Figure 5.5. The omission of these two bridging silica tetrahedra leaves a negative charge of 4. The charges are compensated for by attaching protons to oxygen atoms of Si_4 and Si_2 atoms and adding a calcium atom at the interlayer. The protons that are attached to the oxygen atoms of Si_4 and Si_2 are positioned in such a way that Si_4-O-H and Si_2-O-H forms 108° and also, the O-H distances are always 1.0 A°. Therefore, the count of silicon atoms decreases (from 6 to 4)

in the unit Tobermorite structure. In other words, this increases the Ca-Si ratio from 0.66 to 1.25, which is in reasonable agreement with the ratio of Ca-Si ratio observed in the experiments conducted on bulk cement paste. Therefore, the silicate chains were broken without affecting the charge neutrality of the structure. This forms a dimmer C-S-H i.e., C-S-H that has two silicate tetrahedra as shown in Figure 5.65 The bulk properties of the new C-S-H model were determined using energy minimization methods. Since porosity could not be modeled in the present work, a packing factor is included in the calculation of bulk properties to consider its porous nature which will otherwise be left unaccounted. Porosity is accounted in the current calculations by using a packing factor in the Mori-Tanaka equations to re-calculate the bulk properties of the C-S-H from the previously determined values through GULP code. Manzano et al [51] choose a packing factor of 0.7, this was suggested by Taylor [8]. However, in this work, a packing factor (Φ) of 0.69 is used, obtained by taking an average value of the packing densities of LD and HD C-S-H. The C-S-H gel modeled was assumed to have 31% porosity in its volume. The rescaled bulk (K_{new}) & shear modulus (G_{new}) values were calculated using Mori-Tanaka equations (5.1), (5.3) and (5.2), (5.4) respectively, that involves the packing factor (Mori et.al [54].

$$K_{new} = \Phi \frac{(1-\alpha)}{(1-\alpha\Phi)} K_{cal} \tag{5.1}$$

$$G_{new} = \Phi \frac{(1-\beta)}{(1-\beta\Phi)} G_{cal} \tag{5.2}$$

where,

$$\alpha = \frac{3K_{cal}}{3K_{cal} + 4G_{cal}} \tag{5.3}$$

$$\beta = \frac{6K_{cal} + 12G_{cal}}{15K_{cal} + 20G_{cal}} \tag{5.4}$$

The bulk properties thus found, K=22 GPa, G=14 GPa E = 34 GPa, were comparable to the experimental and simulation results. [K=18 GPa, G=9.7 GPa, E = 20-30 GPa] – Manzano.H (2007). Hence, it can be deduced from this work that the length of the silicate

chains does have a significant effect on the mechanical properties of C-S-H. Also, the newly constructed Dimmer C-S-H could be a possible representative structure for C-S-H.

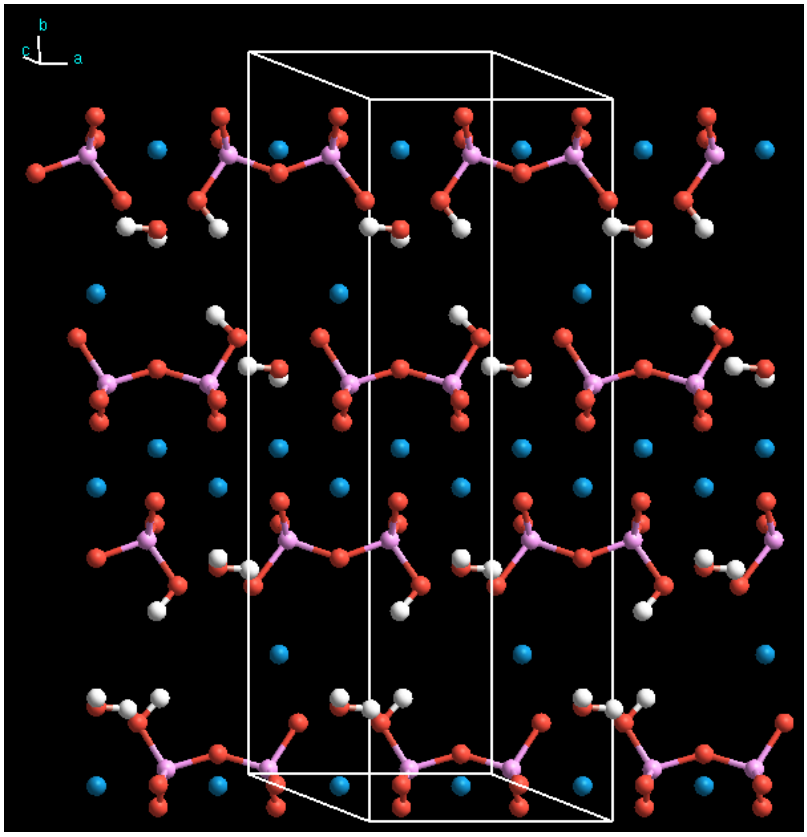

Figure 5.6 Proposed Structure for C-S-H

5.3 Stress–Strain Behavior of Calcium Silicate Hydrate structures

In this study, a uniaxial tension and compression test was performed on two atomic structures of Calcium Silicate Hydrate. The first structure is a Tobermorite crystal (structure has continuous silicate chains) and the second structure is a proposed C-S-H structure (structure has dimmer silicate chains). The maximum strain allowed for both atomic structures is 0.0005(tension) and 0.005(compression). The responses of both structures to a strain rate of 0.00002/ps are shown in Figure 5.7 and Figure 5.8. Attractive stresses (tensile) are negative and repulsive stresses (compression) are positive. At low strains (from 0 to 0.0005) Ang/Ang the tensile stress response for both C-S-H units is non linear and the stress fluctuate from attractive stresses to repulsive stresses. In Figure 5.1a, the stress-strain data for Tobermorite, shows a maximum stress of about 600MPa for a strain of 0.0005. In Figure 5.8a, the stress-strain data for the proposed C-S-H structure, reveals a maximum stress of about 50 MPa for a strain of 0.005. Both structures exhibit similar behaviors when loaded in uniaxial compression. Both stress–strain curves show a compressive stress response of about 600 MPa for a strain of 0.005

The graphically represented data has shown that the constitutive response of calcium silicate hydrate structures when subjected to uniaxial loading (tension and compression) are magnitudes higher than the macro level data for cement paste for the same strain values. In addition, the strain at failure cannot be observed from the stress-strain data of both structures as compared to macro level data for cement paste. The strain at failure for cement at macro level is 0.003(compression) and 0.0003(tension). The strain at failure at the atomic level may be greater than the strain at failure at the macro level. However, the MD simulations indicate that at low strains the C-S-H unit with continuous silicate chains (Tobermorite) is able to resist tensile stresses of 600 MPa or greater, as a result of attractive electrostatic forces and silicate bond forces. However, it was observed that the C-S-H unit with dimmer silicate chains (proposed C-S-H) was only able to resist tensile stresses around 50 MPa. It is believed that in C-S-H unit with dimmer silicate chains has less O-Si-O bonding due to breaks in the silicate chains. Breaks in silicate chains leads to reduction in tensile strength.

In order to visualize the strain at failure at the atomic level this would require the simulation to run for more than two weeks. Therefore, a higher strain rate (0.0002/ps) was applied to both atomic structures to reduce computational time to two days. Even at high strain rates the tensile response to strains ranging from (0 to 0.0005) Ang/Ang are nonlinear but the data is more scattered. The responses of both structures are shown in Figure 5.9 and Figure 5.10. The strain at failure for Tobermorite (0.35 Ang/Ang) and the proposed C-S-H (0.05 Ang/Ang) was found to be much higher than the corresponding values at macro scale (0.0003 Ang/Ang). This could possibly be attributed to the higher loading rates. The tensile stresses of the Calcium Silicate Hydrate structures are three magnitudes higher than the macro level (2MPa). The compressive stresses are two magnitudes higher than the macro level (20-60 MPa).

The stress response (tension and compression) is almost linear up to a maximum stress then decreases to zero. In Figure 5.9a, the stress-strain data for Tobermorite, shows a tensile stress of about 12000 MPa (12 GPa) for a strain of 0.35. In Figure 5.10a, the stress-strain data of the proposed C-S-H, shows a maximum tensile stress of about 4000 MPa (4 GPa) for a strain of 0.05. At zero stress the forces acting on each atom is nearly zero. It was also observed in Figure 5.9b and 5.10b that both structures exhibit similar behavior when loaded in compression, however in tension, both structures exhibit dissimilar behavior due to bond breakage. In addition the Tobermorite crystal (continuous silicate chain) is as strong in tension as in compression. The tensile strength (~12,000MPa) is 80% of the compressive strength (~15,000MPa). This is not the case for the proposed C-S-H (dimmer silicate chains). The tensile strength (~3500 MPa) is approximately 23% of the compressive strength (~15,000 MPa). A magnification of the tensile response of the proposed C-S-H (dimmer silicate chains) is shown in Figure 5.5.

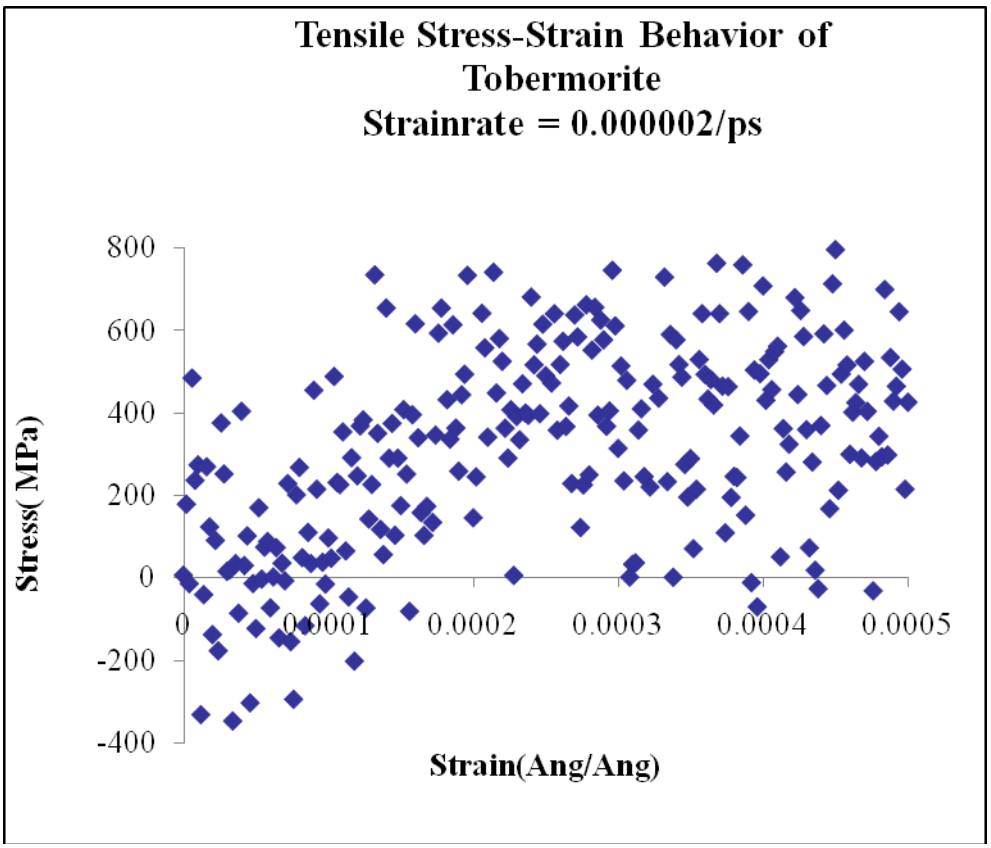

Figure 5.7(a) Tensile Stress-Strain Behavior of Tobermorite

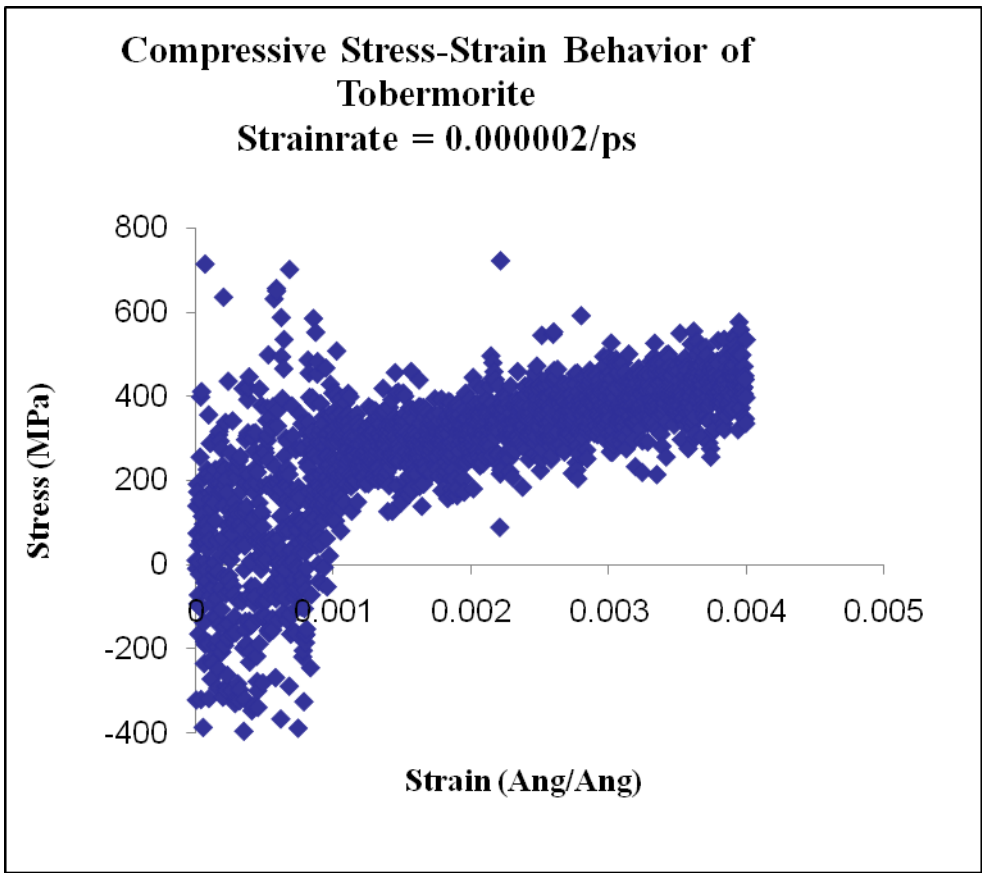

Figure 5.7 (b) Compressive Stress-Strain Behavior of Tobermorite

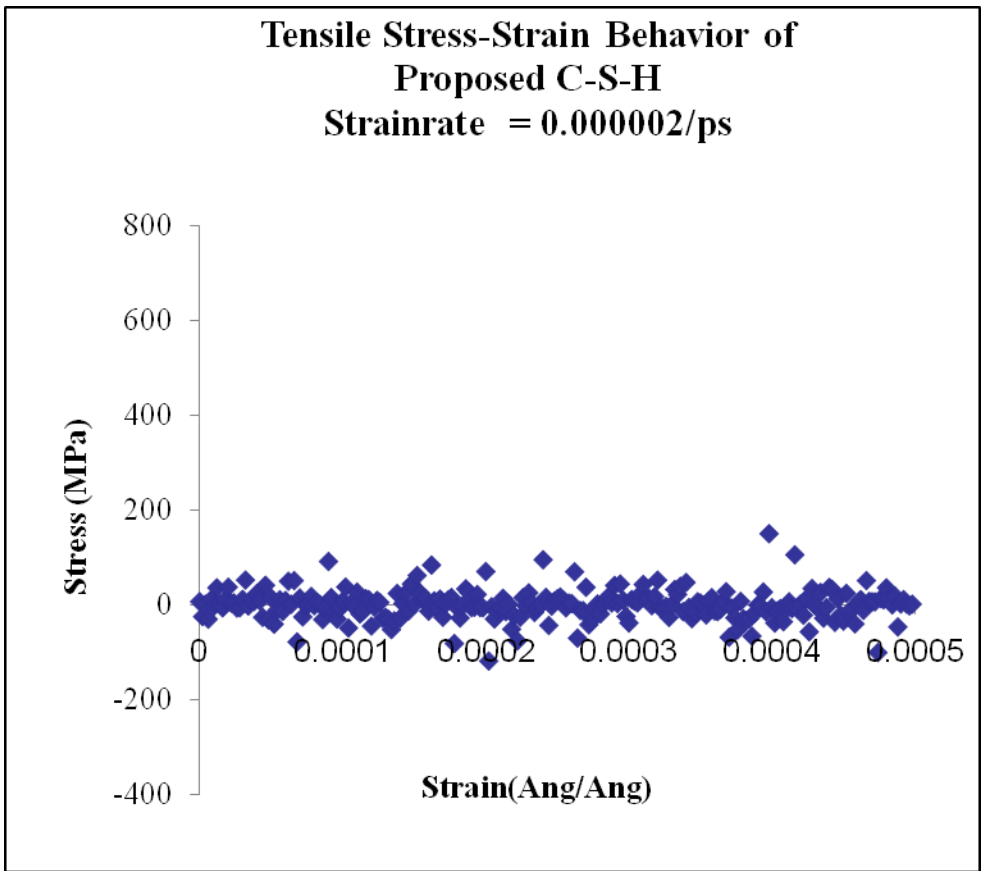

Figure 5.8 (a) Tensile Stress-Strain Behavior of Proposed C-S-H

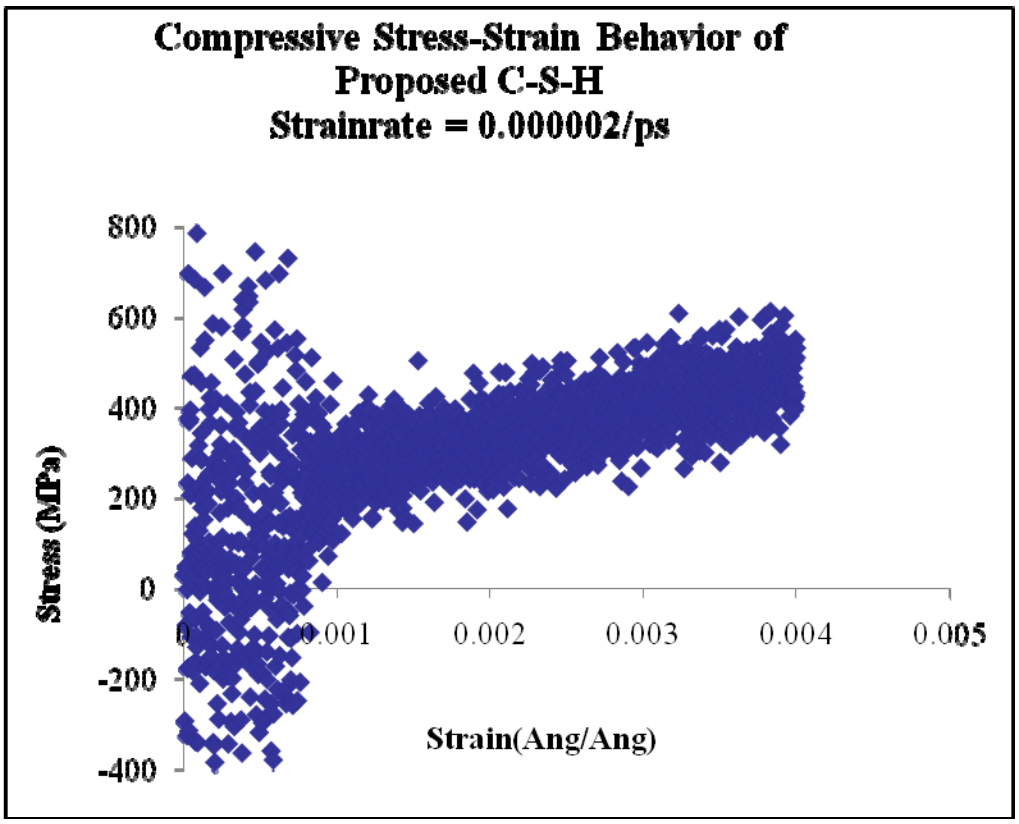

Figure 5.8 (b) Compressive Stress-Strain Behavior of Proposed C-S-H

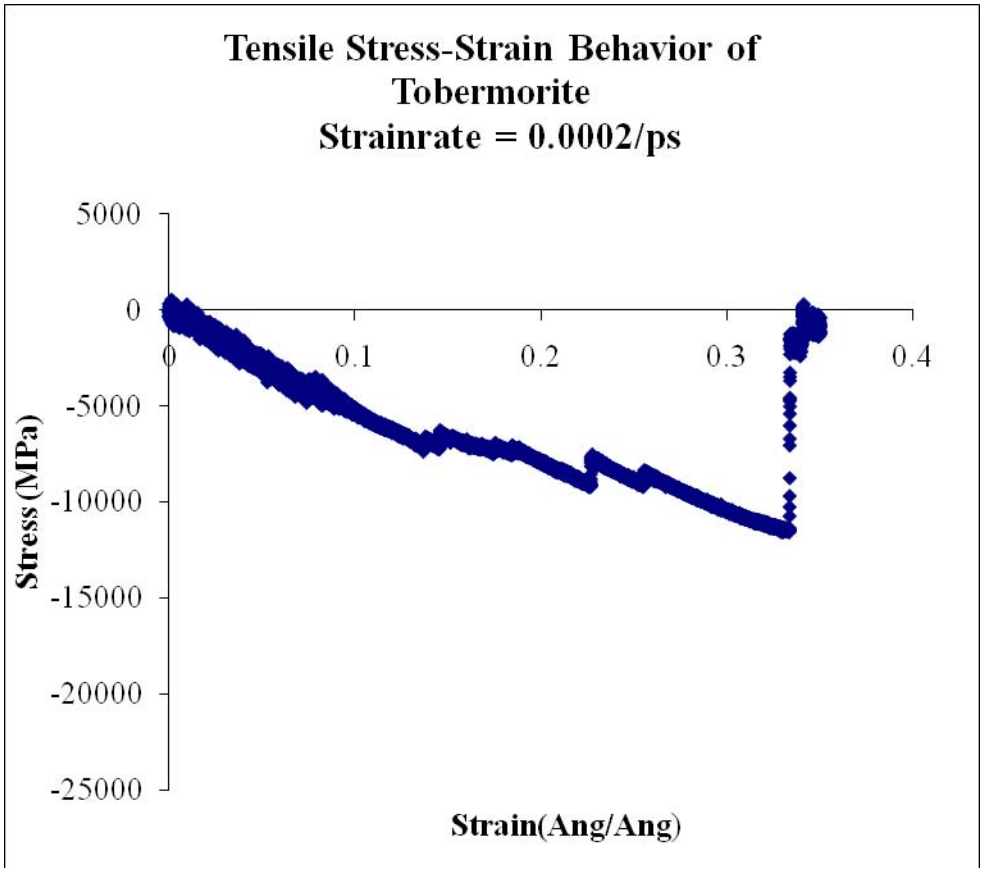

Figure 5.9 (a) Tensile Stress-Strain Behavior of Tobermorite

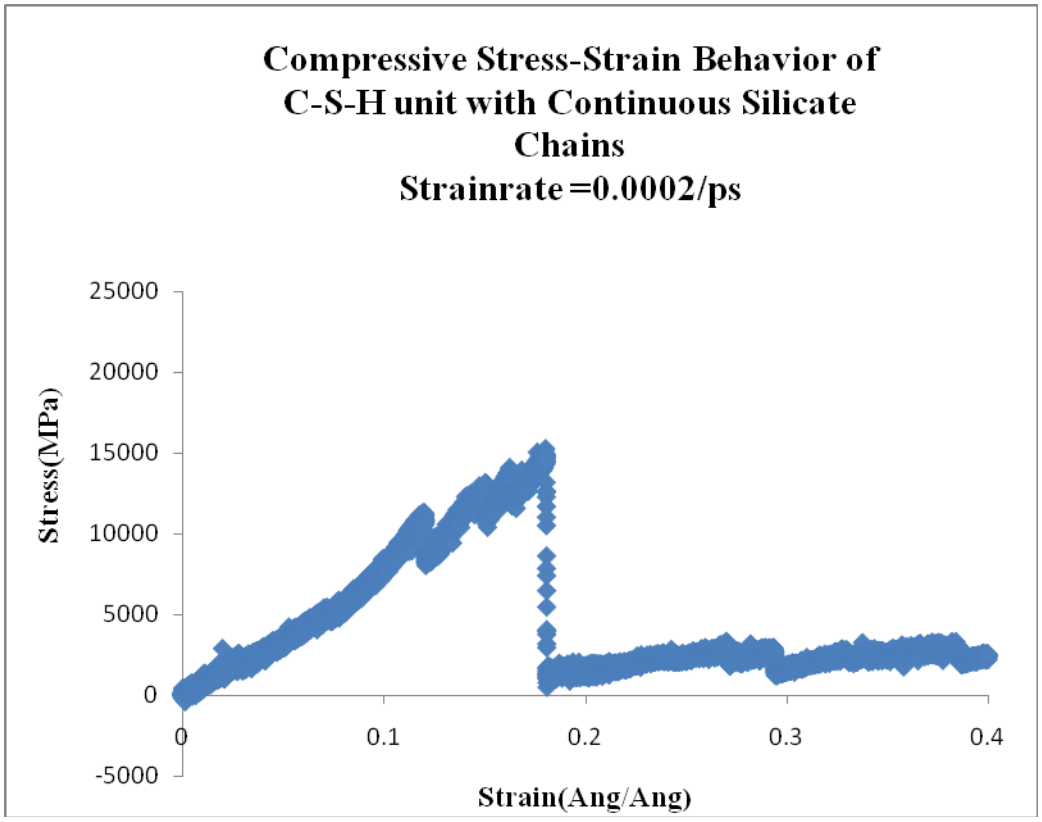

Figure 5.9 (b) Compressive Stress-Strain Behavior of Tobermorite.

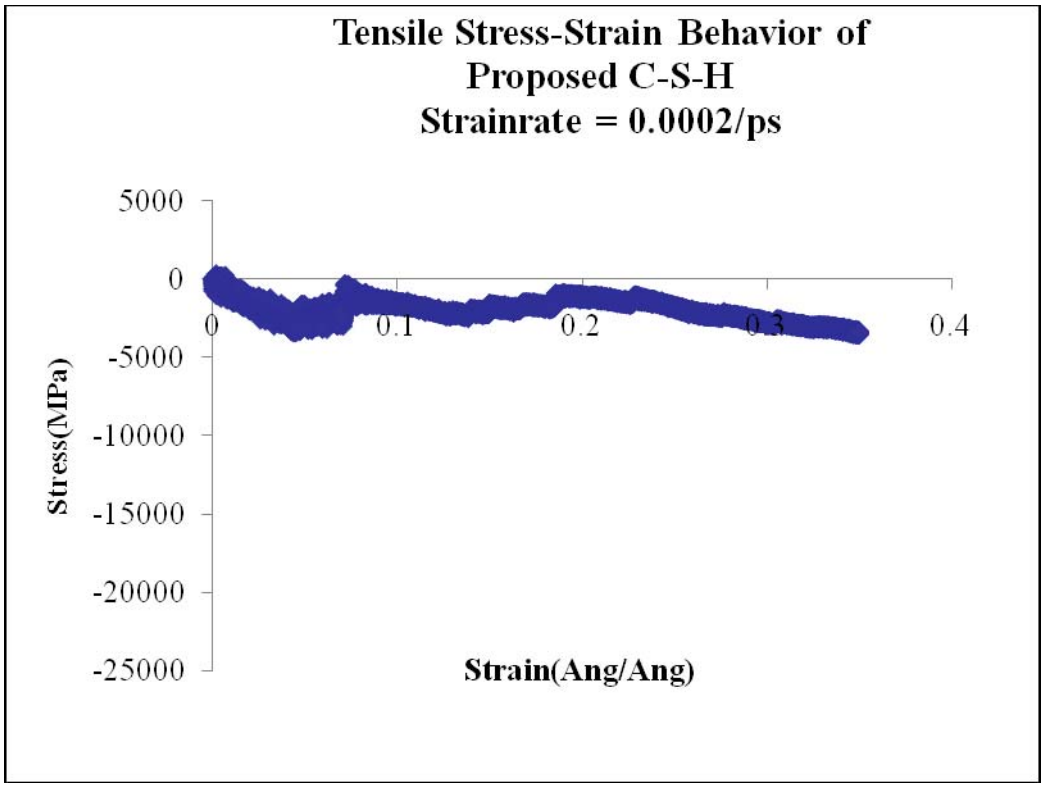

Figure 5.10 (a) Tensile Stress-Strain Behavior of Proposed C-S-H

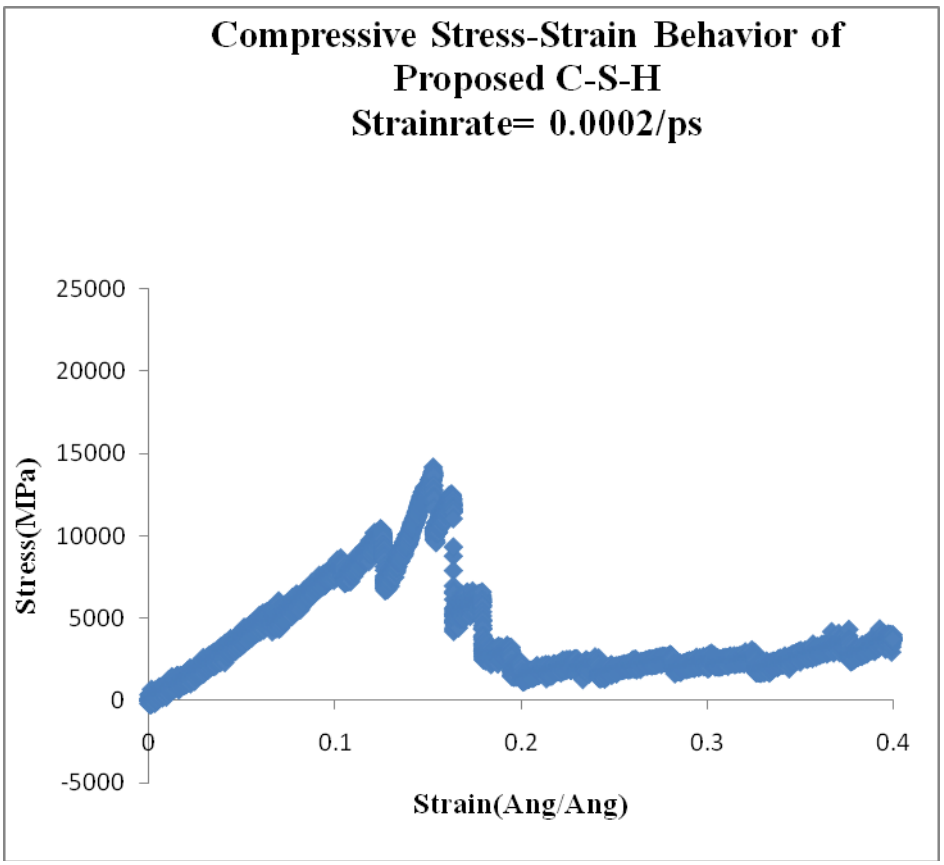

Figure 5.10 (b) Compressive Stress-Strain Behavior of Proposed C-S-H

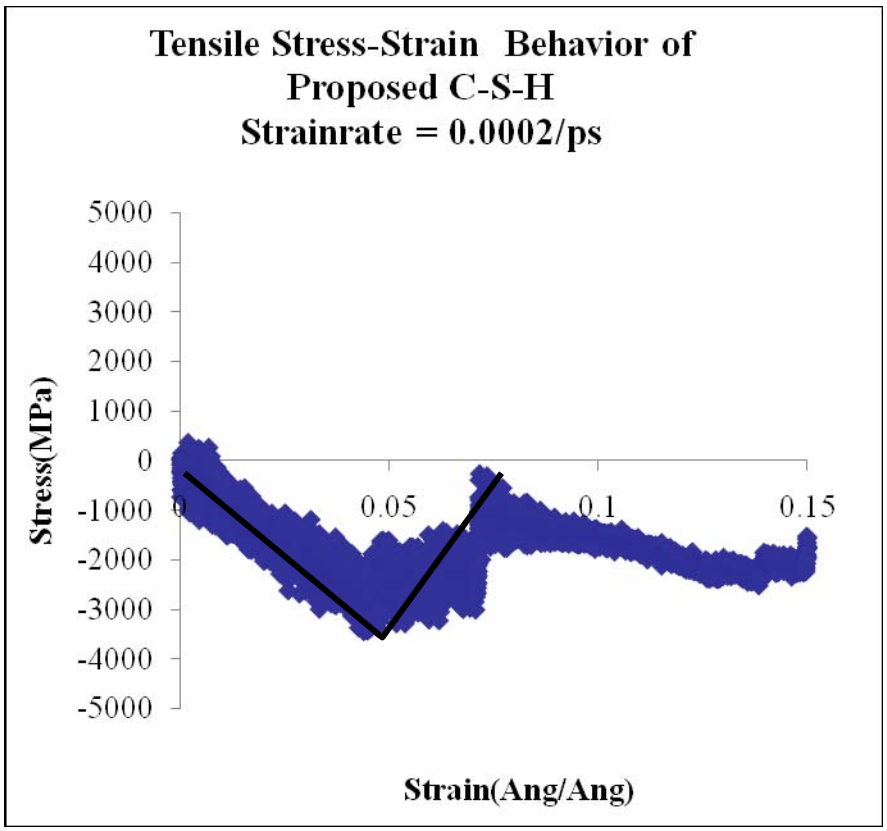

Figure 5.11 Magnification of the Tensile Stress-Strain Behavior of Proposed C-S-H

5.3.1 Computation of Elastic Modulus and Tensile Strength

In the stress-strain graphs shown in Figures 5.9a and 5.10a, a linear portion can be observed and hence the elastic modulus can be ascertained. The elastic modulus of both structures was computed from the slope of the linear portion of the tensile stress-strain curve. The linear portion evaluated is from the origin to the point corresponding to 0.4 times the maximum stress. Table 5.3 presents computed elastic modulus and strength of both structures. Based on the simulation results, the Young's modulus of the Proposed C-S-H and Tobermorite in the b direction [100] were determined to be 70,000 and 96,000MPa respectively, and the ultimate strength (tension) are 12,000 and 3,500 MPa, as shown in Figure 5.9a and 5.10a, respectively, and the ultimate strength (compression) are 15,000 MPa and 15,000 MPa as shown in Figure 5.9b and 5.10b, respectively, at a strain rate of 0.0002/ps.

Overall MD, simulations are in reasonable agreement with the results reported by Pellenq[9] and Vikramraja[15], Table 5.3 Pellenq[9] reported a maximum cohesion pressure (tensile strength) of 5,000 MPa between C-S-H lamella (layers) structures in C-S-H units using Ab Inito modeling techniques. The elastic modulus of the both C-S-H structures is comparable with other studies. Subramani[15], using molecular statics, calculated an elastic modulus of 65,000 MPa for the C-S-H unit with dimmer silicate chains. However, Subramani [15] multiplied a porosity factor to the calculated results from his research to account for porosity; the recalculated values were found to be comparable with macro level experimental results for cement paste. Pellenq [9] reported an elastic modulus of 89,000 MPa Tobermorite structure (Ca/Si =1).

Table 5.3 Elastic Modulus and strength of Calcium Silicate Hydrate Structures

C-S-H Model	Estimated Elastic Modulus (10^3)(MPa)	Estimated Elastic Modulus (10^3)(MPa)	Tensile Strength (MPa)	Compressive Strength (MPa)
Tobermorite	96	89[1]	-12 **(10^3)**	15**(10^3)**
Proposed C-S-H	70	65[2]	-3.5**(10^3)**	15**(10^3)**
Cement Paste (macroscopic)	20-30	34[2]	2[3]	20-60[3]

[1]Pellenq, [9]
[2] Subramani, [15]
[3]Pretorious [55]

5.3.2 Limitations of Computational Model

This computational model did not consider the presence of impurities in C-S-H gel i.e. sulphate or aluminate . Impurities may have an effect on the stiffness and strength values of C-S-H gel and should be considered in future work. Also porosity is not accounted for in this computational model. Instead this work suggests a method to account for porosity based on packing calcium silicate hydrate structures in a simulation cell to a specified density

5.4 Mechanical Properties of Tobermorite structures Packed Together

Molecular Statics via GULP code was used to calculate the mechanical properties of Tobermorite (crystalline calcium silicate hydrate) packed together. The tobermorite structures are spaced a few angstroms apart. This spacing was done to incorporate bond breakage in the silicate chains. The calculated mechanical properties are shown in Table 5.4. It can be seen that as the density of C-S-H unit favored the density of C-S-H found in experiments; the computed elastic moduli are in reasonable agreement with nano indentation experiments. At the nano meter length scal, C-S-H gel exists in two forms; Low Density C-S-H and High Density C-S-H. The dry density values for low density and high density C-S-H gel are 1.44 g/cm^3 and 1.75 g/cm^3 respectively. Nanoindentation experiments show that the range of elastic modulus corresponding to low density C-S-H is 13-26 GPa and the range of elastic moduli corresponding to high density C-S-H is 26 -39 GPa. This packing method may be a possible way to account for porosity in C-S-H. Figure 5.12 present visualizations of the three simulation cells constructed. The simulation cells are referred to as Stack 1, Stack 2 and Stack 3. The red square represents a single Tobermorite unit cell.

Table 5.4 Mechanical Properties of Tobermorite Structures Packed Together

C-S-H Model	Density g/cm3	Bulk modulus K GPa	Shear modulus G GPa	Poissons ratio γ	Elastic modulus E GPa
Stack 1	2.24	46	23	0.29	59
Stack 2	1.93	39	23	0.25	58
Stack 3	1.55	21	12	0.30	30
Experimental Data High Density C-S-H	2.13	n/a	n/a	n/a	26-39
Experimental Data Low Density C-S-H	1.44	n/a	n/a	n/a	13-26

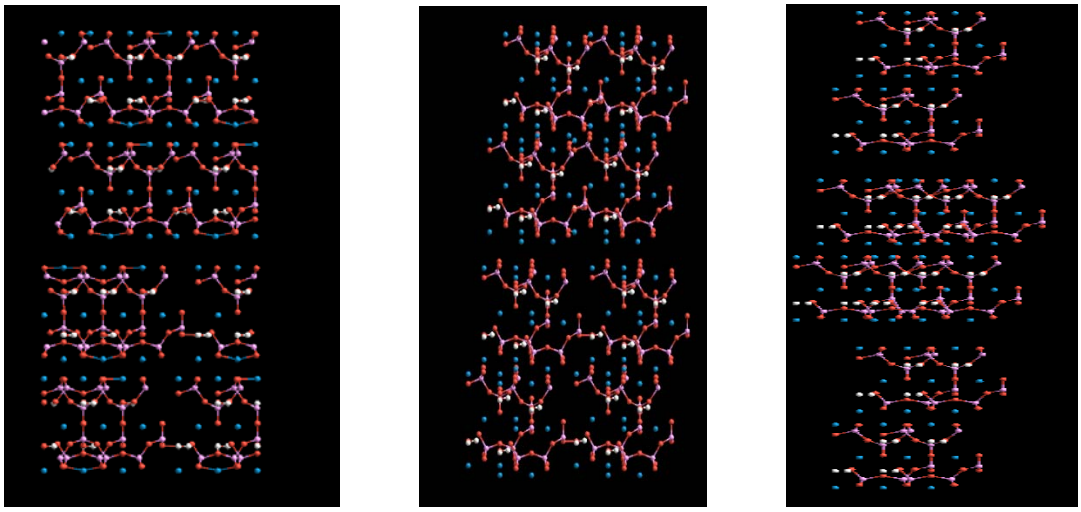

(a) (b) (c)

Figure 5.12 Packing of Crystalline Calcium Silicate Hydrate . (a) Stack 1, (b) Stack 2 and (c) Stack 3

5.5 Case study 1: Mechanism of deterioration of concrete structures upon subjection to aggressive environment

The performance properties of concrete get severely affected concrete undergoes chemical and physical degradation due to several factors. Hence to design concrete for a specified minimum service life, it is very essential to couple properties to environmental factors during design. Concrete structures deteriorate when subjected to different kinds of aggressive environment. For ex: Attack of chlorides, alkali, sulphates etc Examination of deteriorated concretes often revealed that there were more than one form of attack has been operative and this is because one form of attack makes the concrete more susceptible to damage by another.

For instance, attack of Magnesium salts on concrete structures is presented here. Higher concentrations of Magnesium salts are found in ground/sea water, industrial effluent, etc. Upon prolonged exposure to Magnesium salts, the calcium ions from the cement are leached out, which in turn triggers the deterioration of the concrete structures. The deterioration is initiated by the substitution of the less stable calcium ions in the

cementitious materials by Magnesium ions. For this study, Hamid's [34] Tobermorite 11 A° has been considered to represent the C-S-H structure.

5.5.1 Site potentials of Calcium atoms

Knowledge on the potential energies of Calcium atoms at its site (also called as site potentials) in the Tobermorite structure could shed more light on its exchange/substitution capacities. The site potentials of Calcium atoms in the Tobermorite structure for different Ca/Si ratios (0.66, 0.83 and 1.00) were determined using GULP. Figure 5.13 shows the stability of calcium atoms in the Tobermorite structure. The potential energy data that are encircled in the graph below are those that correspond to the interlayer Calcium atoms. The number of calcium atoms at the interlayers of the Tobermorite structure varies with Ca/Si ratio. For example: none in 0.66, one in 0.83 and two in 1.0. The potential energies of interlayer Calcium atoms (corresponding to site 5 & 6) are much higher than the potential energies of the lattice Calcium atoms (site 1, 2, 3 and 4). This suggests that the lattice Calcium atoms are far more stable than the interlayer calcium atoms. Hence, the interlayer Calcium atoms are the most vulnerable atoms for cationic-exchange or substitution.

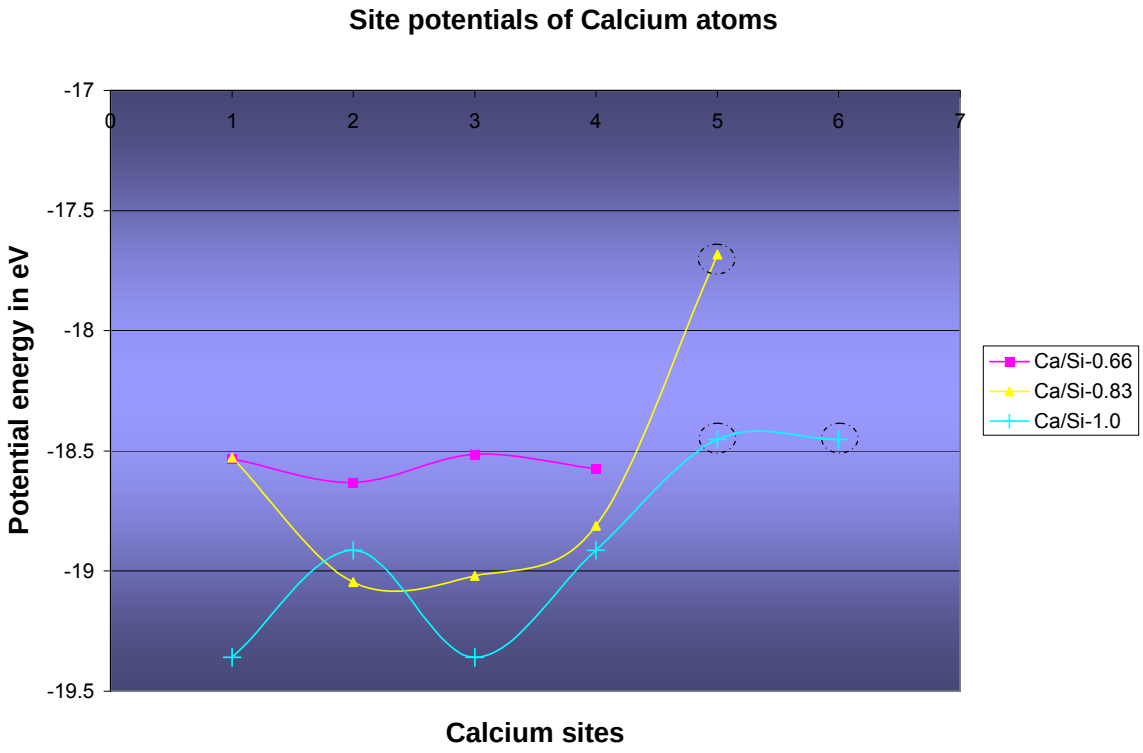

Figure 5.13 Site potentials of Calcium atoms

5.5.2 Substitution of Calcium by Magnesium

Magnesium ions from the water substitute the energetically less stable interlayer Calcium atoms in the C-S-H structure. In this case, only the substitution of interlayer Ca2+ions by Mg2+ is considered. Figure 5.14 shows the Magnesium substituted C-S-H.

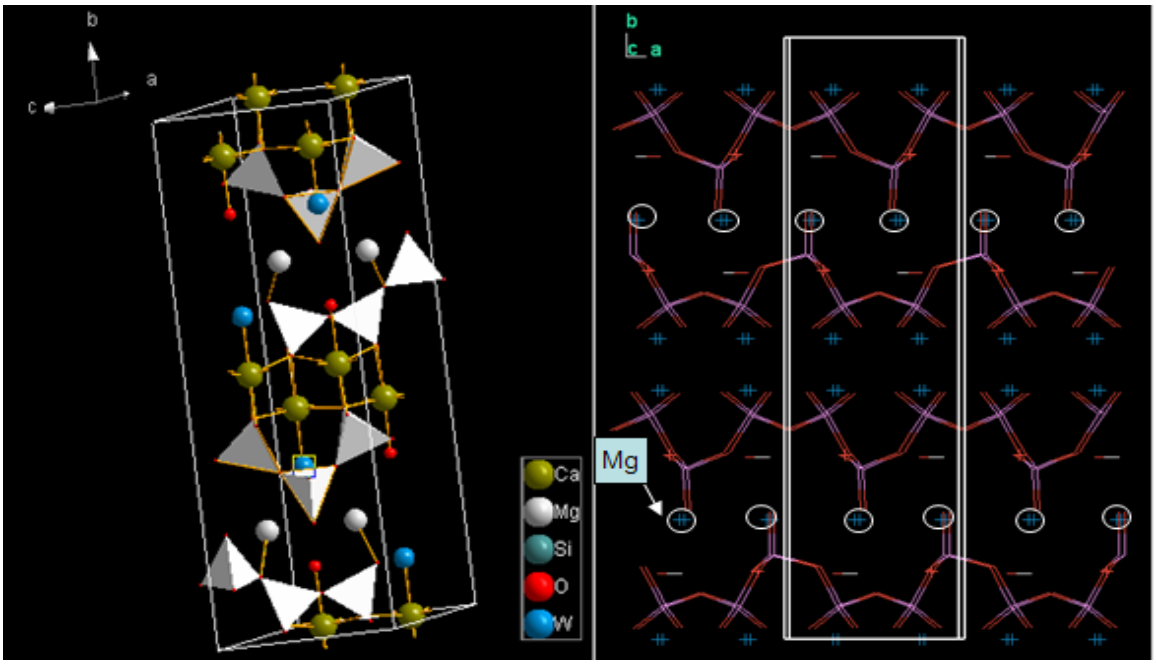

Figure 5.14 Magnesium substituted C-S-H.

Noticeable decrease in Elastic modulus value was observed for Mg substituted C-S-H structures as shown in Table 5.5. Leaching of Calcium leads to the reduction in the strength, stiffness and durability of concrete; eventually loses its cohesive nature. When all Calcium atoms in the C-S-H structures are substituted and occupied by Magnesium ions it results in the formation of Magnesium Silicate Hydrates; ultimately results in loss of cementitious characteristics and eventually leads to deterioration of rigid cement paste into a non-cohesive mass.

Table 5.5 Comparison of the bulk properties of Magnesium substituted Tobermorite with unsubstituted Tobermorite

Species	Dopant	Bulk Modulus	Shear Modulus	Elastic Modulus	Poissons ratio
		K	G	E	ν
		(GPa)	(Gpa)	(Gpa)	
Tobermorite 11 A° [34]	Without Mg	79	37	96	0.3
Tobermorite 11 A° [34]	With Mg (only the Interstitial Calcium is substituted with Mg)	68	27	71	0.32

5.6 Case study 2: Chemical and physical compatibility of composite cement

Composite cement contains one or more inorganic materials that takes part in the hydration reactions and contribute significantly to the hydration product. Fly ash is one of the most important sources of such inorganic materials that can readily be mixed with cement. Fly ash is known to be rich in Al2O3 and SiO2. This case study attempts to explain the mechanism of different possible cationic substitutions that can take place during the hydration of composite cement. Hamid's [34] Tobermorite 11 A° is considered as the C-S-H model for this study. To perfrom this study, it is critical to know which of the six silicon atoms in the C-S-H model need to be substituted. Calculation of the site potentials of all the silicon atoms in the C-S-H structure will provide a good idea about its exchange capacities.

5.6.1 Substitution of Silicon by Aluminium

As it is evident from Figure 7.6, the potential energy of silicon atoms at site 3 and 5 for Ca/Si-0.83 were found to be much lesser than those at other sites (1, 2, 3 and 4). Thus, the bridging silicon atoms have the least cohesive energy and are less stable compared to non bridging silicon atoms. Hence Si3 and Si5 are the preferential sites for substitution. The Aluminium ions available from the fly ash also participate in the hydration mechanism by substituting the silicon atoms in the C-S-H structures. As Al3+ions tend to form tetrahedral coordination similar to silicon atoms, it substitutes the energetically less stable bridging silicon atoms. But this substitution leaves a negative charge induced into the C-S-H structure. The charge compensation can be done in two ways: a) Bridging silicon atoms can be substituted by two Al3+ ions & one Ca2+ ion (in interlayer) b) Bridging silicon atoms can be substituted by two Al3+ ions & two protons attached to the oxygen atoms (all oxygen atoms connected to bridging silicon atoms are hydroxylated). Figure 5.15 shows the structure of C-S-H with Aluminium substituted only at the bridging silicon sites.

The aluminium substitution reaction in the silicate chains of C-S-H can also be viewed with another perspective. During the initial stages of hydration of the cement-based materials, the formation of dimmeric C-S-H structures is favored. Alumina

available from the flyash gets hydrated to Aluminium hydroxide (Al(OH)3). Since Aluminium is also tetrahedrally coordinated, Al(OH)3 acts a bridging molecule between dimmeric silicate chains. Thus, the addition of flyash favors the transformation of Dimmeric silicate chains to Drierketten type silicate chains. Only that the silicon in the bridging tetrahedra is substituted by Aluminium in this case. Also, the silica available from the flyash interacts with the calcium hydroxide in the cement paste and thus, forms additional C-S-H.

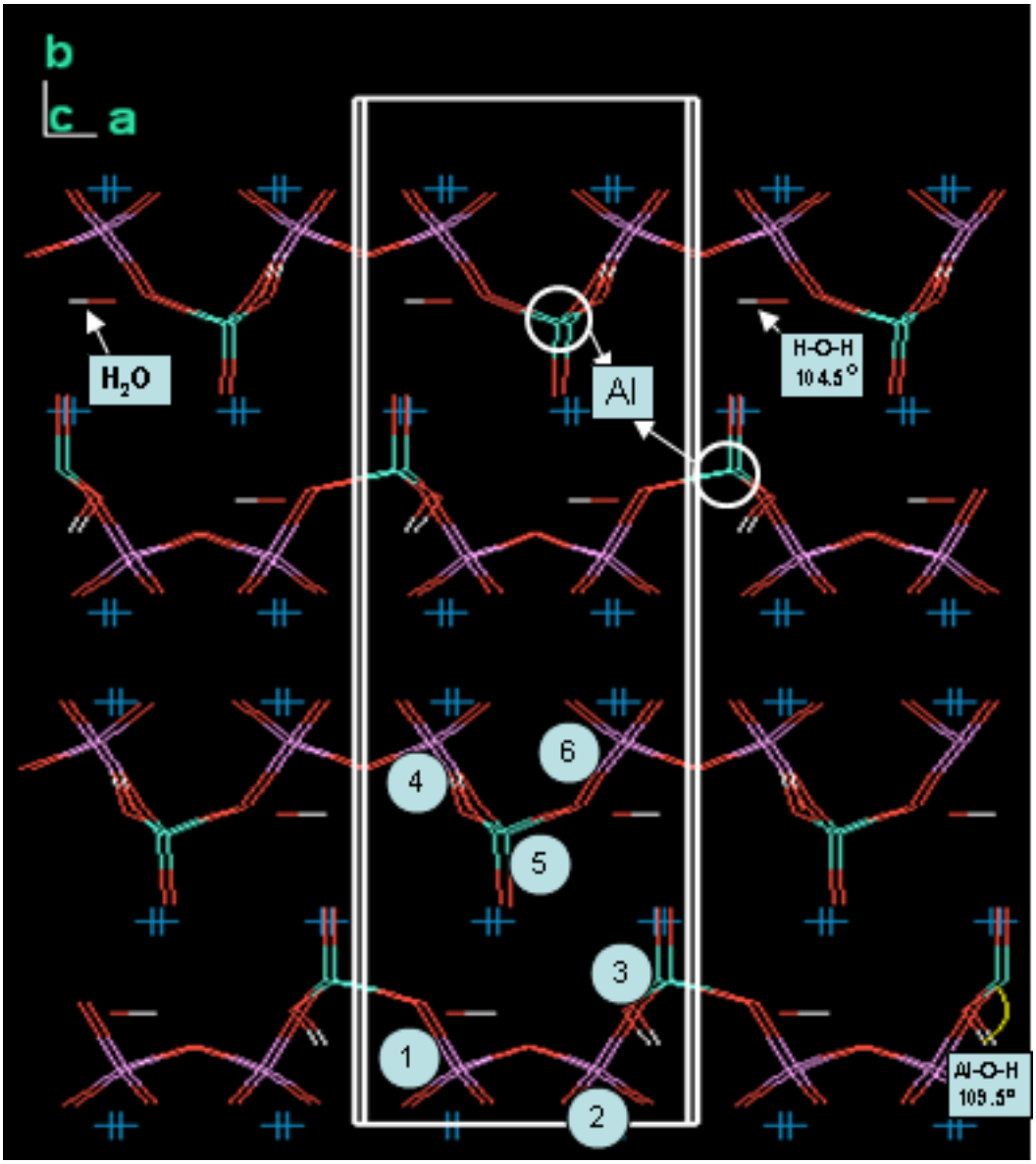

Figure 5.15 Aluminium substituted C-S-H

For Case (a), the two negative charges induced by the displacement of two Si^{4+} by two Al^{3+} were compensated by addition of one Ca^{2+} ion to the labile layer. Since the addition of a calcium atom in the interlayer was adequately sufficient to compensate the charge deficit induced near the bridging silicon atoms, this substitution did not provoke rupture in the tetrahedral silica chains. This shows the chemical compatibility of inorganic material additions to cement from the 'atomic structure' point of view. On the other hand, substitution of aluminium ions in non-bridging silicon sites induced rupture in the tetrahedral chains. Though the charge deficit can be compensated theoretically by adding Calcium ions or adding protons to the oxygen atoms of bridging silicon atoms, the charge compensation was poor because the protons to compensate for the charge deficit are relatively at a far distance from aluminium. This poor charge compensation near the non bridging silicon sites substituted by aluminum, induce a rupture in the chains.

However, the calculated properties of Aluminium substituted C-S-H (on bridging silicon sites) did not differ much from the un-substituted C-S-H (Table 5.6). The results justify the physical compatibility of inorganic material additions (such as fly ash rich in alumina and silica) to cement. The following two cases were also studied but are not reported here. 1) Substitution of Aluminium in place of Bridging silicon atoms with two protons attached to the oxygen atoms (hydroxylated) for charge compensation and 2) Substitution of Aluminium in place of Non bridging silicon atoms.

Table5.6 Comparison of the bulk properties of C-S-H with/without Aluminium substitution.

C-S-H model Ca/Si- 0.83	Tobermorite 11 A° (Hamid [34])	
Si Substitution by Al & Ca	No substitution	Si3 & Si5 sites
Bulk Modulus K (GPa)	62	69
Shear Modulus G (GPa)	34	36
Elastic modulus E (GPa)	86	0.28
Poissons ratio	0.27	

CHAPTER 6: SUMMARY

6.1 Summary

The tensile strength of cement paste is the most important factor affecting the nucleation of shrinkage cracks in cement based materials. Cement pastes which exhibit low tensile strength, tend to exhibit greater shrinkage crack potential and reduced durability. If the tensile strength in cement paste can be increased, then the shrinkage cracking potential can be minimized. It is believed that the strength and cohesion of cement paste is controlled by the formation of Calcium Silicate Hydrate (C-S-H) gel.

Currently, there is no adequate theory as to the source of the strength or cohesion of Calcium Silicate Hydrate (C-S-H) gel. The bonding scheme within C-S-H gel is believed to be the source of cohesion in cement paste. Vandamme et. al [2] shed some light on the factors that affects setting and hardening of the cement paste. Strong reasons were provided that the short and medium range attractive electrostatic forces were the prime components of the cohesion of C-S-H. Other evidences indicate that the surface forces between C-S-H particles are solely responsible for the cohesion in the cement. . If C-S-H gel can be made more functionalized, i.e. C-S-H gel with better cohesive properties, this can lead to better improvements in mechanical properties (strength and stiffness) of cement based materials. The process of making C-S-H gel more functional requires reliable information about the structure and properties of C-S-H gel.

Over the past decade there has been several experimental investigation of the nanostructure of main hydration product of cement paste, calcium silicate hydrate (C-S-H gel). It is believed that C-S-H gel controls properties such as cohesion and strength. X-ray diffraction (XRD) data of C-S-H gel suggests that structure is amorphous (i.e no long range order exists). In order words, it lacks the orderliness in the arrangement of atoms unlike a perfect crystal (bulk Copper, silicon etc..,). Experimental techniques such as Scanning Electron Microscopy (SEM), Transmission Electron Microscopy (TEM) found that Ca/Si ratio ranges from 0.6 to 2.0[8]. Also, the amorphous nature of C-S-H makes it very difficult to measure the amount of “bound” (chemically bound) & “unbound” water in cement pastes and thus, makes the quantitative measurements extremely challenging.

Although, the structure of C-S-H is not completely understood, some of the features of C-S-H have already been identified and recognized globally. C-S-H has a layered structure, at short length scales (1 to 5) nanometers. C-S-H layered structure, similar to the structure of Tobermorite and Jennite minerals, with a lamellae thickness in the nanometer range [9].

The main objective of this project is to determine the atomic structure of C-S-H at a length scale (1 to 5) nanometers. This structure can be used to study the fundamental behavior at the atomic level and predict mechanical properties.

To achieve this objective two possible atomic structures of C-S-H were considered. These were (i) crystalline minerals and (ii) crystalline minerals with bonds broken.

Molecular Statics calculations were performed on crystalline minerals like Tobermorite, Foshagite etc. to calculate the key physical properties such as Young's modulus, Bulk modulus, Shear modulus and Poissons ratio etc. The calculated bulk properties of the crystalline minerals were found to overestimate the existing experimental data by 4 to 5 times. The reasons for the overestimation were investigated: a) the atomic structure of the crystalline minerals considered do not resemble the actual C-S-H, they are perfect crystals. b) The crystalline minerals have an infinite length of silicate chains c) Porosity was not modeled in the input atomic structure. Therefore, two different methods were employed to modify and mimic the structure of C-S-H derived from Tobermorite 11 A°: a) Introduced defects by limiting the silicate chains to a finite length (dimmer C-S-H) b) Accounted porosity by including a packing factor of 0.69 using Mori-Tanaka scheme. The bulk properties of the newly constructed dimmer C-S-H was found to be K=22 GPa, G=14 GPa E = 34 GPa, which are now very much comparable to the experimental and simulation data [K=18 GPa, G=9.7 GPa, E = 20-30 GPa] – Manzano.H [51]. The length of the silicate chains had a significant effect on the key mechanical properties of C-S-H. From this work, a plausible atomic structure of C-S-H is proposed.

Molecular Dynamics simulations of uniaxial tension and compression were conducted on two atomic structures, namely, the proposed atomic structure of C-S-H (unit with dimmer silicate chains) and a Tobermorite mineral (unit with continuous

silicate chains) to determine their mechanical properties (tensile/compressive strength and elastic modulus). A uniaxial strain rate is applied to the both atomic structures and the response (stress) of structure is calculated and given as output. Stress-Strain graphs were derived from the MD output data and from these graphs the maximum strength [tensile and compressive] and elastic moduli were determined.

The simulations suggest the following:

1. Simulations of uniaxial tension and compression test conducted on the, C-S-H unit with dimmer silicate chains and the C-S-H unit with silicate chains (crystalline calcium silicate hydrate) showed both structures exhibit a linear elastic behavior up to the ultimate stress.
2. The strain at failure was found to be much higher than the corresponding values at macroscale, possibly due to the higher loading rates used.
3. The Young's modulus of Tobermorite and the proposed C-S-H structure in the b direction [100] was found to be 70,000 and 96,000 MPa, respectively. The ultimate strength in tension is 10,000 and 3,500 MPa, respectively. The ultimate strength in compression is 15,000 MPa and 15,000MPa respectively.
4. The maximum tensile and compressive strength of both C-S-H structures are magnitudes higher than the tensile and compressive strength at the macro level.
5. The trend in the stress-strain behavior of the C-S-H unit with dimmer silicate chains in tension and compression is reasonably comparable to that at the macroscopic level, i.e. the tensile strength is 23% of the compressive strength. This infers that bond breakage at the atomic level may potentially be the reason for the low tensile strength in cement pastes.

One limitation of this MD computational model is that porosity of C-S-H gel is not considered. Previous studies of the mechanical properties of C-S-H gel accounted for porosity by multiplying a packing factor to the computed mechanical properties. This work suggests a possible way to account for porosity directly into a computational model of C-S-H gel based on packing units of calcium silicate hydrate to a specified density. Molecular statics was used to compute the mechanical properties (elastic modulus) on packed Tobermorite structures and found that as the density of the packed Tobermorite

structures favored experimental data, the elastic modulus are in reasonable agreement with experimental data of C-S-H gel.

6.2 Future Work

1. This study concluded that bond breakage in C-S-H gel at the atomic level is responsible for low tensile strength of C-S-H gel. Future work is needed to determine ways to improve the bond at the atomic level, and increase tensile strength of C-S-H gel.
2. In molecular dynamics the strain rates used are normally very high in comparison with experiments. Future work is needed to determine the effect of strain rate on the strength of C-S-H gel. This could help resolve whether the strength of C-S-H gel is strain rate dependent and to determine an optimum strain rate.
3. Normally, concrete structures are subjected to triaxial loading not uniaxial loading. Future work is needed to determine the strength of C-S-H gel due to triaxial loading. This could help determine the true "strength" value of C-S-H gel.
4. Nanoindentation experiments have revealed that high density C-S-H gel is stronger than low density C-S-H gel. Future work can be done to investigate the atomic configuration of high density and low density C-S-H and determine the strength of these structures.
5. In addition, current nanoindenation experiments are not able to observe atomic scale deformation of C-S-H gel. Molecular Modeling can be used to investigate the atomic scale mechanisms of deformation during virtual indentation of high density or low density C-S-H gel. Predict the hardness and elastic modulus of C-S-H gel and compare with experiments. This work can be done to observe the atomic-scale mechanisms of deformation in C-S-H gel and to investigate the factors that affect hardness. This finding may serve as a backbone for the development of sustainable cement based materials.
6. Develop a model to investigate surface forces between Calcium Silicate Hydrate (C-S-H) particles in C-S-H gel. The cohesion of cement grains is caused by surface forces acting between C-S-H particles in interstitial electrolytic solution. Plassard et al (5) used atomic force microscopy (AFM) to investigate the

interaction between two Calcium Silicate Hydrates surfaces in air and different aqueous solutions. AFM measurements showed the existence of medium range forces of attraction between Calcium Silicate Hydrate particles in solutions (calcium hydroxide solution) similar to the pore solution of a hydrating cement paste. The attraction occurs on a relatively large range of pH and does not require a high calcium concentration. The pressure between C-S-H particles is about 30 MPa. Furthermore, at a fixed pH, the adhesion force seems to be lowered when part of the calcium counterions is replaced by sodium or potassium. Pure repulsion can only occur at low calcium concentration in the bulk solution. A precise model is needed to evaluate the surface forces measured in Plassard's work to determine the relationship between surface force and tensile strength of cement paste. A model of the atomic details of C-S-H surface can be proposed. In addition this work can provide avenues for improving the tensile strength of cement based materials at the nano scale. This work can be done using the following steps:

a. Develop a modified model that describes the packing arrangement of C-S-H particles in C-S-H Gel. This model should account for variations in Ca/Si ratio. This can be done by using a combination crystalline C-S-H crystal. For example: using both Tobermorite-like and Jennite- like crystals or using crystalline C-S-H crystal with variable chain length (dimmer, pentamer and continuous) as shown in Figure 6.1. In addition the density and surface area of C-S-H gel should comply with Low density C-S-H or High Density C-S-H.

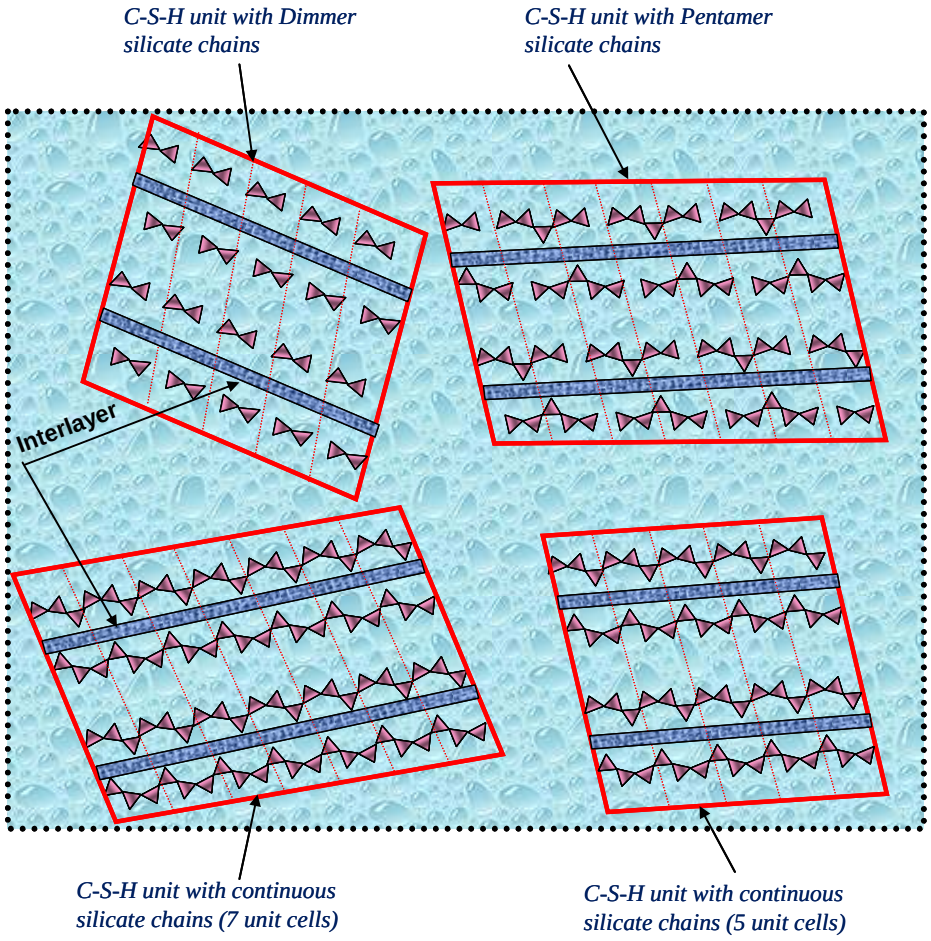

Figure 6. 1 Schematic diagram of the packing of C-S-H nanoparticles[15]

b. Use molecular mechanics to determine the bulk mechanical properties of C-S-H gel and compare with experiments.
c. Evaluate the interaction forces between C-S-H nanoparticles suspended in aqueous liquid (calcium hydroxide solution) using molecular dynamics and compare with experiments.
d. Once the structure and intermolecular forces within C-S-H gel is known, determine the tensile strength of the structure.

7. Use nanotechnology to investigate ways to manipulate the intermolecular forces between C-S-H particles and improve the tensile strength of cement based materials.

REFERENCES

1. Popovics, S. 1998. *Strength and related properties of concrete*: A Quantitative Approach. New York. John Wiley & Sons Inc.
2. Van Damme, H. and R.J-M Pellenq. 2004. Why Does Concrete set? The Nature of Cohesion Forces in Hardened cement based materials. *MRS Bulletin*
3. Richardson, I.G.1999.The nature of C-S-H in hardened cements. *Cement and Concrete Research* 29:1131-1147.
4. Hubbard, A.T. 2002. *Encyclopedia of Surface and Colloid Science.* CRC Press.
5. Plassard C., I Pochard, C. Labbez, A. Norat, E.Lesnniwsha , B. Jonsson. 2005. Nanoscale investigation of the particle interaction at the origin of the cohesion of cement. *Langmuir* 21:7263-7270
6. Plassard, C., E.Lesniewska, I.Pochard, and A.Nonat. 2004. Investigation of the surface structure and elastic properties of calcium silicate hydrates at the nanoscale. *Ultramicroscopy* 100: 331–338.
7. Gmira, A., J. Minet, A. Francischini, N. Lequeux, R.J-M. Pellenq, H.Van Damme.2008. Molecular engineering of the cohesion in neat and hybrid cement hydrates. *American Concrete Institute* 254:29-40.
8. Taylor, H. F.W.1997. *Cement Chemistry.* Thomas Telford Ltd. 2nd edition
9. Pellenq R. J.M., Lequex N., and Van Damme H.2008. Engineering the bonding scheme in C-S-H; the ionic-covalent framework. *Cement and Concrete Research* 38:159-174.
10. Constantinides.G and .F.J. Ulm.2003. The effect of two types of C-S-H on the elasticity of cement-based materials: Results from nanoindentation and micromechanical modeling. *Cement and Concrete Research* 34: 67-80.
11. Jennings,H.M .2000. A model for the microstructure of Calcium Silicate Hydrate in cement paste. *Cement and Concrete Research* 30: 101-116.
12. Jennings, H.M., J. Thomas, Julia S. Gevrenov, Georgios Constantines and Franz-Josef Ulm .2005. Relating the nanostructure of Concrete to

Engineering Properties. *2nd International Symposium on Nanotechnology in Construction*.

13. Donev, A., Cisse, I., Sachs D., Variano, E.A., Stillinger, F.H., Connely, R., Torquato, S., Chaikin, P.M.2004.Improving the density of jammed disordered packings using ellipsoids. *Science* 303:990–993.
14. Thomas, J. 2004. A colloidal interpretation of chemical aging of the C-S-H gel and its effect on concrete properties of cement paste. *Cement and Concrete Research*.36: 30-38
15. Subramani, V. S. 2008. Potential Applications of Nanotechnology for improved performance of Cement based materials. M.S Thesis, University of Arkansas.
16. Bensted, J. 2001. *Structure and Performance of cements.* Taylor and Francis.
17. Double,D.D, P.C Hewlett., K.S.W Sing and J.F Raffle.1983. New developments in understanding the chemistry of cement hydration, Philosophical Transactions of the Royal society of London. Series A. *Mathematical and Physical sciences* 310: 53-66.
18. Garboczi, E.J. and D.P. Bentz. 1995. Microstructure – Property relationships in concrete: from nanometer to centimeter". Second (2nd) Canmet/ACI. *Advances in Concrete Technology. International Symposium. Supplementary Papers* 573-585.
19. U.S. Department of Transportation Federal Highway Department .Petrographic Methods of examining hardened concrete: A Petrographic Manual. Chapter 14, http://www.fhwa.dot.gov/pavement/pccp/pubs/04150/chapt14.cfm.
20. Jennings, H.M, .J.J Thomas, .J.S Gevrenov, G. Constantinides and F.J Ulm. 2007. A multi-technique investigation of the nanoporosity of cement paste. *Cement and Concrete Research* 37: 329- 336.
21. Allen, M.P and Tildesley.D.J.1987. *Computer Simulation of Liquids*.
22. Bentz, D. P., D.A Quenard, V. Baroghel-Bounty, E. J. Garbocz1, H.M. Jennings.1995. Modeling drying shrinkage of cement paste and mortar Part – Structural Models from nanometer to millimeter. *Materials and Structures* 28:450-458.

23. Maekawa, K. T. Ishida and T.Kishi.2003. Multiscale modeling of concrete performance integrated material and structural mechanics. *Journal of Anvanced Concrete Technology* 1 (2): 91-126

24. Introduction to X-ray Diffraction. http://www.panalytical.com/index.cfm?pid

25. Wikepedia. http://www.wikipedia.org/

26. Taylor, H.F.W and Mohan.K (1981), Analytical Electron Microscopy of Cement pastes: IV, β-DiCalcium Silicate pastes. *Journal of American Ceramic Society 64*. 717-719.

27. Silicates.http://www.homepage.usask.ca/~mjr347/prog/geoe118/geoe118.007.html

28. Gonzalez, R .2002. Aggregation of Nanoparticles in 1D.Unpublished article

29. Richardson, I.G. 2004. Tobermorite /Jennite and Tobermorit/Calcium Hydroxide based models for the structure of C-S-H: Applicability to hardened pastes of Tricalcium Silicate, β-dicalcium silicate, Portland Cement, and blends of Portland with Blast-furnace Slag, Metakaolin, or silica fume. *Cement and Concrete Research* 34:1733-1777

30. Richardson, I.G .2004. The nature of C-S-H in hardened Cements. *Cement and Concrete Research* 29:1131-1147.

31. Walsh, D., M. A. Otooni, M. E. Taylor Jr and M. J. Marcinkowski. 1974. Study of portland cement fracture surfaces by scanning electron microscopy techniques. Modeling drying shrinkage of cement paste and mortar Part – Structural Models from nanometer to millimeter. *Journal of Materials and Scienc*e 9:423-429.

32. Acker, P. 2001. Micromechanical analysis of creep and shrinkage mechanism

33. Aligaizaki, Kalliopi K.2005. Pore structure of Cement Based Materials. Taylor & Francis Group.

34. Hamid, S.A .1981. The crystal structure of the 11A° Natural Tobermorite Ca2.25[Si3O7.5 (OH) 1.5].H2O.*Zeitschrift fur Kristallographie* 154:189-198.

35. Merlino, S, Bonaccorsi.E, and Armbruster.T .1999. Tobermorites: Their real structure and order-disorder (OD) character. *American Minerologist* 84: 1613-1621.

36. Merlino, S., Bonaccorsi.E, and Armbruster.T .2000. The real structures of Clintobermorite and Tobermorite 9 A°: OD character, polytypes, and structural relationships. *Eur.J. Mineral* 12: 411-429.

37. Faucon,P., Delaye. J.M. and Virlet.J .1996. Molecular Dynamics Simulation of the Structure of Calcium Hydrates. *Journal of Solid State Chemistry* 127: 92-97.

38. Faucon, P., .J.M Delaye. J Virlet., Jacquinot.J.F and Adenot.F.1997. Study of the structural properties of the C-S-H(I) By molecular dynamics simulation. *Cement and Concrete Research* 27(10):1581-1590

39. Dolado J.S., Griebel.M., and Hamaekers.J.2007. A Molecular Dynamic Study of Cementitious Calcium Silicate Hydrate (C-S-H) Gel. *Journal of the American Ceramic Society* 90 :3938-3942

40. Gmira, A., Zabat.M, Pellenq. R.J.M, Van Damme. H .2004. Microscopic physical basis of the poromechanical behaviour of cement based materials. *Materials and Structures/ Concrete Science and Engineering* 37: 3-14.

41. Manzano, H., Dolado.J.S, Guerrero.A and Ayuela.A .2007. Mechanical properties of crystalline Calcium-silicate-hydrates: comparison with cementitious C-S-H gels *Phys. stat. sol*. 204:1775–1780.

42. Introduction to Molecular Modeling. Chapter 2. http://chemistry.ncssm.edu/book/Chap2MolModel.pdf

43. Leach, A.2001. *Molecular Modeling: Principles and Applications*

44. Shewchuk, J.R .1994. An introduction to the Conjugate Gradient method without the agonizing pain. Unpublished article.

45. Brown, F.C.1967. *The Physics of solids - Ionic Crystals, Lattice vibrations, and Imperfections.*

46. Gale, J.D .1997. A computer program for the symmetry adapted simulation of solids. *JCS Faraday Trans* 93: 629.
47. LAMMPS Molecular Dynamic Simulator. http://lammps.sandia.gov/
48. Erccolessi, Furio. A molecular dynamic primer. University of Udine, Italy
49. Lewis,G.V and Catlow.C.R.A .1985. Potential models for ionic oxides. J.Phys.C: *Solid State Phys.* 18: 1149-1161.
50. Gale,J.D and Rohl.A.L .2003.The General Utility Lattice Program, Mol.Simul. 29:291.
51. Watanabe, T.,Hiroki F., Hidekazu N., Tadatsugu H., Iwao O. New Interatomic Potential Energy Function for Si-O Mixed Systems.1999. *Journal of Applied Physics*. 38: 366-369
52. CRD-C166-92 .Standard Test Method for Static Modulus of Elasticity of Concrete . www.wbdg.org/ccb/ARMYCOE/COESTDS/crd_c166.pdf
53. Pretorius, J.M.2008. Materials. Chapter 2. http://witsetd.wits.ac.za:8080/dspace/bitstream/123456789/4784/13/Research_Project_02_Materials.pdf

APPENDIX A: INPUT PARAMETERS TO GULP

A.1 Chemical formula:

The C-S-H structure (Ca/Si =1) has the following chemical formula $Ca_6Si_6O_{18}.2H_2O$. (As per Hamid's (1981) model)

A.2 Space group:

P21 ($P12_11$)
 # 4

A.3Unit cell dimensions:

a = 7.3900 A°; b = 22.7790 A°, c = 6.69 A°

$\alpha = 90°$; $\beta = 123.49°$; $\gamma = 90°$
Note that the coordinate axis (as mentioned in Hamid et.al (1981) are rotated in the clockwise direction as per the Right hand rule.

A.4 Fractional coordinates:

Sl. No.	*Atom*	*Type*	*x/a*	*y/b*	*z/c*
1	*Ca1*	*core*	*0.25*	*0*	*0.75*
2	*Ca1*	*core*	*0.75*	*0*	*0.75*
3	*Ca1*	*core*	*0.75*	*0.413*	*0.75*
4	*Ca1*	*core*	*0.25*	*0.413*	*0.75*
5	*Ca2*	*core*	*0.38*	*0.198*	*0.506*
6	*Ca2*	*core*	*0.88*	*0.198*	*0.506*
7	*Si*	*core*	*0.287*	*0.056*	*0.25*
8	*Si*	*core*	*0.707*	*0.056*	*0.25*
9	*Si*	*core*	*0.909*	*0.141*	*0.068*
10	*Si*	*core*	*0.207*	*0.373*	*0.25*
11	*Si*	*core*	*0.414*	*0.282*	*0.084*
12	*Si*	*core*	*0.787*	*0.373*	*0.25*
13	*O1*	*shel*	*0.17*	*0.12*	*0.25*
14	*O1*	*shel*	*0.137*	*0.0189*	*0.015*
15	*O1*	*shel*	*0.372*	*0.0189*	*0.484*
16	*O1*	*shel*	*0.83*	*0.12*	*0.25*
17	*O1*	*shel*	*0.5*	*0.077*	*0.25*
18	*O1*	*shel*	*0.622*	*0.0189*	*0.015*
19	*O1*	*shel*	*0.856*	*0.0189*	*0.484*
20	*O1*	*shel*	*0.909*	*0.211*	*0.068*
21	*O1*	*shel*	*0.785*	*0.113*	*-0.18*

22	*O1*	*shel*	*0*	*0.348*	*0.25*
23	*O1*	*shel*	*0.357*	*0.4108*	*0.484*
24	*O1*	*shel*	*0.122*	*0.4108*	*0.015*
25	*O1*	*shel*	*0.335*	*0.31*	*0.25*
26	*O1*	*shel*	*0.425*	*0.213*	*0.1*
27	*O1*	*shel*	*0.645*	*0.31*	*0.25*
28	*O1*	*shel*	*0.638*	*0.4108*	*0.015*
29	*O1*	*shel*	*0.872*	*0.4108*	*0.484*
30	*O1*	*shel*	*0.288*	*0.306*	*-0.175*
31	*O2*	*shel*	*0.75*	*0.303*	*0.75*
32	*O2*	*shel*	*0.25*	*0.11*	*0.75*
33	*H1*	*core*	*0.8396*	*0.303*	*0.92921*
34	*H1*	*core*	*0.8494*	*0.303*	*0.69257*
35	*H1*	*core*	*0.3396*	*0.11*	*0.92921*
36	*H1*	*core*	*0.3494*	*0.11*	*0.69257*
37	*O1*	*core*	*0.17*	*0.12*	*0.25*
38	*O1*	*core*	*0.137*	*0.0189*	*0.015*
39	*O1*	*core*	*0.372*	*0.0189*	*0.484*
40	*O1*	*core*	*0.83*	*0.12*	*0.25*
41	*O1*	*core*	*0.5*	*0.077*	*0.25*
42	*O1*	*core*	*0.622*	*0.0189*	*0.015*
43	*O1*	*core*	*0.856*	*0.0189*	*0.484*
44	*O1*	*core*	*0.909*	*0.211*	*0.068*
45	*O1*	*core*	*0.785*	*0.113*	*-0.18*
46	*O1*	*core*	*0*	*0.348*	*0.25*
47	*O1*	*core*	*0.357*	*0.4108*	*0.484*
48	*O1*	*core*	*0.122*	*0.4108*	*0.015*
49	*O1*	*core*	*0.335*	*0.31*	*0.25*
50	*O1*	*core*	*0.425*	*0.213*	*0.1*
51	*O1*	*core*	*0.645*	*0.31*	*0.25*
52	*O1*	*core*	*0.638*	*0.4108*	*0.015*
53	*O1*	*core*	*0.872*	*0.4108*	*0.484*
54	*O1*	*core*	*0.288*	*0.306*	*-0.175*
55	*O2*	*core*	*0.75*	*0.303*	*0.75*
56	*O2*	*core*	*0.25*	*0.11*	*0.75*

A.5 Charges

Sl.No.	*Atom*	*Type*	*Charge*	*No. of atoms*	*Total charge*
1	*Ca1*	*core*	*2*	*4*	*8*
2	*Ca2*	*core*	*2*	*2*	*4*
3	*Si*	*core*	*4*	*6*	*24*
4	*O1*	*core*	*0.86902*	*18*	*15.64236*
5	*O1*	*shel*	*-2.86902*	*18*	*-51.64236*
6	*O2*	*shel*	*-2.05*	*2*	*-4.1*
7	*O2*	*core*	*1.25*	*2*	*2.5*
8	*H1*	*core*	*0.4*	*4*	*1.6*
Charge of the system – Neutral					*0*

A.6 Potentials:

Note: Atoms with label Ca2 are the interstitial calcium atoms; O1 are the free oxygen atoms. O2 are the oxygen atoms from the water molecule. There are no oxygen atoms from hydroxyl group for Ca/Si =1 (Hamid's (1981) model).

Buckingham potential

Atom 1	Type	Atom 2	Type	A (eV)	rho (A°)	C_6 in eV * A°^{6}	r_{min} (A°)	r_{max} (A°)
Ca1	core	O1	shell	1090.4	0.3437	0	0	12
Si	core	O1	shell	1283.9	0.32052	10.66158	0	12
O1	shell	O1	shell	22764	0.149	27.879	0	12
H1	core	O2	shell	396.27	0.25	0	0	12
Ca2	core	O2	shell	777.27	0.3437	0	0	12
Ca2	core	O1	shell	1090.4	0.3437	0	0	12
Ca1	core	O2	shell	777.27	0.3437	0	0	12
Si	core	O2	shell	983.556	0.32052	10.66158	0	12
O1	shell	O2	shell	22764	0.149	13.94	0	12
O1	shell	H1	core	311.97	0.25	0	0	12

Morse potential

Atom 1	Type	Atom 2	Type	D (eV)	α (A° $^{-1}$)	R_o (A°)	r_{min} (A°)	r_{max} (A°)
H1	Core	O2	shell	6.203713	2.22003	0.92376	1	1.4

Three body potential

Atom 1	Atom 2	Atom 3	β (eV rad^{-2})	Θo (°)	Rmax (1-2) (Å)	Rmax (1-2) (Å)	Rmax (1-2) (Å)
Si core	O1 shell	O1 shell	2.09720	109.47	1.8	1.8	3.2
O2 shell	H1 core	H1 core	4.19978	108.69	1.2	1.2	1.8

Lennard Jones potential

Atom 1	Type	Atom 2	Typel	A (eV A°^{12})	B (eV A°^{12})	r_{min} (A°)	r_{max} (A°)
O2	Shell	O2	shell	39344.98	42.15	0	12

Core – shell spring potential

Atom	eV A° ^{2}
O1	74.92
O2	209.45

APPENDIX B: SAMPLE GULP INPUT FILE

```
opti prop conp pot
name C-S-H Ca/Si ratio 0.83 pot sites
cell
7.3900  22.7790 6.69 90.000000 123.49 90.000
frac
Ca1       core      0.25      0.000     0.75
Ca1       core      0.75      0.000     0.75
Ca1       core      0.75      0.413     0.75
Ca1       core      0.25      0.413     0.75
Ca2       core      0.88      0.198     0.506
Si        core      0.287     0.056     0.25
Si        core      0.707     0.056     0.25
Si        core      0.909     0.141     0.068
Si        core      0.207     0.373     0.25
Si        core      0.414     0.282     0.084
Si        core      0.787     0.373     0.25
O1        shel      0.17      0.12      0.25
O1        shel      0.137     0.0189 0.015
O1        shel      0.372     0.0189 0.484
O1        shel      0.83      0.12      0.25
O1        shel      0.5       0.077     0.25
O1        shel      0.622     0.0189 0.015
O1        shel      0.856     0.0189 0.484
O1        shel      0.909     0.211     0.068
O2        shel      0.785     0.113     -0.18
H1    core  0.866  0.078 -0.18
O1        shel      0.000     0.348     0.25
O1        shel      0.357     0.4108 0.484
O1        shel      0.122     0.4108 0.015
O1        shel      0.335     0.31      0.25
O1        shel      0.425     0.213     0.100
O1        shel      0.645     0.31      0.25
O1        shel      0.638     0.4108 0.015
O1        shel      0.872     0.4108 0.484
O2        shel      0.288     0.306     -0.175
H1    core  0.250  0.348     -0.175
O3        shel      0.75      0.303     0.75
O3        shel      0.25      0.11      0.75
H2        core      0.8396 0.303 0.92921
H2        core      0.8494 0.303 0.69257
H2        core      0.3396 0.11       0.92921
H2        core      0.3494 0.11       0.69257
O1        core      0.17      0.12      0.25
O1        core      0.137     0.0189 0.015
O1        core      0.372     0.0189 0.484
O1        core      0.83      0.12      0.25
O1        core      0.5       0.077     0.25
O1        core      0.622     0.0189 0.015
O1        core      0.856     0.0189 0.484
O1        core      0.909     0.211     0.068
O2        core      0.785     0.113     -0.18
O1        core      0.000     0.348     0.25
```

```
O1      core    0.357   0.4108 0.484
O1      core    0.122   0.4108 0.015
O1      core    0.335   0.31    0.25
O1      core    0.425   0.213   0.1
O1      core    0.645   0.31    0.25
O1      core    0.638   0.4108 0.015
O1      core    0.872   0.4108 0.484
O2      core    0.288   0.306   -0.175
O3      core    0.75    0.303   0.75
O3      core    0.25    0.11    0.75
space
4
species
Ca1 core  2.00
Ca2 core  2.00
Si core  4.000
O1 core 0.869020
O1 shel -2.869020
O2 shel -2.295
O2 core 0.869
O3 shel -2.05
O3 core 1.25
H1 core 0.426
H2 core 0.4000
buckingham
Ca1 core O1 shell 1090.4 0.34370 0.00000 0.0 12.0
Ca1 core O2 shell 777.27 0.34370 0.00000 0.0 12.0
Si core O1 shell 1283.9 0.32052 10.66158 0.0 12.0
Si core O2 shell 983.50 0.32052 10.66158 0.0 12.0
O1 shell O1 shell 22764. 0.14900 27.87900 0.0 12.0
O1 shell O2 shell 22764. 0.14900 13.94000 0.0 12.0
O2 shell O2 shell 22764. 0.14900 6.97000 0.0 12.0
H1 core O1 shell 311.97 0.25000 0.00000 0.0 12.0
Morse
H1 core O2 shell 7.0525 3.1749 0.9428 1.0 1.4
Three
Si core O1 shell O1 shell 2.0972 109.47 1.8 1.8 3.2
Si core O1 shell O2 shell 2.0972 109.47 1.8 1.8 3.2
Buck
H2 core O3 shell 396.27 0.25000 0.00000 0.0 12.0
Morse
H2 core O3 shell 6.203713 2.220030 0.92376 1.0 1.4
Three
O3 shell H2 core H2 core 4.199780 108.69 1.2 1.2 1.8
Lennard
O3 shell O3 shell 39344.98 42.15000 0.0 12.0
Buck
Ca2 core O3 shell 777.27 0.34370 0.00000 0.0 12.0
Buck
Ca2 core O1 shell 1090.4 0.34370 0.00000 0.0 12.0
Ca2 core O2 shell 1090.4 0.34370 0.00000 0.0 12.0
Buck
Ca1 core O3 shell 777.27 0.34370 0.00000 0.0 12.0
Si core O3 shell 983.556 0.32052 10.66158 0.0 12.0
H1 core O3 shell 311.97 0.25000 0.00000 1.2 12.0
O1 shell O3 shell 22764.0 0.14900 13.94000 0.0 12.0
```

O2 shell O3 shell 22764.0 0.14900 6.97000 0.0 12.0
O1 shell H2 core 311.97 0.25000 0.00000 0.0 12.0
O2 shell H2 core 311.97 0.25000 0.00000 0.0 12.0
spring
O1 74.920000
spring
O2 74.920000
spring
O3 209.45

APPENDIX C: DATA FILE FOR ATOMIC STRUCTURE OF TOBERMORITE

C.1 Title

Data File for crystalline C-S-H (Ca/Si = 1.00)

C.2 Number of atoms

144 atoms

C.3 Types of atoms

4 atom types

C.4. Simulation cell dimensions:

	Low (Ang)	High(Ang)
x	0.000	11.160
y	0.000	7.390
z	0.000	22.770

C.5 Atomic Mass

Atom type	Mass (amu)
1	40.080
2	28.090
3	16.000
4	1.000

C.6 Atomic coordinates:

Atom I.D.	Atom Type	Charge	x	y	z
1	1	2	5.580	0.000	0.000
2	1	2	5.580	3.700	0.000
3	1	2	5.580	3.700	9.400
4	1	2	5.580	0.000	9.400
5	1	2	4.220	1.860	4.510
6	1	2	4.220	5.560	4.510
7	2	4	2.790	2.120	1.280
8	2	4	2.790	5.230	1.280
9	2	4	1.780	7.390	3.210
10	2	4	2.790	1.530	8.490
11	2	4	1.860	3.670	6.420
12	2	4	2.790	5.820	8.490
13	3	-2	2.790	1.260	2.730
14	3	-2	1.480	1.880	0.430
15	3	-2	4.100	1.880	0.430
16	3	-2	2.790	6.130	2.730
17	3	-2	2.790	3.700	1.750
18	3	-2	1.480	5.470	0.430
19	3	-2	4.100	5.460	0.430
20	3	-2	1.780	7.390	4.800
21	3	-2	0.390	7.390	2.570
22	3	-2	2.790	0.000	7.920
23	3	-2	4.100	1.770	9.350
24	3	-2	1.480	1.770	9.350
25	3	-2	2.790	2.480	7.060
26	3	-2	1.950	3.700	4.850
27	3	-2	2.790	4.770	7.060
28	3	-2	1.480	5.580	9.350
29	3	-2	4.100	5.580	9.350
30	3	-2	0.420	3.700	6.970
31	3	-2	5.580	3.700	6.900
32	3	-2	5.580	0.000	2.510
33	4	1	6.580	3.700	6.900
34	4	1	5.260	4.640	6.900
35	4	1	6.580	0.000	2.510
36	4	1	5.260	0.950	2.510
37	1	2	11.160	3.700	0.000

38	1	2	11.160	7.390	0.000
39	1	2	11.160	7.390	9.400
40	1	2	11.160	3.700	9.400
41	1	2	9.800	5.560	4.510
42	1	2	9.800	9.250	4.510
43	2	4	8.370	5.820	1.280
44	2	4	8.370	8.920	1.280
45	2	4	7.360	11.090	3.210
46	2	4	8.370	5.230	8.490
47	2	4	7.440	7.370	6.420
48	2	4	8.370	9.510	8.490
49	3	-2	8.370	4.950	2.730
50	3	-2	7.060	5.580	0.430
51	3	-2	9.680	5.580	0.430
52	3	-2	8.370	9.830	2.730
53	3	-2	8.370	7.390	1.750
54	3	-2	7.060	9.160	0.430
55	3	-2	9.680	9.160	0.430
56	3	-2	7.360	11.090	4.800
57	3	-2	5.970	11.090	2.570
58	3	-2	8.370	3.700	7.920
59	3	-2	9.680	5.470	9.350
60	3	-2	7.060	5.470	9.350
61	3	-2	8.370	6.170	7.060
62	3	-2	7.530	7.390	4.850
63	3	-2	8.370	8.460	7.060
64	3	-2	7.060	9.280	9.350
65	3	-2	9.680	9.270	9.350
66	3	-2	6.000	7.390	6.970
67	3	-2	11.160	7.390	6.900
68	3	-2	11.160	3.700	2.510
69	4	1	12.160	7.390	6.900
70	4	1	10.840	8.340	6.900
71	4	1	12.160	3.700	2.510
72	4	1	10.840	4.640	2.510
73	1	2	8.370	1.850	11.390
74	1	2	8.370	5.540	11.390
75	1	2	8.370	5.540	20.790
76	1	2	8.370	1.850	20.790
77	1	2	7.010	3.710	15.900
78	1	2	7.010	7.410	15.900

79	2	4	5.580	3.970	12.660
80	2	4	5.580	7.070	12.660
81	2	4	4.570	9.240	14.600
82	2	4	5.580	3.380	19.880
83	2	4	4.650	5.520	17.810
84	2	4	5.580	7.660	19.880
85	3	-2	5.580	3.100	14.120
86	3	-2	4.270	3.730	11.820
87	3	-2	6.890	3.730	11.820
88	3	-2	5.580	7.980	14.120
89	3	-2	5.580	5.540	13.140
90	3	-2	4.270	7.310	11.820
91	3	-2	6.890	7.310	11.820
92	3	-2	4.570	9.240	16.190
93	3	-2	3.180	9.240	13.960
94	3	-2	5.580	1.850	19.310
95	3	-2	6.890	3.620	20.740
96	3	-2	4.270	3.620	20.740
97	3	-2	5.580	4.320	18.450
98	3	-2	4.740	5.540	16.240
99	3	-2	5.580	6.610	18.450
100	3	-2	4.270	7.430	20.740
101	3	-2	6.890	7.430	20.740
102	3	-2	3.210	5.550	18.360
103	3	-2	8.370	5.540	18.290
104	3	-2	8.370	1.850	13.890
105	4	1	9.370	5.540	18.290
106	4	1	8.050	6.490	18.290
107	4	1	9.370	1.850	13.890
108	4	1	8.050	2.790	13.890
109	1	2	13.950	5.540	11.390
110	1	2	13.950	9.240	11.390
111	1	2	13.950	9.240	20.790
112	1	2	13.950	5.540	20.790
113	1	2	12.590	7.410	15.900
114	1	2	12.590	11.100	15.900
115	2	4	11.160	7.660	12.660
116	2	4	11.160	10.770	12.660
117	2	4	10.150	12.930	14.600
118	2	4	11.160	7.070	19.880
119	2	4	10.230	9.220	17.810

120	2	4	11.160	11.360	19.880
121	3	-2	11.160	6.800	14.120
122	3	-2	9.850	7.420	11.820
123	3	-2	12.470	7.430	11.820
124	3	-2	11.160	11.680	14.120
125	3	-2	11.160	9.240	13.140
126	3	-2	9.850	11.010	11.820
127	3	-2	12.470	11.000	11.820
128	3	-2	10.150	12.930	16.190
129	3	-2	8.760	12.930	13.960
130	3	-2	11.160	5.540	19.310
131	3	-2	12.470	7.320	20.740
132	3	-2	9.850	7.310	20.740
133	3	-2	11.160	8.020	18.450
134	3	-2	10.320	9.240	16.240
135	3	-2	11.160	10.310	18.450
136	3	-2	9.850	11.130	20.740
137	3	-2	12.470	11.120	20.740
138	3	-2	8.790	9.240	18.360
139	3	-2	13.950	9.240	18.290
140	3	-2	13.950	5.540	13.890
141	4	1	14.950	9.240	18.290
142	4	1	13.630	10.180	18.290
143	4	1	14.950	5.540	13.890
144	4	1	13.630	6.490	13.890

APPENDIX D: DATA FILE FOR ATOMIC STRUCTURE OF PROPOSED C-S-H

D.1 Title

Data File for proposed C-S-H (Ca/Si = 1.25)

D.2 Number of atoms

124 atoms

D.3 Types of atoms

4 atom types

D.4. Simulation cell dimensions:

	Low (Ang)	High(Ang)
x	0.000	11.160
y	0.000	7.390
z	0.000	22.770

D.5 Atomic Mass

Atom type	Mass (amu)
1	40.080
2	28.090
3	16.000
4	1.000

D.6 Atomic coordinates:

Atom I.D.	Atom Type	Charge	a	b	c
1	1	2	5.580	0.000	0.000
2	1	2	5.580	3.700	0.000
3	1	2	5.580	3.700	9.400
4	1	2	5.580	0.000	9.400
5	1	2	4.220	5.560	4.510
6	2	4	2.790	2.120	1.280
7	2	4	2.790	5.220	1.280
8	2	4	2.790	1.530	8.490
9	2	4	2.790	5.820	8.490
10	3	-2	2.790	1.260	2.730
11	3	-2	1.480	1.880	0.430
12	3	-2	4.100	1.880	0.430
13	3	-2	2.790	6.130	2.730
14	3	-2	2.790	3.700	1.750
15	3	-2	1.480	5.460	0.430
16	3	-2	4.100	5.460	0.430
17	3	-2	2.790	0.000	7.920
18	3	-2	4.100	1.770	9.350
19	3	-2	1.480	1.770	9.350
20	3	-2	2.790	2.480	7.060
21	3	-2	2.790	4.770	7.060
22	3	-2	1.480	5.580	9.350
23	3	-2	4.100	5.580	9.350
24	3	-2	5.580	3.700	6.900
25	3	-2	5.580	0.000	2.500
26	4	1	2.900	1.930	3.480
27	4	1	2.930	1.840	6.220
28	4	1	6.580	3.690	6.900
29	4	1	5.260	4.640	6.900
30	4	1	6.580	0.000	2.500
31	4	1	5.260	0.950	2.500
32	1	2	11.160	3.700	0.000
33	1	2	11.160	7.390	0.000
34	1	2	11.160	7.390	9.400
35	1	2	11.160	3.700	9.400
36	1	2	9.800	9.250	4.510
37	2	4	8.370	5.820	1.280

38	2	4	8.370	8.920	1.280
39	2	4	8.370	5.220	8.490
40	2	4	8.370	9.510	8.490
41	3	-2	8.370	4.950	2.730
42	3	-2	7.060	5.580	0.430
43	3	-2	9.680	5.580	0.430
44	3	-2	8.370	9.830	2.730
45	3	-2	8.370	7.390	1.750
46	3	-2	7.060	9.160	0.430
47	3	-2	9.680	9.160	0.430
48	3	-2	8.370	3.700	7.920
49	3	-2	9.680	5.470	9.350
50	3	-2	7.060	5.460	9.350
51	3	-2	8.370	6.170	7.060
52	3	-2	8.370	8.460	7.060
53	3	-2	7.060	9.280	9.350
54	3	-2	9.680	9.270	9.350
55	3	-2	11.160	7.390	6.900
56	3	-2	11.160	3.700	2.500
57	4	1	8.480	5.620	3.480
58	4	1	8.510	5.530	6.220
59	4	1	12.160	7.390	6.900
60	4	1	10.840	8.340	6.900
61	4	1	12.160	3.690	2.500
62	4	1	10.840	4.640	2.500
63	1	2	8.370	1.850	11.390
64	1	2	8.370	5.540	11.390
65	1	2	8.370	5.540	20.790
66	1	2	8.370	1.850	20.790
67	1	2	7.010	7.400	15.900
68	2	4	5.580	3.970	12.660
69	2	4	5.580	7.070	12.660
70	2	4	5.580	3.380	19.880
71	2	4	5.580	7.660	19.880
72	3	-2	5.580	3.100	14.120
73	3	-2	4.270	3.730	11.820
74	3	-2	6.890	3.730	11.820
75	3	-2	5.580	7.980	14.120
76	3	-2	5.580	5.540	13.140
77	3	-2	4.270	7.310	11.820
78	3	-2	6.890	7.310	11.820

79	3	-2	5.580	1.850	19.310
80	3	-2	6.890	3.620	20.740
81	3	-2	4.270	3.620	20.740
82	3	-2	5.580	4.320	18.450
83	3	-2	5.580	6.610	18.450
84	3	-2	4.270	7.430	20.740
85	3	-2	6.890	7.430	20.740
86	3	-2	8.370	5.540	18.290
87	3	-2	8.370	1.850	13.890
88	4	1	5.690	3.780	14.870
89	4	1	5.720	3.680	17.610
90	4	1	9.370	5.540	18.290
91	4	1	8.050	6.490	18.290
92	4	1	9.370	1.850	13.890
93	4	1	8.050	2.790	13.890
94	1	2	13.950	5.540	11.390
95	1	2	13.950	9.240	11.390
96	1	2	13.950	9.240	20.790
97	1	2	13.950	5.540	20.790
98	1	2	12.590	11.100	15.900
99	2	4	11.160	7.660	12.660
100	2	4	11.160	10.770	12.660
101	2	4	11.160	7.070	19.880
102	2	4	11.160	11.360	19.880
103	3	-2	11.160	6.800	14.120
104	3	-2	9.850	7.420	11.820
105	3	-2	12.470	7.430	11.820
106	3	-2	11.160	11.680	14.120
107	3	-2	11.160	9.240	13.140
108	3	-2	9.850	11.010	11.820
109	3	-2	12.470	11.000	11.820
110	3	-2	11.160	5.540	19.310
111	3	-2	12.470	7.320	20.740
112	3	-2	9.850	7.310	20.740
113	3	-2	11.160	8.020	18.450
114	3	-2	11.160	10.310	18.450
115	3	-2	9.850	11.130	20.740
116	3	-2	12.470	11.120	20.740
117	3	-2	13.950	9.240	18.290
118	3	-2	13.950	5.540	13.890
119	4	1	11.270	7.470	14.870

120	4	1	11.300	7.380	17.610
121	4	1	14.950	9.240	18.290
122	4	1	13.630	10.180	18.290
123	4	1	14.950	5.540	13.890
124	4	1	13.630	6.490	13.890

APPENDIX E: INPUT PARAMETERS INTO LAMMPS

E.1 MD Conditions:

Name of Condition	Crystalline C-S-H (Tobermorite 11 Å)	Non-Crystalline C-S-H (Subramani (2008))
Cell Size (Å)	11.16 x 7.39 x 22.7	11.16 x 7.39 x 22.7
No. of Atoms	144	124
Molecular Tools	LAMMPS	LAMMPS
Interatomic Potentials	Buckingham, Stillinger-Weber, Coulomb	Buckingham, Stillinger-Weber, Coulomb
Energy Minimization tool	Conjugate Gradient	Conjugate Gradient
MD Ensemble	NPT	NPT
Temperature (°K)	300	300
Pressure (GPa)	0	0
Temperature and Pressure Control	Noose-Hover Barostat and thermostat	Noose- Hover Barostat and thermostat
Time Step (fs)	1	1
Dynamics time for NPT (ps)	100 – 300 ps	100 – 300 ps
Strainrate	0.000002	0.000002
Dynamics time for Strainrate Application (ps)	1000 – 3000 ps	1000 – 3000 ps

E.2 Potentials:

Buckingham Potential

Atom 1	Type	Atom 2	Type	A (eV)	rho (A°)	C_6 in eV * A^{o6}	$R_{total\ (A°)}$
Ca	Core	Ca	core	4369.010	0.290	0.000	5.000
Si	Core	Si	core	1171.520	0.290	0.000	5.000
O	Shell	O	core	452.505	0.290	0.000	5.000
H	Core	H	core	21.221	0.350	0.000	5.000
Ca	Core	O	core	3557.620	0.290	0.000	5.000
Ca	Core	Si	core	1382.481	0.290	0.000	5.000
Ca	Core	H	core				5.000
Si	Core	H	core	430.657	0.290	0.000	5.000
Si	Core	O	core	1848.717	0.290	0.000	5.000
O	Shell	H	core	248.632	0.290	0.000	5.000

Three body term (Stillinger and Weber)

Atom 1	Atom 2	Atom 3	Epsilon	Sigma	a	lambda	gamma	costtheta0
Si	Si	Si	2.168	2.095	1.600	16.404	1.047	-0.333
Si	Si	O	0.000	0.000	0.000	10.667	0.250	-0.333
Si	O	Si	0.000	0.000	0.000	10.667	0.250	-0.333
Si	O	O	2.168	2.095	1.650	3.189	0.322	-0.333
O	Si	Si	2.168	2.095	1.400	2.957	0.718	-0.616
O	Si	O	0.000	0.000	0.000	0.000	0.000	-0.333
O	O	Si	0.000	0.000	0.000	0.000	0.000	-0.333
O	O	O	0.000	0.000	0.000	0.000	0.000	-0.333

Three body term (Stillinger and Weber) (cont.)

Atom 1	Atom 2	Atom 3	A	B	p	q	tol
Si	Si	Si	7.050	0.602	4.000	0.000	0.000
Si	Si	O	0.000	0.000	0.000	0.000	0.000
Si	O	Si	0.000	0.000	0.000	0.000	0.000
Si	O	O	0.000	0.000	0.000	0.000	0.000
O	Si	Si	115.364	0.909	2.590	2.394	0.000
O	Si	O	0.000	0.000	0.000	0.000	0.000
O	O	Si	0.000	0.000	0.000	0.000	0.000
O	O	O	12.292	0.000	0.000	2.244	0.000

Coulumb Potential

Total Cutoff distance (r) = 5.000 Angstroms

APPENDIX F: SAMPLE INPUT FILE FOR LAMMPS

```
# 3d csh stress calc
 log             log.pressurew.csh
 units           metal
 boundary        p p p
 atom_style      charge
 pair_style      hybrid/overlay buck 3.0 sw coul/long 3.0
 kspace_style    ewald 0.0001

 read_data       data4.hamid
 pair_coeff    1 1 buck 4369.01 0.29 0.0
 pair_coeff      2 2 buck 1171.52 0.29 0.0
 pair_coeff      3 3 buck 452.5051 0.29 0.0
 pair_coeff      4 4 buck 21.228 0.35 0.0
 pair_coeff      1 2 buck 1382.4811 0.29 0.0
 pair_coeff      1 3 buck 3557.62 0.29 0.0
 pair_coeff      2 3 buck 1848.7174 0.29 0.0
 pair_coeff      3 4 buck 248.6324 0.29 0.0
 pair_coeff      2 4 buck 430.6566 0.29 0.0
 pair_coeff    * * coul/long
 pair_coeff      * * sw  SiOOO.sw NULL Si O NULL

 neighbor        2.0 bin
 neigh_modify    every 1 delay 0 check yes

# equilibrate
 min_style       cg
 thermo          5
 minimize        1.0e-4 1.0e-6 120 1000

# 300-NPT
 velocity all create 300.0 5812775
# fix             1 all npt 300.0 300.0 0.001 xyz 0.0 0.0 1.0 drag 1.0
 fix             1 all npt 300 300 0.001 aniso 0.0 0.0 0.0 0.0 0.0 0.0 0.005 drag 2.0
 thermo        1000
 thermo_style   custom step temp etotal press vol
 thermo_modify   flush yes
 timestep        0.0001
 run             2000000
 unfix           1


# 300-NPT
  fix            2 all npt 300.0 300.0 0.001 aniso 0.0 0.0 NULL NULL 0.0 0.0 0.005 drag 2.0


# Deform
# ------
 fix             3 all deform 1 y erate .00000002
 compute        deftemp all temp/deform
 compute        4 all pressure deftemp
 thermo          10000
 thermo_style    custom step temp etotal pxx pyy pzz  press  vol lx ly lz
```

```
# dump          2 all custom 1000 out.tensionlong.csh tag type x y z
 reset_timestep    0
 timestep          0.0001
 run               20000000
```

APPENDIX G: INPUT PARAMETERS INTO GULP FOR PACKED TOBERMORITE STRUCTURES

G.1 Chemical formula:

The C-S-H structure (Ca/Si =1) has the following chemical formula $Ca_6Si_6O_{18}.2H_2O$. (As per Hamid's (1981) model)

G.2 Space group:

Space group #1 - no symmetry

G.3 Potentials:

Buckingham Potential

Atom 1	Type	Atom 2	Type	A (eV)	rho (A°)	C_6 in eV * A^{o6}	$r_{min\ (A°)}$	$r_{max\ (A°)}$
Ca	Core	Ca	core	4369.010	0.290	0.000	0.000	5.500
Si	Core	Si	core	1171.520	0.290	0.000	0.000	5.500
O	Shell	O	core	452.505	0.290	0.000	0.000	5.500
H	Core	H	core	21.221	0.350	0.000	0.000	5.500
Ca	Core	O	core	3557.620	0.290	0.000	0.000	5.500
Ca	Core	Si	core	1382.481	0.290	0.000	0.000	5.500
Ca	Core	H	core					5.500
Si	Core	H	core	430.657	0.290	0.000	0.000	5.500
Si	Core	O	core	1848.717	0.290	0.000	0.000	5.500
O	Shell	H	core	248.632	0.290	0.000	0.000	5.500

Three body term (Stillinger and Weber)

Atom 1	Atom 2	Atom 3	K (eV)	Θo (°)	rho (A°)	Rmax (1-2) (Å)	Rmax (1-2) (Å)	Rmax (1-2) (Å)
Si	O	O	149.794	109.5	2.8	3	3	6

APPENDIX H: FORTRAN CODE TO BUILD THE ATOMIC STRUCTURE OF PACKED TOBERMORITE STRUCTURES

```
c.....
c....SHANIQUE MURRAY
c....DATE: MARCH 10TH, 2009
c....TRIAL1
c....CONFIGURATION OF NANOPARTICLES IN C-S-H GEL
c.....
      IMPLICIT REAL*8 (A-H,O-Z)
      DIMENSION X(30000),Y(30000),Z(30000),IC(30000),AM(30000),
     &CH(30000),XR(30000),YR(30000),ZR(30000),XT(30000),YT(30000),
     &ZT(30000),XS(30000),YS(30000),ZS(30000),XO(30000),
     &ZO(30000),YO(30000),XP(30000),YP(30000),ZP(30000),XM(30000),
     &YM(30000),ZM(30000),XE(30000),YE(30000),ZE(30000),
     &XB(30000),YB(30000),ZB(30000)

c.....ICOLOR DETAILS
c     CA  Si  O  H
C     1   2   3   4
C.....READ ALL ATOM POSITION IN C-S-H particle
C.....XSH  YSH   ZSH
c      b     c     a
C.....OPEN THE DATA FILE
      OPEN (91, FILE='tob.txt')
      OPEN (92, FILE='tob1.txt')
   11  format(2I4,4F15.7)
C.....LOOP READS THE COORDINATES FROM THE .TXT FILE AND STORES THEM IN
C.....6 ARRAYS X,Y,Z,IC,AM AND CH. COORDINATES ARE IN A°
C.... WRITE(92,11)

      NPQ = 144

      DO I=1,NPQ
      READ (91,*) X(I),Y(I),Z(I),IC(I),CH(I)
      WRITE (92,11) I,IC(I),CH(I),X(I),Y(I),Z(I)
      END DO

C.....TRANSLATING COORDINATES ALONG Y DIRECTION TO CREATE PARTICLE 2

      XSH = 00.00
      YSH = 12.61
      ZSH = 0.00

      NPC1= NPQ

      CALL TRAN(X,Y,Z,IC,AM,CH,NPQ,XSH,YSH,ZSH,XT,
     &YT,ZT,NPC1)
```

```
C.....TRANSLATING COORDINATES ALONG Z DIRECTION TO CREATE PARTICLE 3

      XSH2 = 0.00
      YSH2 = 0.00
      ZSH2 = 28.00

      NPC2 = 2*NPQ

      CALL TRAN(X,Y,Z,IC,AM,CH,NPQ,XSH2,YSH2,ZSH2,XS,
     &YS,ZS,NPC2)

C.....TRANSLATING COORDINATES ALONG Y and Z DIRECTION TO CREATE
c     PARTICLE 4

      XSH3 = 00.00
      YSH3 = 12.61
      ZSH3 = 28.00

      NPC3 = 3*NPQ

      CALL TRAN(X,Y,Z,IC,AM,CH,NPQ,XSH3,YSH3,ZSH3,XO,
     &YO,ZO,NPC3)

      END

      SUBROUTINE TRAN(X,Y,Z,IC,AM,CH,NPQ,XSH,YSH,ZSH,XT,
     &YT,ZT,NPC)
      IMPLICIT REAL*8 (A-H,O-Z)
      DIMENSION X(30000),Y(30000),Z(30000),IC(30000),AM(30000),
     &CH(30000),XT(30000),YT(30000),ZT(30000)

      DO I=1,NPQ

      XT(I)=X(I)+XSH
      YT(I)=Y(I)+YSH
      ZT(I)=Z(I)+ZSH
      IC(I)=IC(I)
      CH(I)=CH(I)

      WRITE (92,11) I+NPC,IC(I),CH(I),XT(I),YT(I),ZT(I)
   11  format(2I5,4F15.7)

      END DO

      RETURN
      END
```